HYPERSPECTRAL ANALYSIS OF SEAGRASS IN REDFISH BAY, TEXAS

A Dissertation

by

JOHN S. WOOD

Submitted
in Partial Fulfillment of the Requirements for the Degree of

DOCTOR OF PHILOSOPHY
in
Coastal and Marine Systems Science

Texas A&M University-Corpus Christi

Corpus Christi, Texas

December, 2012

HYPERSPECTRAL ANALYSIS OF SEAGRASS IN REDFISH BAY, TEXAS

A Dissertation
By

JOHN S. WOOD

Dr. James Gibeaut, Chair

Dr. John W. Tunnell, Jr., Co-Chair

Dr. Gary Jeffress, Committee Member

Dr. James Simons, Committee Member

Dr. Stacey Lyle, Graduate Faculty Representative

JoAnn Canales, PhD.
Interim Dean, College of Graduate Studies

December, 2012

December 2012

ABSTRACT

Remote sensing using multi- and hyperspectral imaging and analysis has been used in resource management for quite some time, and for a variety of purposes. In the studies to follow, hyperspectral imagery of Redfish Bay is used to discriminate between species of seagrasses found below the water surface.

Water attenuates and reflects light and energy from the electromagnetic spectrum, and as a result, subsurface analysis can be more complex than that performed in the terrestrial world. In the following studies, an iterative process is developed, using ENVI image processing software and ArcGIS software. Band selection was based on recommendations developed empirically in conjunction with ongoing research into depth corrections, which were applied to the imagery bands (a default depth of 65 cm was used). Polygons generated, classified and aggregated within ENVI are reclassified in ArcGIS using field site data that was randomly selected for that purpose. After the first iteration, polygons that remain classified as ‘Mixed’ are subjected to another iteration of classification in ENVI, then brought into ArcGIS and reclassified. Finally, when that classification scheme is exhausted, a supervised classification is performed, using a ‘Maximum Likelihood’ classification technique, which assigned the remaining polygons to the classification that was most like the training polygons, by digital number value. Producer’s Accuracy by classification ranged from 23.33 % for the ‘MixedMono’ class to 66.67% for the ‘Bare’ class; User’s Accuracy by classification ranged from 22.58% for the ‘MixedMono’ class to 69.57% for the ‘Bare’ classification. An overall accuracy of 37.93% was achieved. Producers and Users Accuracies for *Halodule* were 29% and 39%,

respectively; for *Thalassia*, they were 46% and 40%. Cohen's Kappa Coefficient was calculated at .2988.

We then returned to the field and collected spectral signatures of monotypic stands of seagrass at varying depths and at three sensor levels: above the water surface, just below the air/water interface, and at the canopy position, when it differed from the subsurface position. Analysis of plots of these spectral curves, after applying depth corrections and Multiplicative Scatter Correction, indicates that there are detectable spectral differences between *Halodule* and *Thalassia* species at all three positions. Further analysis indicated that only above-surface spectral signals could reliably be used to discriminate between species, because there was an overlap of the standard deviations in the other two positions. A recommendation for wavelengths that would produce increased accuracy in hyperspectral image analysis was made, based on areas where there is a significant amount of difference between the mean spectral signatures, and no overlap of the standard deviations in our samples.

The original hyperspectral imagery was reprocessed, using the bands recommended from the research above (approximately 535, 600, 620, 638, and 656 nm). A depth raster was developed from various available sources, which was resampled and reclassified to reflect values for water absorption and water scattering, which were then applied to each band using the depth correction algorithm. Processing followed the iterative classification methods described above.

Accuracy for this round of processing improved; overall accuracy increased from 38% to 57%. Improvements were noted in Producer's Accuracy, with the 'Bare' classification increasing from 67% to 73%, *Halodule* increasing from 29% to 63%,

Thalassia increasing slightly, from 46% to 50%, and ‘MixedMono’ improving from 23% to 42%. User’s Accuracy also improved, with the ‘Bare’ class increasing from 69% to 70%, *Halodule* increasing from 39% to 67%, *Thalassia* increasing from 40% to 7%, and ‘MixedMono’ increasing from 22.5% to 35%.

A very recent report shows the mean percent cover of seagrasses in Redfish Bay and Corpus Christi Bay combined for all species at 68.6%, and individually by species: *Halodule* 39.8%, *Thalassia* 23.7%, *Syringodium* 4%, *Ruppia* 1% and *Halophila* 0.1%. Our study classifies 15% as ‘Bare’, 23% *Halodule*, 18% *Thalassia*, and 2% *Ruppia.* In addition, we classify 5% as ‘Mixed’, 22% as ‘MixedMono’, 12% as ‘Bare/*Halodule* Mix’, and 3% ‘Bare/*Thalassia* Mix’. Aggregating the ‘Bare’ and ‘Bare/*species*’ classes would equate to approximately 30%, very close to what this new study produces. Other classes are quite similar, when considering that their study includes no ‘Mixed’ classifications.

This series of research studies illustrates the application and utility of hyperspectral imagery and associated processing to mapping shallow benthic habitats. It also demonstrates that the technology is rapidly changing and adapting, which will lead to even further increases in accuracy. Future studies with hyperspectral imaging should include extensive spectral field collection, and the application of a depth correction.

DEDICATION

This humble body of work is dedicated to:

…The memory of my father, Howard Anthony Wood, Sr., who taught me that hard work, integrity, and perseverance is worth it in the end,

…To Dennis Pridgen, a friend and colleague who shared his love of the study area with me over a warm cup of coffee on a cold sunny day with very little wind, with the icy water lapping at the sides of our boats hitched side by side, and his desire to protect and understand it, and who passed from this world at far too young an age,

…To my son, with the knowledge that it may not be perfect, but does strive to be so,

…To my grandchildren, with the hope that this may someday make a difference in your lives, and in the world in which I hope you live a long, long time, and always have time to enjoy,

…To my family and friends, who often encouraged me and seldom questioned my mental state,

… and last but not least to my dear wife, for always being there, supporting me, encouraging me and refusing to let me give up.

ACKNOWLEDGEMENTS

Over the last arduous and seemingly everlasting seven and one half years, there have been many who have contributed both support and encouragement, in large and small ways to the completion of this endeavor. I would be remiss if I did not acknowledge Ed Harte and the Harte family, who had the vision to create the Harte Research Institute, and the inspiration for many of us to ‘make a difference’. My dissertation committee, composed of Jim Gibeaut, Wes Tunnell, Jim Simons and Gary Jeffress, has been a valuable asset in the quest to become a better scientist. Those who have offered advice and encouragement along the way will be silently remembered. To those who have funded this research and invested considerable time (Jim Gibeaut, Wes Tunnell, and Larry McKinney, NOAA Environmental Cooperative Science Center) ‘thanks!’ will never be enough. To my long-time mentor and friend, Liz Smith, who always has an encouraging word, I can only hope to repay you by being as good a mentor to someone else along the way.

TABLE OF CONTENTS

Page

LIST OF FIGURES

Page

Page

Page

LIST OF TABLES

Page

Page

CHAPTER I: BACKGROUND AND HYPOTHESES

INTRODUCTION[1]

The Texas coast is widely known for its rich natural resources (Tunnell and Judd 2002), and much of this richness and high biodiversity is attributable to vast estuarine seagrass-dominated communities (Pulich and Onuf 2004). A small (6,180 hectares) but important part of this coastal area is Redfish Bay, a major component of the 75,150 hectare Mission-Aransas National Estuarine Research Reserve (MANERR) (Beyer *et al.* 2007). This research reserve was established in 2007 and tasked with the mission to ensure that coastal management decisions benefit flora and fauna, water quality, and people by bringing together scientists, landowners, policy-makers, and the public (Bittler 2011). Redfish Bay is located between Aransas Pass and Port Aransas, and *Halodule wrightii* and *Thalassia testudinum* are co-dominant seagrass species (Fry and Parker 1979) in this shallow estuarine ecosystem.

These seagrass beds have undergone intense research: Cowper (1978) studied the drift algae community found interspersed within the blades; Pulich *et al.* (1976) studied the trace metal cycles; Fry and Parker (1979) studied the animal diets within the meadows; McMillan (1991) studied the longevity of the seed reserve; and Major and

---

[1] *Format: Ecology*

Dunton (2002) studied the effects of the variations in light-harvesting characteristics. Short and Wyllie-Echeverria (1996) studied the effects of propeller scarring.

Between 2005 and 2040, the population of Texas coastal counties is predicted to rise 108%. Furthermore, populations are becoming more mobile, and an increasingly large number of coastal habitat users are coming from larger cities hundreds of miles from the coast. With these increases come increasing stresses on the estuaries and coastal environments that serve as an interface between the mainland and the seaward barrier islands (Cohen *et al.* 1997).

These estuaries also are subject to increased environmental pressures from nutrient enrichment in the watersheds that feed them (Montagna and Kalke 1992). As populations in these areas increase, so have the industrial and agricultural influences. Other influences include decreased freshwater inflows due to increasing demands for fresh water, and increases in recreational and commercial fishing have increased turbidity levels. Increased dredging to accommodate the growing populations has had a similar effect. All of these stressors can impact the sustainability of our estuaries and coastal habitats and systems. The goal of coastal management is to monitor and evaluate the conditions of these habitats, which are recognized as essential to the well-being of fauna, flora and the quality of human existence along the coast (Diaz *et al.* 2004). Remote sensing provides a means to monitor many of these conditions on a regional or landscape scale.

BACKGROUND AND RELEVANCE

Submerged aquatic vegetation (SAV) is a group of vascular plants that grow below the water surface, but do not emerge, and includes what is commonly known as seagrass. Seagrasses in the bays and estuaries of the northern Gulf of Mexico (Handley *et al.* 2007) are important on national and even global scales. Figure 1.1 shows the global diversity and distribution of seagrasses (Short *et al.* 2007). The meadows found in the northern Gulf of Mexico cover the majority of the total distribution in the US, and over 5% of all seagrass found world-wide (Beck *et al.* 2007). In Texas, 85% of the total seagrass vegetation for the entire coastal zone is found in the Laguna Madre. These seagrass meadows cover over 730 km^2 of bay bottom, and are comprised of five different species (Onuf and Ingold 2007). Five of 50 species found worldwide are in Coastal Bend estuaries (Duarte 1999): *Thalassia testudinum, Halodule wrightii, Syringodium filiforme, Halophila engelmanni,* and *Ruppia maritima*, with *Halodule* and *Thalassia* dominant.

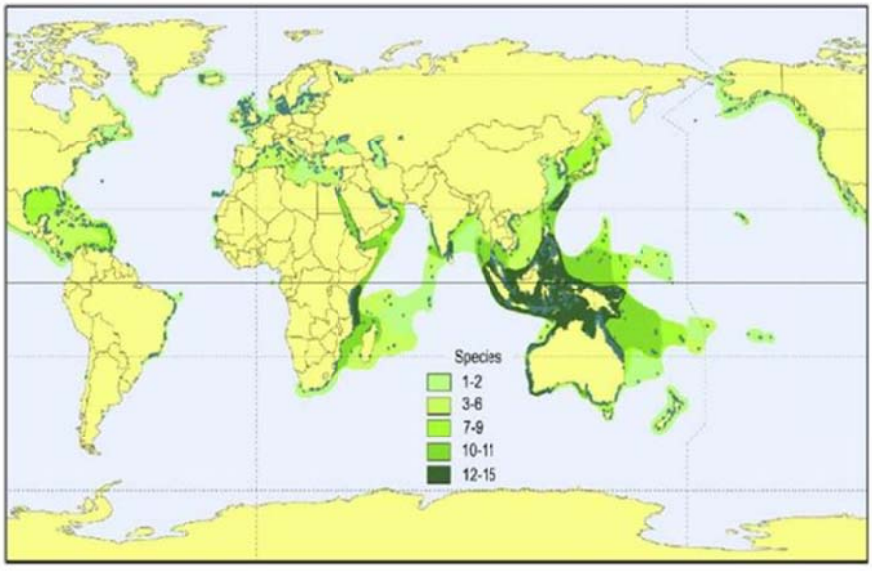

Figure 1.1. The extent of global seagrass diversity and distribution. From 2005 UNEP-WCMC, as adapted by Short (2007).

Seagrass meadows perform or contribute to at least twelve of the 17 recognized ecosystem services, including gas regulation (regulation of atmospheric chemical composition, such as CO_2/O_2 balance, O_3 levels for UVB protection, and SO_x levels), disturbance regulation (including dampening the ecosystem responses to storms, floods and droughts and other environmental variability), hydrologic flow regulation, erosion control, soil formation, nutrient cycling, waste treatment, habitat and refuge, food production, raw materials and recreational services (Costanza *et al.* 1997). Seagrasses provide vital nursery and spawning habitat for many marine and estuarine fishes (Jagtap *et al.* 2003), and they provide protected areas for juvenile and adult fish and shellfish. Seagrasses and detrital material from them also serve as food sources for a variety of microbes, juvenile fishes and benthic organisms, which in turn feed larger organisms, fishes, molluscs, crustaceans, and echinoderms (Jagtap *et al.* 2003) which then serve as a food source for waterfowl, turtles and mammals (Orth *et al.* 2006). They add oxygen to the water column, help stabilize sediments (Jagtap *et al.* 2003), and diffuse and absorb wave energy (Fonseca and Cahalan 1992). They alter water flows and trap sediments (Orth *et al.* 2006). By affecting the currents and flows through the estuary, they collect both organic and inorganic materials, which also help stabilize and bind the sediments (Wood *et al.* 1969), preventing erosion and preserving the microflora found in sediments and at the sediment/water interface. Seagrasses also support an extensive community of macrophytes and epiphytes, further aiding in the trophic structure and diversity of estuarine ecosystems (Harlin 1975). Detritus also provides organic matter necessary for sulfur reduction and cycling. The vast beds of seagrasses are recognized as important indicator species for estuarine environments (Ward 1987).

Remote sensing enables spatial analysis of seagrass and benthic habitats on a landscape scale (Weng 2002). Researchers have used remote sensing to monitor and analyze benthic habitats, algae, SAV distribution, and coral reef ecosystems, using a variety of scales and both aerial and satellite platforms (Mishra *et al.* 2005). Much of this research has been accomplished using multispectral imagery, often using the shorter visible bands that have higher water penetration. In addition to monitoring the present condition of these habitats, time series analysis can be performed with images from different time periods (Dobson and Dustan 2000). The Near-Infrared (NIR) region of the spectrum is seldom used due to its high spectral attenuation through water, despite serving as the primary cue for discriminating vegetation type and a critical component for vegetation indices such as the Normalized Difference Vegetation Index (Cho and Lu 2010), Green Leaf Area Index (Bréda 2003), MERIS Terrestrial Chlorophyll Index (Dash and Curran 2004) and Wide-Dynamic Range Vegetation Index (Gitelson 2004).

Several states have attempted to estimate the economic value of their seagrass habitat. The Texas Parks and Wildlife Department estimates the value of seagrass habitat at $9,000 to $28,000 per acre in commercial, recreational and hydrologic economic benefits (Handley *et al.* 2007). Likewise, the Florida Department of Environmental Protection estimates a total economic benefit of $55.4 billion, equating to approximately $20,500 per acre (Handley *et al.* 2007). Costanza *et al.* (1997) have calculated the value in 2010 dollars to $34,000 per acre per year.

Seagrass habitats are declining

Declines in seagrass habitats have been occurring on local, regional and global scales. The decline has been attributed to various anthropogenic and natural disturbances,

including dredging (Onuf 1994), nutrient enrichment, and propeller scarring from recreational and commercial fishing boats (Quammen and Onuf 1993, Dunton and Schonberg 2002, Burfeind and Stunz 2006). Loss of seagrass habitat has been documented since the mid-1970s (Merkord 1978); Onuf performed a vegetation survey in the Laguna Madre in 1988 (Onuf 1996), confirming a 140 km^2 decrease in cover between the mid-60s and 1988. Much of this loss is attributed to increased turbidity (Baden *et al.* 2003) resulting in low light levels reaching the sediment layers. In Laguna Madre, this is at least partly a result of maintenance dredging of the Gulf Intracoastal Waterway (Quammen and Onuf 1993).

Degradation of seagrass habitats is a cause for concern for communities throughout the northern Gulf of Mexico. Over the last 50 years, seagrass habitat losses are estimated in ranges from 20-100% for most estuaries in Gulf coastal regions. As coastal populations increase (Cohen *et al.* 1997), further stresses can be expected. Increased nutrient loading, dredging, shoreline development, and boating are all expected to increase simultaneously (Handley *et al.* 2007).

Irresponsible boating in shallow waters can contribute to undesirable changes in the seagrass habitats by causing increased fragmentation. Propeller scarring creates channels through the matrix of seagrass vegetation, dissecting continuous beds into smaller patches causing an increase in edge-to-area ratios. These scars can have permanent effects (Dunton and Schonberg 2002), although most will heal to some extent in two to ten years (Uhrin and Holmquist 2003).

There are also natural stresses on seagrass habitats, including the hydrodynamics and fetch of individual bay and estuary systems. Storms erode the sediments or bury

seagrasses beneath them. Changes in water levels expose seagrass to harsh climatic conditions. Outbreaks of disease, overgrazing by nekton, and freshwater-caused changes in salinity (Pulich 2007) also put great stresses on seagrasses. Light shading and oxygen depletion are often caused by an overgrowth of macroalgae, as shown in Figure 1.2.

Figure 1.2. Macroalgae covering *Thalassia* bed, possibly causing oxygen depletion and light shading.

Between 1990 and 1997, the microalga *Aureoumbra lagunensis* bloomed constantly in the Laguna Madre (Buskey *et al.* 1998). This 'brown tide' bloom began after an extended drought, which raised salinities in the hyper-saline lagoon far above normal, to as much as ~60 PSU (Buskey *et al.* 1998). Reduced water clarity reduced the distribution of seagrass from deeper water by reducing the amount of light available (Dunton 1994, Onuf 1996, Burfeind and Stunz 2006). Stressed seagrass beds often signal stresses on the whole coastal ecosystem. Along with a reduction in seagrass, reductions in biomass and diversity of grazers were noted during the brown tide (Buskey and Hyatt 1995).

The role of seagrass as an indicator species

The evaluation and assessment of the environmental status of ecosystems is often accomplished with the use of indicators and indices (Casazza *et al.* 2002, Fonseca *et al.* 2002). By analyzing the parameters of an appropriate indicator, information can be gained about a complex system beyond what is directly associated with that indicator (Casazza *et al.* 2002). Living organisms represent the most appropriate indicators for the environmental quality of a water body, as they integrate biotic and abiotic components through their adaptive responses (Casazza *et al.* 2002).

Seagrass is often considered to be a biological indicator for estuarine ecosystem health. Bio-indicators are essential for monitoring the coastal environment because they send complex messages in simplified and useful ways, providing insights about a trend or event that cannot be observed directly. Because seagrass communities are stationary, and tend to respond cumulatively to the effects of eutrophication, seagrasses can be used as bio-indicators for long-term water quality (Harlin 1975). When used as a bio-indicator, seagrass can serve as an early warning system of pollution or a degrading ecosystem, helping to sustain other interrelated critical resources (Harlin 1975, Linton and Warner 2003). By observing and analyzing changes signaled by bio-indicators, managers can monitor the state of the coastal environment and measure the effects of management strategies, as well as environmental, social, and economic activities. Changes may be indicated by seagrass presence/absence, condition, and growth rate. Declines in shoot biomass and density can signal increased eutrophication levels. Excess nutrients increase epiphyte loads (Harlin 1975), decrease irradiance (Tomasko and Lapointe 1991) and

lower seagrass productivity (Sand-Jensen 1977). These stressors can ultimately result in seagrass die-off.

As an environmental status indicator, seagrass can provide a means of measuring the results of policies and actions, as well as a means to monitor the impacts of anthropogenic and other stressors. Seagrass can be used to assess current trends and conditions, project future trends, and show the connections between social, environmental and economic policies or actions (Linton and Warner 2003). Finding patterns, such as quantitative differences in abundance and diversity of macrofaunal organisms, root-to-shoot ratios, habitat use by sciaenid larvae and early juveniles, as well as spatial and structural pattern characteristics such as patchiness, density, contiguousness, biomass and blade length can indicate what stresses are present and help identify the sources of stressors (Lewis *et al.* 1983, Edgar and Robertson 1992, Irlandi *et al.* 1995, Rooker *et al.* 1998, Fourqurean *et al.* 2001). Measurements of growth rates, rates of change, enzyme activities, and other biologic and physical parameters can highlight the effects of those stressors on the community. Since communities generally respond to stressors with a reduction in diversity and an increase in dominance by species more tolerant to the particular type of stress, these changes may indicate what types of stressors are active (Linton and Warner 2003). Seagrasses also require higher light levels than most plants, and thus are sensitive to environmental changes that alter light availability such as turbidity, suspended solids and water clarity (Orth *et al.* 2006). Increased sediment loads directly affect seagrass productivity by reducing the light intensity, which drives the photosynthesis in canopy tissue pigments (Ferwerda *et al.* 2007).

Seagrass as a filter/sediment trap

One of the greatest threats to the ecological integrity of coastal ecosystems is nutrient pollution. The world-wide trend of increasing human population densities in coastal areas (Cohen *et al.* 1997) will shift population impacts from forested, agricultural, suburban and urban land use areas to the coastal areas, with increasing delivery of nutrients and sediments to these systems. This increase is a major stress to coastal ecosystems, increasing turbidity and decreasing available light levels (Beck *et al.* 2007).

In tropical areas, sediments and nutrients (primarily phosphorous and nitrogen compounds from agricultural fertilizers and the burning of fossil fuels) in freshwater runoff are filtered first by coastal forests and then mangrove wetlands (Smith *et al.* 1999). Seagrass beds provide a final filtration. This system of filters provides a buffer zone for offshore reefs, and helps to create the oligotrophic conditions under which they thrive. Reefs then act as a buffer between the open ocean and the onshore communities (Linton and Warner 2003). In the Texas Coastal Bend area, there is no substantial offshore reef system for many miles, thus the filtering process serves as the final filter between the onshore communities and the open ocean.

Historically, the coastal system has been able to absorb large quantities of these nutrients and sediments. For instance, results extrapolated from a study by Short and Short (1984) showed nitrogen removal by seagrasses from the Indian River Lagoon in Florida to be approximately 3890 metric tons annually, 11% of the nutrient load of the Indian River. The system binds them up in plant biomass and the sediments that support them, thereby improving water quality with lower water column nutrient concentrations and phytoplankton biomass (McGlathery *et al.* 2007). Microalgae are able to bind up

these nutrients for periods measured in days, and macroalgae are able to tie them up for weeks, while seagrasses bind them on the scale of weeks to months (Valiela *et al.* 1992). After this temporary sequestration, these nutrients are often re-mineralized or transferred to microbial and other trophic systems and then excreted by grazers. These retention times are often on the scale of years rather than months, further slowing the transport of the nutrients to the sea (Duarte and Cebrian 1996).

In some areas, seagrass canopies are able to remove as much as 70% of the suspended particles present within the canopy in less than an hour. There are two processes involved: passive trapping occurs when the particles become attached to the leaf surfaces, and active trapping occurs when the particles are ingested by phagotrophic protozoans or filtered by suspension feeders in the seagrass community (Agawin and Duarte 2002). The removal of phytoplankton from the water column by the epifauna (hydrozoans, bryozoans, barnacles, and amphipods) found on seagrass leaves serves as an important sink for phytoplankton biomass and seston loading in shallow seagrass communities. Seagrass communities also trap and filter picophytoplankton, which may explain negative picophytoplankton biomass and population growth rates found in some seagrass meadows, even though the individual growth rates are high (Agawin and Duarte 2002).

Seagrass meadows provide another valuable ecosystem service by altering the hydrologic flows and sediment deposition in lagoons and estuaries (Fonseca and Fisher 1986). Different species tend to alter friction and flows differently and thus affect the deposition of sediments and nutrients. The different sizes, shapes and characteristics of the seagrasses affect the flow of water over, around and through the seagrass beds, which

in turn influences the sediment and particle types which are either deposited or eroded (Fonseca and Fisher 1986). These changes can affect not only the estuary and its inhabitants; they also influence the systems beyond, such as mangrove and reef systems.

Seagrass serves as a nursery habitat

A nursery habitat is defined as one in which a species recruits to the adult population at a greater rate than other areas, due to any combination of density, growth, survival and movement to adult habitats (Beck *et al.* 2001). The coastal ecosystem is recognized as one of the most productive ecosystems, supporting a diverse variety of macrofauna and invertebrates (Quammen and Onuf 1993, Beck *et al.* 2001). The structurally complex coastal ecosystems provide nursery habitat for diverse juvenile marine and estuarine fish species (Tolan *et al.* 1997), offering protection from predation, providing abundant food supplies, and encouraging high growth and survival rates (Stunz *et al.* 2002). Maximizing growth rates and minimizing time spent in vulnerable size classes can have positive effects on population demographics (Stunz *et al.* 2002). The relative values of coastal habitats are often determined by the density of nekton species. High values are determined by high densities, and indicate high productivity, habitat quality and preference (Rozas and Minello 1998). Seagrass meadows provide a habitat that will support high densities of juveniles for commercial and recreational fisheries (Quammen and Onuf 1993). However, the protection of these valuable habitats is not solely dependent on conserving the habitats; protecting the ecological processes that help support the increased growth and survival rates of species using them is also important (Burfeind and Stunz 2006).

Monitoring seagrass ecosystems

Ecosystem-based management is one of the most effective ways to conserve and protect valuable seagrass habitats (Chen *et al.* 2007, Barbier *et al.* 2008, Halpern *et al.* 2008). Recent studies have demonstrated that anthropogenic activities have had a major impact on all remaining coral reefs, seagrass beds and mangroves (Halpern *et al.* 2008). Monitoring these changes is one of the key themes of ecosystem-based management (Grumbine 1994). Many indicators of seagrass health have been identified and regular monitoring of those indicators is needed to respond quickly and efficiently to a variety of changes in the ecosystem (Beck *et al.* 2007, Chen *et al.* 2007). For example, estuarine water quality management plans should focus on understanding and mitigating inputs from storm water, river run-off, and dredging, as well as recreational and transportation activities (Chen *et al.* 2007). Mapping and monitoring aids in quantifying and understanding the spatial distribution of human impacts, helping in the evaluation of trade-offs between human use and ecosystem conservation (Halpern *et al.* 2008).

Monitoring results are also an indispensable aid to policy makers and resource managers (Coles 2004). Maps of seagrass distribution and change provide coastal resource managers with valuable information that can be used in the continuing assessment of estuarine health (Dekker *et al.* 2005). There are several methods of monitoring and mapping seagrass and other benthic habitats in coastal areas, and each has shown varying degrees of success. Seagrass monitoring programs must consider the localized mechanisms which propagate stress responses. It is critical to continue seagrass status and trends monitoring at the landscape level on a 2 to 3 year interval basis (Pulich *et al.* 1997).

Swimming transect surveys

Traditional surveys of seagrass beds in shallow waters involved swimming transects through the bed and estimating coverage along the transect line (Merkord 1978). Data collected typically includes species and the location along the transect line where species or coverage changes occur. Attempts to standardize the coverage estimates are sometimes facilitated with photographs. To shorten the time involved in this type of survey, submersible video equipment has been employed. Video techniques involve photographing the site along with some sort of scale indication, and then later estimating coverage in the laboratory (Duarte and Kirkman 2001, Yamamuro *et al.* 2002). This method can be used to develop very accurate habitat maps, but it is expensive, labor intensive, and best suited for particular sites rather than for landscape or regional-scale projects.

Remote sensing of benthic habitats

As pollution and habitat degradation escalates with coastal zone population increases, legislation is being introduced at national, regional and local levels, requiring, in part, more extensive monitoring. The demands of extensive monitoring of large areas pose difficulties for conventional monitoring techniques. Aerial remote sensing provides methods to assess and monitor large areas efficiently (Cracknell 1999), and terrestrial landscape monitoring using aerial remote sensing has proven highly effective. The coastal zone, however, may be the last frontier to benefit fully from modern aerial remote sensing techniques.

Image analysis of terrestrial habitats requires corrections for variability in atmospheric conditions; benthic habitats pose additional challenges in that many of the conditions that confound analysis are in a near-constant state of flux in terms of area and time. Tides can alter the chemical and biologic constituents on an hourly basis, stirring up sediments and changing the levels of salinity and particulates. Turbidity and production levels can change within hours, and wind velocities can increase almost instantaneously (Finkbeiner *et al.* 2001). Changes can occur in gradients over a study area, thus requiring collection of extensive field data from the entire study area, as close to the collection time as possible. In addition, sun angles change continuously, producing glare and glint rather than useable data streams if preflight planning doesn't preclude it. Table 1.1 shows recommended conditions for aerial acquisitions over benthic habitats, while Figure 1.3 shows the effects of haze and/or glint.

Table 1.1. Recommended minimum conditions for aerial imagery collection, adapted from Finkbeiner *et al.* (2001).

Recommended Conditions for Aerial Imagery Flights	
Turbidity	As low as possible. Avoid seasonal phytoplankton blooms, periods following heavy rains or persistent strong winds. Water clarity should be confirmed the day of the flight.
Phenology	It is best to consider times of overlapping phenology, when biomass is highest for the dominant species, if all other conditions are acceptable.
Sun Angle	Ideal sun angles are between 30 and 45 degrees for images at nadir
Tidal Stage	Generally, the lower the tide, the better. Rising tides may improve the clarity by bringing in clear marine water; however, this flow may also re-suspend sediments.
Wind and Surface Waves	Winds should be less than 7-10 mph. The direction, persistence, and fetch should all be considered. Whitecaps, wrack or debris lines, should not be visible from the air or in the imagery.
Clouds and Haze	Maximum recommended cloud cover is 5%. Haze should be minimal.

Figure 1.3. The effects of sun angle and haze. Left: 2004 NAIP RGB imagery, flown November 4-7 2004, Right: 2008 (Summer) NAIP Imagery flown May 2008. Note that the image on the right shows very little detail of the seagrasses found below the surface of the water, while the image on the left shows a greater amount of detail.

Multispectral imaging

Researchers in the 1970s began using satellite-borne multispectral scanners to map seagrass habitats (Ferwerda *et al.* 2007). Multispectral sensors collect data in a small number of very broad bands, generally in the red, blue, green or near-infrared parts of the spectrum (Figure 1.4). These satellite images proved to be of little use for ecosystem monitoring. The resolution of these images (the old LANDSAT – Multi-Spectral data had a resolution of 80 m, LANDSAT Thematic Mapper imagery has a resolution of 15 –30 m) does not permit enough detail for landscape scale mapping of estuarine and coastal habitats (Malthus and Mumby 2003), although others have used Landsat Thematic

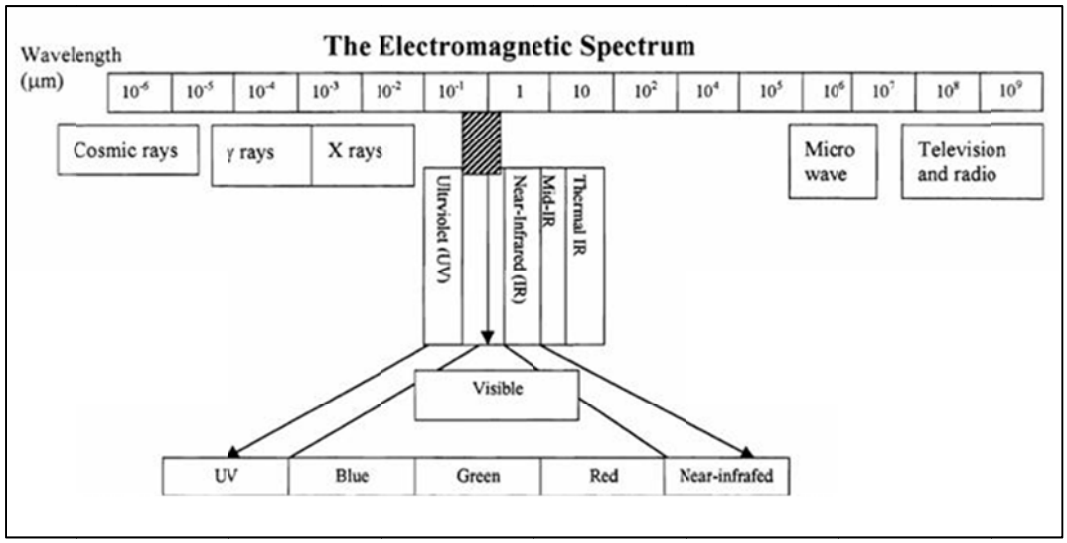

Figure 1.4. The portion of the electromagnetic spectrum most often used for digital imagery. In addition to the visible range, it includes both the ultraviolet and the infrared spectrums. Adapted from Shull (2000).

Mapper (TM) and Landsat Multispectral Scanner (MSS) imagery to detect two species of seagrass, *Zostera marina* and *Ruppia maritima*, and Armstrong used the visible bands of Landsat TM to form an empirical estimate of seagrass biomass in the Bahamas (Ackleson and Klemas 1987, Armstrong 1993). Temporal resolution, the time between subsequent

images, is also a concern (Cracknell 1999). Newer, higher resolution satellite imagery is available, but it is expensive for mapping large areas (Kelly *et al.* 2001). The remote sensing community has always been challenged to find affordable, high resolution data sets. IKONOS, QuickBird, RapidEye, and SPOT are costly and can be disadvantageous for regional mapping due to their small footprint and often limited spectral resolution (Watts *et al.* 2011).

In the 1990s, benthic habitat and ecosystem researchers used true color analog aerial photography, which was then digitized, rectified, and manually interpreted to obtain estimates of coverage of seagrass and other benthic habitat types (Malthus and Mumby 2003). The resolution of aerial photography is quite good, often in the range of 0.25 m. The data derived from this imagery is often used as a historic baseline for seagrass habitat loss studies (Ferwerda *et al.* 2007). However, because the imagery has to be digitized and then individually rectified, there are often problems with the spatial accuracy. The rectification process is labor intensive and photo interpretation is also subject to interpretation errors (Dekker *et al.* 2005).

Fortunately, there have been numerous recent improvements in aerial photography, digital photogrammetry and imagery, and automated/semi-automated interpretation software (Malthus and Mumby 2003). Commercial remote sensing companies such as ENVI (Environment for Visualizing Images), ERDAS (Earth Resource Data Analysis Systems, and ER Mapper (Earth Resource Mapper) have developed processes and algorithms that can incorporate not only the digital number value of a pixel in an image, but also those pixels that surround that individual pixel and other ancillary data, into processes that will produce vector polygon data sets that

segment or group like areas which are in close proximity, according to parameters selected by the user. Object oriented programming can then be used to classify the polygons according to user input values. The processes described are referred to as 'automated' processing; the computer is performing the calculations and using the algorithms that are developed without further human input. Very seldom is the output from such automated processing sufficient for habitat mapping purposes, thus, the user must use 'semi-automated' processing to supervise, manipulate and complete processing of the data. Semi-automated processing usually involves manual selection or digitizing to correct flaws in the data.

In the early twenty-first century, digital multispectral and hyperspectral sensors mounted on specialized aircraft considerably reduced the costs associated with digital imagery acquisition (Malthus and Mumby 2003). These aircraft employ real-time Global Positioning Systems (GPS) and in-flight tilt and yaw compensation to deliver an imagery product that eliminates almost all post-processing rectification, and has superior positional and radiometric accuracy. Often, calibration and positional data are recorded simultaneously with the image. Many imagery characteristics, such as color balance and contrast, can be adjusted while in flight. Various resolutions can be obtained, with higher acquisition costs directly related to higher resolution. While analog imagery provides a map-based view of several square kilometers in each frame, many digital sensors collect imagery in continuous rows or bands, thus eliminating edge-matching and other tedious procedures necessary with analog imagery. While the equipment costs associated with advanced digital imagery collection are great, considerable savings are realized when the post-processing tasks are eliminated or reduced.

Hyperspectral imaging

Hyperspectral scanning systems, also referred to as imaging spectrometers, can capture numerous very narrow (1.5 - 30 nm) bands within the spectral region of approximately 400-920 nm (Shull 2000). The high spatial and spectral resolution of these systems allows accurate mapping of terrestrial vegetation to the species level when the plants are spectrally distinct (Fyfe 2003). Hyperspectral imaging has also been used to study benthic habitats. Fyfe (2003) used hyperspectral imaging to differentiate Australian seagrass species, and developed a set of guidelines for selecting suitable bands for hyperspectral discrimination of seagrasses. Fyfe's guidelines state that the optimal wavelengths for discrimination of seagrass species in coastal areas lie between 500 - 630 nm. Further, researchers should select one or two regions of good separation between species in the absorption troughs and reflectance peaks of both the photosynthetic and the accessory pigments found in local seagrass species. One region should be selected where spectral separation is poor for use as a reference. Lastly, one or two regions of the spectrum should be selected where epiphytic fouling is an obvious feature, such as are found around 570, 595 and 620 nm. Figure 1.5 illustrates an effective selection of spectral regions for seagrasses found in Australia (Fyfe and Dekker 2001). Each of these bands form an additional 'layer' of data, which, when analyzed simultaneously, produce the information for a particular pixel location.

Other researchers, including Mumby *et al.* (1998), have used hyperspectral imaging to delineate coral reefs. Durand *et al.* (2000) developed algorithms to obtain bathymetry, bottom coverage, and calculate water clarity and reflectance using hyperspectral imagery (Mishra *et al.* 2007). Holden and LeDrew (2002), Maritorena

(1996), Albert and Mobley (2003) and others have developed models, commonly called 'water column corrections' (Mumby *et al.* 1998), to adjust for the optical properties of the water column, sea surface condition and other climatic and reflectance properties on hyperspectral analysis, altering Lyzenga's method for calculating a 'depth-invariant index'(Lyzenga 1981). The Lyzenga method is based on ratios of reflectance values between hyperspectral bands (Tassan 1996). The alterations above have relied on a variety of techniques, including using spectral libraries, measuring the spectral characteristics of benthic habitat *in situ* (Maritorena 1996, Holden and LeDrew 2002), or using the ratio of irradiance reflectance to the remote sensing reflectance (Albert and Mobley 2003). Figure 1.6 shows uncorrected spectral response curves for two common species of seagrass *(personal communication, Cho 2008).*

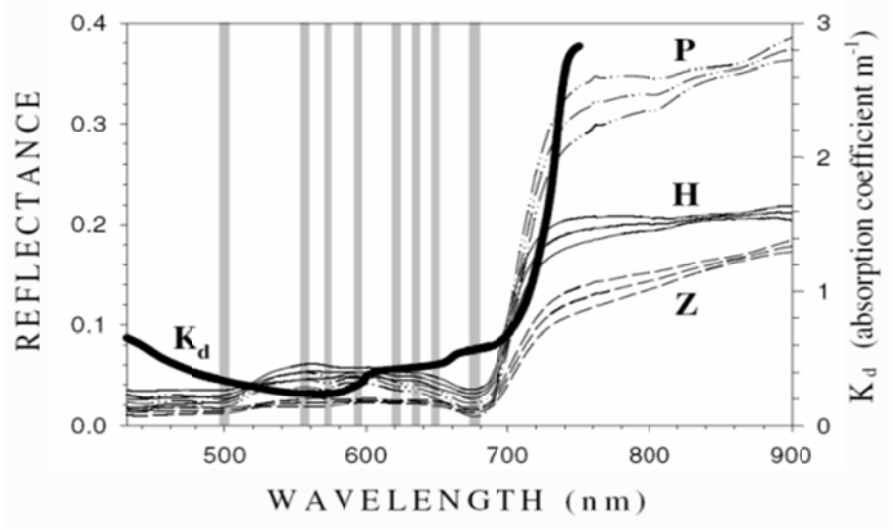

Figure 1.5. Relationship between spectral absorption (K_d) by an estuarine water column of 2.1 m and the mean + SD spectral reflectance of 3 seagrass species (*Posidonia australis*, *Halophila ovalis* and *Zostera capricorni*) with leaf epibionts. The grey bars indicate suggested locations of wavebands for the remote sensing of benthic vegetation (Fyfe and Dekker 2001). The thick solid line represents the spectral absorption.

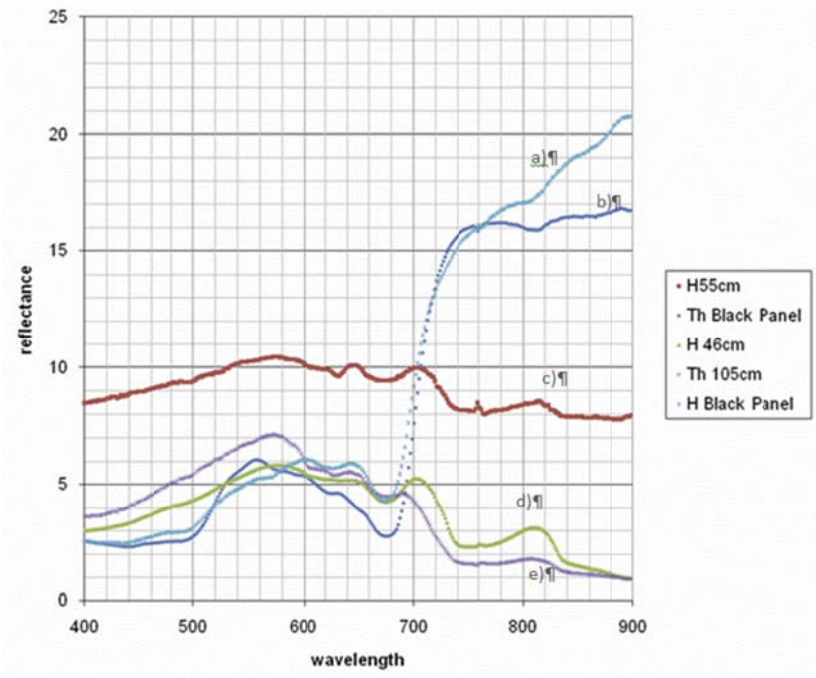

Figure 1.6. Spectral responses for a) *Halodule* against a black panel, b) *Thalassia* against a black panel, c) *Halodule* at 55 cm depth, d) *Halodule* at 46 cm, and e) *Thalassia* at 105 cm depth *(personal communications, Cho 2008)*. These spectral curves have not been corrected for depth. Data collected during Redfish Bay fieldwork, collected and processed by H.J. Cho, and combined and charted by the author.

Hyperspectral imaging opens up new dimensions in remote sensing of habitats; however, it is more labor intensive, costly and time-consuming than multi-spectral imaging. Sophisticated procedures requiring skills in mathematics, software, physics, hardware and biogeochemistry are often required to derive data from hyperspectral images.

Choices among monitoring techniques

There are many sources of digital imagery, and federal, state and local jurisdictions often archive historic imagery, which is accessible by the public (Finkbeiner *et al.* 2001). The data sets derived from these images can be used in Geographical Information Systems (GIS), making remote sensing a valuable tool for assessing and monitoring coastal habitats (Kelly *et al.* 2001).

Recent studies (Pulich 2007) have implied that the best approach to mapping benthic habitats at a landscape or regional scale is manual digitization of 1:9,600 scale (presumably 0.4 m resolution, as in Table 1.2 and Table 1.3, below) aerial photography. This result was determined by comparison of manual digitization of 1:9,600 scale images with the manual digitization of 1:24,000 (presumably 1 m resolution, as in Table 1.2) imagery (Pulich 2007). However, the manual digitization approach ignores recent advancements in automated digital processing. Studies as early as 1998 have shown that coastal areas can be mapped successfully using digital imagery and automated processing at pixel sizes of 5 m or less (Finkbeiner *et al.* 2001). Digital imagery also allows for more objective differentiation between objects that would appear similar in color to a photo interpreter, but have slight differences in digital signature (Shull 2000). Minute amounts of an object, such as sparse but continuous patches of seagrass, undetectable to the naked eye even at extremely small scales, may affect the signature within a pixel or group of pixels much larger than the object itself (Shull 2000).

Table 1.2. Conversion of photo scale to resolution, in meters or feet, for images scanned at 600 dots per inch (DPI) or pixels per inch (PPI) for common scales or resolutions. Adapted from Finkbeiner *et al.* (2001) and Pulich (2007).

Photo Scale 1: XXXX	**Pixel Size in m**	**Pixel Size in ft**
1:1,200	0.051	0.167
1:2,400	0.102	0.333
1:4,800	0.203	0.667
1:9,600	0.406	1.333
1:10,000	0.423	1.389
1:12,000	0.508	1.667
1:20,000	0.847	2.778
1:24,000	1.016	3.333
1:40,000	1.693	5.556
1:48,000	2.032	6.667
1:58,000	2.455	8.056

Table 1.3. Conversion of pixel size to photo scale. Adapted from Finkbeiner et al. (2001).

Pixel Size (m)	Scale
0.1	1: 2,362
0.25	1: 5,906
0.5	1:11,811
0.75	1:17,717
1.0	1:23,622
1.5	1:35,433
2.0	1:47,244
2.5	1:59,055

Resource managers are faced with choosing from a variety of monitoring options, and those choices are best made after considering the scale of the research being conducted. Patterns and processes in a local ecosystem can only be understood by examining an area in a variety of scales and resolutions and levels of detail (Boström *et al.* 2006). Recognizing this, a three-tiered approach has been suggested (Dunton *et al.* 2011), including a regional scale, incorporating a large geographic area such as an entire bay or bay system, a landscape scale, covering a smaller area mapped from higher resolution imagery (0.25 m - 0.5 m), and a more local or site-level scale, where field data would be collected and sampled for biomass, root-to-shoot ratio, blade width and length, shoot density, species composition, percent cover, water and sediment quality, light response indicators, and plant nutrient response indicators (Dunton *et al.* 2011).

PURPOSE, OBJECTIVES AND HYPOTHESES

The purpose of this research is to examine the use of hyperspectral imagery in characterizing the benthic habitats in coastal waters, and develop protocols for processing the imagery. The first approach will examine the utility of hyperspectral analysis, a relatively new technique, and its use to differentiate benthic habitats in a submerged area of seagrass beds in Redfish Bay. The second objective will be to improve the processes and protocols developed in the first objective, and the third objective will be to apply those improvements and measure their effect.

Objectives and hypotheses

Objective 1.

To develop and evaluate hyperspectral techniques for mapping seagrass species in a shallow, microtidal lagoon: Redfish Bay State Scientific Area, Texas. This research will develop a protocol for hyperspectral discrimination of species and benthic habitat, allowing future researchers to analyze the changes in status and trends of this coastal lagoon on a species level. This is important because changes in dominant species distribution has numerous effects on the coastal ecosystem, and serves as an indicator of system health.

Hypothesis 1.

Species of seagrasses can be differentiated in shallow water ecosystems using hyperspectral imagery.

Intended project results.

This project will demonstrate the effectiveness of hyperspectral imagery for mapping benthic habitats in shallow water ecosystems, and discrimination of seagrass species and presence or absence of seagrass coverage. The process will use band selection recommendations from recent literature and employ a previously untested depth correction algorithm found in contemporary literature.

Objective 2.

To compare spectral signatures of the two dominant species of seagrass in this area, and determine if it is possible to discriminate between the species at varying depths, and from three different positions: above the surface, just below the surface, and at canopy level.

Hypothesis 2.

Species of seagrasses are spectrally distinct *in situ*.

Intended project results.

This project will verify that species of seagrasses are spectrally distinct, and will investigate methods for determining the best spectral bands for separation. A depth correction will be applied, and the data will be normalized and a Multiplicative Scatter Correction applied to the corrected data.

Objective 3.

To apply knowledge gained in the previous two projects to evaluate and confirm that they improve the analysis accuracy of benthic habitats using hyperspectral imagery. Specific differences will be the use of band selection derived from *in situ* data collection, and creation and use of a bathymetric surface.

Hypothesis 3.

Species of seagrass can be discriminated using hyperspectral imagery, and analysis will be improved by using *in situ* data collection to establish which specific spectral bands will best facilitate that analysis. Inclusion of bathymetric data will further enhance the accuracy of the analysis.

Intended project results.

This project will confirm the selection of bands and the application of the depth correction algorithm with a bathymetric dataset will significantly increase accuracy of hyperspectral image analysis of benthic habitats.

STUDY AREA

The study area is the Redfish Bay area of the Mission-Aransas National Estuary Research Reserve in the Coastal Bend area of Texas (Figure 1.7). This area is typical of many of the dynamic 'grass flats' and inland bays formed by the barrier islands found along the Texas coast (Oppenheimer 1963). These estuarine habitats are subjected to changes in salinity, depth, and temperature (McMillan and Moseley 1967), and

occasionally ravished by tropical storms and hurricanes (Oppenheimer 1963). The climate for the area is classified as dry sub-humid (Kornicker 1964). The area of study is bordered on the northeast by the Lydia Ann Channel, on the south by the Aransas Pass Channel and Causeway, and on the west by the Gulf Intracoastal Water Way, and Corpus Christi Bayou on the east side. The more open areas to the west are bisected by a series of intermittent islands and submerged rocks, which once served as the bed of a railroad track (Kornicker 1964). Other navigational hazards found in the area include shallow oyster reefs and mud flats.

Figure 1.7. Location and general layout of Redfish Bay, Texas. The study area is bounded by Corpus Christi Bayou and Aransas Bay on the east, Aransas Channel on the south, the Gulf Intracoastal Waterway on the west.

DISSERTATION ORGANIZATION

This dissertation is organized into five chapters. Chapter I presents an introduction, the background and relevance, the hypothesis and purpose and objectives of the research, and a description of the study area. Chapters II, III, and IV, will describe the research. These chapters are presented as suitable for publishing, and follow the *Ecology* journal format. Chapter V is brief summary and conclusions drawn from the creation of this dissertation. References for the entire document will follow the fifth and final chapter. Chapters may be taken from this dissertation and submitted for publication, so each contains individual introductions and conclusions.

CHAPTER II: HYPERSPECTRAL DISCRIMINATION OF BENTHIC HABITAT TYPES

ABSTRACT

This study examines the use of hyperspectral imagery to map and classify benthic habitats found in Redfish Bay, located in the Coastal Bend area of Texas. The area is a shallow water estuary co-dominated by two species of seagrass: *Halodule wrightii* and *Thalassia testudinum*. After mosaicking the imagery and applying a depth correction algorithm in ENVI imaging software, the image is classified. An iterative approach is used, employing a combination of supervised and unsupervised classification techniques, and further classification in ESRI's ArcGIS. This iterative technique produces a comprehensive benthic habitat map with an overall thematic accuracy of 37.93%. The results from this study provide an areal estimation of the seagrass species found in Redfish Bay, as well as percent coverage by each species. The largest percentage of habitat (33%) is classified as mixed, while 26% is classified as bare, 19% is *Thalassia testudinum,* 12% is covered with *Halodule wrightii,* and 11% is covered by *Ruppia maritima*. The accuracy of these results is similar to those produced in similar studies at other locations.

INTRODUCTION

The seagrass beds of Redfish Bay, Texas have undergone intense research: Pulich *et al.* (1976) studied the trace metal cycles within the seagrass beds; Fry and Parker (1979) examined the animal diets and McMillian (1991) studied the longevity of the seed reserve, flowering and reproduction of seagrasses. Majors and Dunton (2002) studied the variations in light-harvesting techniques. Green and Finkbeiner (2008) conducted the

first-ever ‘simultaneous’ 3-sensor comparison for coastal mapping, by flying three different sensors over the bay in less than 4 hours. The DMC, UltraCam and ADS40 digital multispectral sensors were flown over the same areas, with near-identical flight and water conditions, and compared for radiometric accuracy, imaging and spectral characteristics, under similar conditions (Green and Finkbeiner 2008).

Redfish Bay seagrasses, primarily *Halodule wrightii* and *Thalassia testudinum* (Fry and Parker 1979), have been mapped extensively (Pulich and Onuf 2004, Pulich 2007, Green and Finkbeiner 2008), however these mapping efforts have, for the most part, been conducted with either (analog) photographic images or multispectral imagery. Hyperspectral imagery has been used to map submerged vegetation and benthic habitats successfully in many areas around the world (Artigas and Yang 2004, Artigas and Yang 2005, Green and Cole 2005, Artigas and Yang 2006, Ciraolo *et al.* 2006, Mishra 2006, Peneva *et al.* 2008). Likewise, Schalles (2012) and others have used hyperspectral imagery to map terrestrial components of these bay systems, such as mangrove canopies.

METHODS

Studies have indicated that the spectral signatures for different species of seagrass can be distinguished in laboratory settings (Ressom *et al.* 2003) and in the field (Fyfe and Dekker 2001). While multi-spectral images lack the spectral information (Louchard *et al.* 2003) necessary to differentiate between bottom types or seagrass species, hyperspectral imagery, which has many spectral bands, is able to capture these differences.

Study area

Redfish Bay is a shallow estuarine ecosystem located between Aransas Pass and Port Aransas in the Coastal Bend area of Texas, and a small (approximately 6,180 acres) but important part of the Mission-Aransas National Estuarine Research Reserve (MANERR) (Beyer *et al.* 2007). MANERR, established in 2007, covers an area of 75,150 acres, and contains a diverse ecosystem with abundant flora and fauna. This area is typical of many of the dynamic grass flats and inland tidal bays found landward of the barrier islands along the Texas coast. While the climate is classified as 'dry sub-humid' (Kornicker 1964), these highly productive estuarine habitats are subject to extremes ranging from droughts that can last decades, to ravaging tropical storms and hurricanes (Oppenheimer 1963). These shallow habitats often are subjected to dramatic shifts in salinity, depth, and temperature, as well as turbidity that can change the depth of the photic zone in a matter of minutes. Redfish Bay is bounded by manmade channels: the Lydia Ann Channel on the east, the Aransas Pass Channel to the south, Gulf Intracoastal Water Way to the west, and is crisscrossed by others. Other than these channels, the bay has an average depth of .75 m and a maximum depth of about 2 m. The study area (Figure 2.1) was reduced from the entire area north of the Aransas causeway to encompass only the area (3,200 hectares) from approximately Corpus Christi Bayou west to the Gulf Intracoastal Water Way, due to clouds and cloud shadows in the imagery. Shallow mud flats, submerged rocks and intermittently submerged oyster beds and islands, and the bed of an old railway add navigational hazards to this challenging location.

Figure 2.1. The Redfish Bay study area encompasses approximately 3,200 hectares.

Field collected data

Prior to fieldwork, a pattern of 6,945 hexagons covering the study area and measuring 100 m across was generated using 'Repeating Shapes for ArcGIS Version 1.5' (Jenness 2011). Hexagons that fell completely on land areas were eliminated. From

these, approximately 350 hexagons were randomly chosen. A target location was then randomly chosen inside of each chosen hexagon. These more specific target locations were considered desirable but not mandatory. When practical, the survey team would get as close to the specific location as possible.

Field work was completed in July, 2008. Although the fieldwork was meticulously planned to coincide with the image acquisition flight, that flight did not occur until October 2008. Two observers navigated to each preselected location with an onboard WAAS enabled GPS. At each location, species presence and approximate percent coverage were noted for a 1 m^2 area, and the precise location was recorded with a Real-Time Kinetic (RTK) -enabled GPS to within 1 m horizontal accuracy. No preconceived classes were used in the collection of this data; all data breaks were developed in the field as different combinations were encountered. Table 2.1 shows the combinations of seagrass species and benthic habitats found in Redfish Bay during this study. The collected data was later transcribed into an Excel 2003 spreadsheet, which was then imported into ArcGIS and converted to an ESRI (Environmental Systems Research Institute) point shapefile.

The points created from the data gathered in the field were later separated into two groups: those used to develop and train the model (training or learning points), and those used later in the process to assess the accuracy of the model.

Table 2.1. Matrix of Seagrass Mixes observed in Redfish Bay. Sediment and Algae were recorded sporadically, as background values.

Halodule	*Thalassia*	*Ruppia*	*Syringodium*	*Halophila*	Sediment	Algae
100	-	-	-	-	-	-
90	-	10	-	-	-	-
80	-	20	-	-	-	-
75	25	-	-	-	-	-
75	-	25	-	-	-	-
70	30	-	-	-	-	-
70	30	-	-	-	-	
50	50	-	-	-	-	-
50	-	50	-	-	-	-
50	-	-	50	-	-	-
40	30	30	-	-	-	-
40	20	40	-	-	-	-
40	-	60	-	-	-	-
25	25	50	-	-	-	-
20	80	-	-	-	-	-
10	90	-	-	-	-	-
10	80	10	-	-	-	-
10	40	50	-	-	-	-
10	40	-	50	-	-	-
10	20	70	-	-	-	-
10	10	-	-	-	80	-
10	-	90	-	-	-	-
-	100	-	-	-	-	-
-	75	25	-	-	-	-
-	50	50	-	-	-	-
-	50	-	50	-	-	-
-	50	-	-	50	-	-
-	40	-	-	-	30	30
-	30	30	-	-	-	40
-	30	-	-	-	30	40
-	20	-	-	-	-	80
-	10	90	-	-	-	-
-	10	-	-	-	90	-
-	-	100	-	-	-	-
-	-	-	100	-	-	-

Acquired imagery data

Hyperspectral imagery for the study area was acquired October 18th and 19th, 2008 using an Airborne Imaging Spectroradiometer for Applications (AISA) Eagle

hyperspectral sensor. The sensor was flown by the Center for Advanced Land Management Information Technologies (CALMIT), in cooperation with the Nebraska Airborne Remote Sensing Program (NARSP) as part of their CALMIT Hyperspectral Aerial Monitoring Program (CHAMP), aboard a specially modified Piper Saratoga aircraft. The AISA hyperspectral imaging system was developed by SPECIM, Spectral Imaging LTD., Finland, and covers a spectral range of 400 to 1000 nm, in a possible 272 bands. It collects a swath approximately 1000 m wide, at 1 m resolution, in a pushbroom fashion, from an approximate altitude of 1418 m. As the aircraft moves forward, the sensor collects "lines" or "frames" of data to build an image, each line 1024 pixels wide and one pixel tall (Green and Cole 2005). The AISA Eagle instrument incorporates a miniature, integrated 3-axial inertial navigation sensor with an integrated solid state gyroscope and real-time GPS. These onboard sensors monitor the aircraft position and attitude, so imagery and positional data are acquired and stored synchronously (Bertels et al. 2005). For added recording capacity, the hard-drives can be swapped in flight. The band settings and bandwidths are programmable on this sensor to as little as 2.3 nm. Table 2.2 shows specifications of the sensor.

Table 2.2. Capabilities of the AISA Eagle sensor used in this project, adapted from Bertels *et al.* (2005).

Characteristic	Value
Field of view (FOV)	39.7º
Instantaneous field of view (IFOV)	0.039 º
Spatial resolution	0.5 - 10 m
Spectral range	400 - 970 nm
Spectral channels	max. 244
Spectral sampling interval	2.3 nm
Spectral resolution (FWHM)	2.9 nm
Dynamic range	12 bits (4096)

Proper interpretation of hyperspectral imagery can require a considerable groundtruthing effort. Most airborne sensors collect hundreds of bands of data for each pixel, and visits to the site at the approximate time of the flight help to select those bands useful for discriminating vegetation species. It is also necessary to determine the depth correction coefficients for volumetric scatter and water absorption, as well as to verify that field conditions are acceptable.

Prior to delivery, the imagery was corrected for atmospheric distortions which are inherent in all aerial imagery. The FLAASH (Fast Line-of-Sight Atmospheric Analysis of Spectral Hypercubes) algorithm was used to remove atmospheric effects caused by molecular and particulate scattering and absorption. Spectral Sciences, Inc. developed this MODTRAN4-based correction code in collaboration with the Air Force Research Laboratory, with assistance from the Spectral Information Technical Applications Center. The FLAASH algorithm takes the following form:

$$L^* = A\rho/(1-\rho_e S) + B\rho_e/(1-\rho_e S) + L^*_a \qquad (2.1)$$

where ρ represents the pixel surface reflectance, ρ_e is a surface reflectance averaged over the pixel and a surrounding region, *S* is the isotropic incident radiation of the atmosphere, L^*_a is the atmospherically backscattered radiance, and *A* and *B* are coefficients that depend on non-surface atmospheric and geometric conditions (Matthew *et al.* 2002). The FLAASH process transforms the data from spectral radiance to spectral reflectance, and was applied in ENVI.

The atmospherically-corrected georectified imagery was received from CALMIT on a portable hard drive. This project was flown with the following parameters: 63 bands, each approximately 9 – 12 nm wide, and at a height to obtain a 1 m pixel, which is approximately 1538.6 m, as shown in Table 2.3. The stated horizontal accuracy was 10 m, and the flight parameters and procedures met National Map Accuracy Standards (NMAS) at the 1:12,000 scale (personal communications, Perk, CHAMP program at UNL, 2012), which states that not more than 10% of the points tested shall be in error by more than 1/30 of an inch on the printed map for maps on publication scales larger than 1:20,000, using well-defined points.

Table 2.3. The flight parameters used for this project (personal communications with Rick Perk, pilot at CHAMP program at UNL, 2012).

	Value
Acquisition Date:	19 October 2008
Acquisition Time:	18:59-20:05 UTC
Flight Direction:	NE/SW
Ground Speed:	120 Knots
Data Rate:	61.7 fps
Integration Time:	14.0 ms
Target Elevation:	0 m MSL
Altitude:	1538.6 m AGL

Thirteen individual images were delivered from CHAMP via CALMIT by FEDEX for the original study area, each approximately 1000 m wide and ranging from 8 to 14 km in length. Of these, 4 images were discarded, as they contained too many clouds and cloud shadows to be usable. From the remaining 9 images with 63 bands each, 5 bands were selected for analysis. After numerous unsuccessful attempts to isolate bands suitable for species separation using Principal Component Analysis and Artificial Neural Networks (ANN), these wavelengths were selected based on personal communications with Dr. Hyun Jung Cho: 553.89 nm, 694.6 nm, 722.88 nm, 741.74 nm, and 808.84 nm.

Image processing

Images were mosiacked in ENVI version 4.8. After mosaicking, a water depth correction algorithm was applied to each of the 5 selected bands, using an assumed mean depth of 65 cm, and no turbidity. This algorithm was applied to each masked pixel in each of the five bands:

$$(R_w/10 - R_w) / (1- A_w/200)^2 \quad (2.2)$$

where R_w is equal to the percent surface and volumetric reflectance for a particular wavelength, and A_W is the absorption by the water column in both upward and downward directions (Cho and Lu 2010). The output from this band math function is a new set of 5-band imagery, adjusted for an average water depth of 65 cm. and no turbidity. Values for A_w and R_w were derived empirically by Cho and Lu (2010), using laboratory water tank spectral studies. Future applications by Cho will allow depth rasters (bathymetry) and turbidity measurements to be included as part of the algorithm input, which will greatly increase the value of this function.

This new corrected 5-band image is then opened in ENVI EX 4.8, where the classification workflow is initiated. The image is clustered into groups of similar pixels which are then categorized into classes, each having similar pixel values. Using a larger number of classes causes the clusters within a category to have less variation (more similarity to each other), while a smaller number would include more variety within a category. ENVI uses the Iterative Self-Organizing Data Analysis Technique (ISODATA) classification algorithm, which starts by calculating the pixel means distributed evenly throughout the data space, and then iteratively clustering the remaining pixels using a Minimum Distance technique. During each iteration of the clustering process mean values are recalculated and pixels are re-clustered with the new means. Clusters are split if the standard deviations are equal or greater than the user-defined threshold, and merged if the distance between them is less than the user-defined threshold (Ball and Hall 1965). The iterations continue until the percent of change meets or exceeds the threshold setting or until the maximum number of iterations is reached. After some experimentation, the defaults (2% change threshold and 10 iterations) were accepted. The default number of categories is five; however, that did not separate the species well, and all categories contained multiple species and species combinations during the ArcGIS processing. Experimentation with this parameter indicated starting with a larger number of categories would increase separation and overall efficiency of the process. Starting with a larger number of categories (25) and decreasing the number of categories at subsequent iterations provided the desired separation and processing efficiency.

The resulting categorized clusters were then aggregated into groups with a minimum of 9 pixels. Until now, the data generated within the process has been in a

virtual raster format, which means the attribute values for the categories are inaccessible but presumably are integer values. These refined categorized clusters were then converted to an ESRI polygon shapefile and exported. The processing in ENVI EX (see the left section of Figure 2.2) produced 143,991 polygons covering 27,064,111 m^2, with a mean area of 487.9 m^2; the largest area was 456,138, and the smallest was 10 m^2.

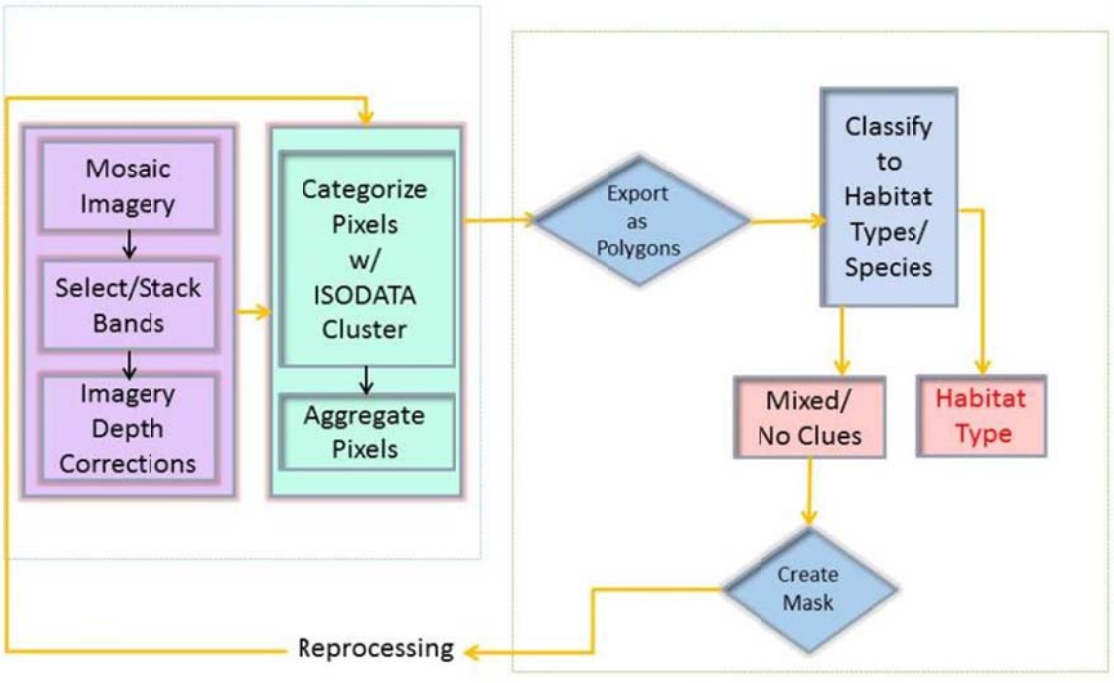

Figure 2.2. The processing flow within the ENVI EX and the ArcGIS software.

Vector processing

The 143,991 polygons generated in ENVI EX are categorized as 'Class 1', 'Class 2', and so on through 'Class 25'. These categories represent groups of clusters with similar pixel values; in order to define what the species makeup within these categories might be, the categories are classified in ESRI's ArcGIS 10.0. The categorized polygons exported from ENVI were imported into ESRI's ArcGIS 10.0 as a shapefile. The data points created from the fieldwork site visits were added to the ArcGIS map document.

These data points were divided evenly into two groups using a random number generator which added an attribute field to the data table, and randomly assigned an even number of '1's or '0's to the field. Each of these groups ('1's or '0's) was exported into a new ESRI point shapefile; 'ones' were named 'Learning Points', and the 'zeroes' 'Accuracy Assessment Points'. The learning points were used to develop and classify the polygons generated in ENVI within the ArcGIS environment. The accuracy assessment points were used within the iteration process to aid in the evaluation of interim processes, as well as to ascertain the accuracy of the final output.

The field 'MainSpecie'

Within the ArcGIS polygon shapefile, all polygons of a class ('Class 1' in Table 2.4) were selected, and then all the learning points that fell within that class were selected. All of the polygons that contained those learning points were then selected. Figure 2.3 displays the Python Model Builder diagram used to automate the selection-reselection process. Each polygon that contained a learning point was labeled with the learning point habitat type and count, such as '1 B100, 2 H100, 1 H50T50', representing 1 'Bare' point, 2 points of 100% *Halodule*, and 1 point that was 50% *Halodule* and 50% *Thalassia* (see the line with the Class_Name 'Class 2' in Table 2.4 below). Once each of the learning points that fell within a 'Class' were noted, all undesignated polygons in the class were assigned a derived attribute with a concatenated listing of the types of learning points(s) that fell within the class. An asterisk was used to denote this derived classification (see the third 'Class 1' in Table 2.4 below).

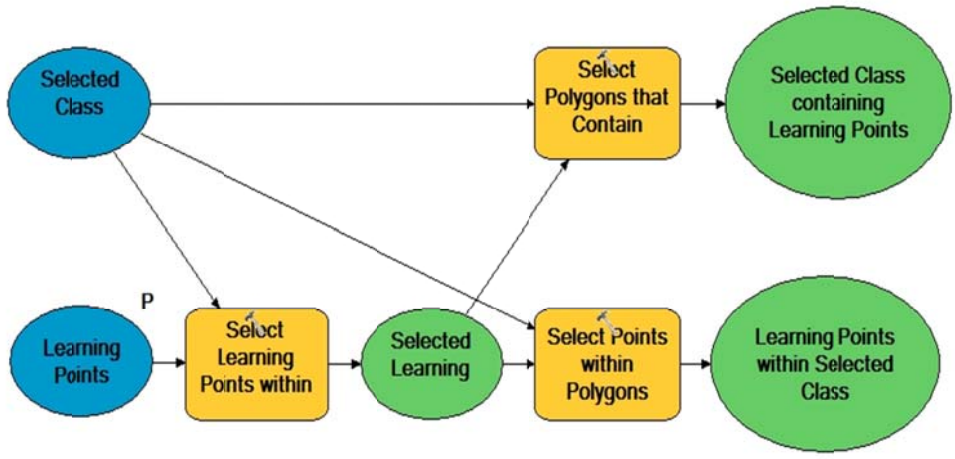

Figure 2.3. The ArcPython Model Builder diagram for the selection process, showing the selection of learning points that lay within the selected polygon class, and then the selection of the polygons containing those learning points.

It is important to remember that each 'Class' (fieldname 'Class_Name') is made up of polygons corresponding to segments with similar pixel values within the five selected bands. The 'MainSpecie' field notes which types of 'learning points' were found within each class, and each polygon within that class that does not contain a learning point is then designated a derived 'MainSpecie' attribute, based on its similarity to those in the same class that do contain a learning point. These derived attributes are denoted with asterisks (*) preceding the learning point designations.

Table 2.4. Portion of an attribute table with classification data for Redfish Bay. Each row represents an individual polygon. Asterisks denote a derived classification.

CLASS_NAME	**AREA**	**MainSpecie**	**grassType**
Class 1	47	1 H100	*Halodule*
Class 1	150,020	1 H75T25	MixedMono
Class 1	4,687	* 1 H100, 1 H75T25	Mixed
…	…	…	…
Class 2	12	* 1 B100, 2 H100, 1 H50T50	Mixed
…	…	…	

The field 'grassType'

As shown in Table 2.4 above, a field named 'grassType' was added to the database. This field would be the final designation of habitat type, based on the 'MainSpecie' types found within each class of polygons. If a polygon contained a learning point, the 'grassType' for that polygon would be the same as the decoded 'MainSpecie' for that polygon (see the 'grassType' field for the first tuple in Table 2.4). If a single polygon contained more than one type of learning point, it received the 'Mixed' attribute. Table 2.6 below contains a description of each 'grassType' attribute value.

If an entire class contained only one species (i.e. *Halodule*), the field 'grassType' for the entire class was filled with the species name as an attribute value, i.e. '*Halodule*' or '*Ruppia'*. The majority of first-iteration classes contained more than one 'MainSpecie' designation, and therefore were classified as 'Mixed' polygons. A 'Mixed' classification could contain any number of permutations of habitats: one learning point of 100% *Halodule*, in the same class as a 'Bare' point, and perhaps two or three learning points that had a combination of *Thalassia* and *Ruppia* or *Syringodium*. When a class of polygons contained learning points of more than one species or species mix, it was classified as 'Mixed' under the field name 'grassType'.

When a point had more than one species or type of habitat within the observed 1 m area in the field, it was designated as a 'MixedMono' point. An example of a 'MixedMono' point would be one where both *Thalassia* and *Halodule* were found in equal proportions. This point would be designated 'H50T50' in the 'MainSpecie' field

for the point file. That value would then be assigned to the 'MainSpecie' field in the polygon database for the polygon containing that point. In the 'grassType' field, it would be designated a 'MixedMono' polygon. This allows a class that has one polygon that is 50% *Halodule* and 50% *Thalassia* to be grouped in the same 'grassType' as one that was 60% *Halodule* and 40% *Thalassia*, but not with one that is 100% *Halodule* or with one that was 100% *Thalassia*.

If a polygon class contained only unclassified polygons, the field 'grassType' was designated an 'Unclassified' class. If a class contained no learning points, it was designated a 'No Clues' class. The polygons designated 'Unclassified', 'No Clues' or 'Mixed' were used to create an inclusion mask for the next iteration of image processing in ENVI.

This process of selecting and assigning attribute values was continued until all 25 classes were designated either as Bare, Bare/*Halodule* Mix, Bare/*Thalassia* Mix, *Halodule*, Mixed, MixedMono, No Clues, *Ruppia*, *Syringodium*, or *Thalassia*. The designation 'No Clues' was used for Classes 13 and 22, because no learning points fell within any of their polygons. The number of polygons and the corresponding area in m^2 is shown in Table 2.5. Figure 2.4 shows the results from this iteration of processing.

Table 2.5. Summary of the ArcGIS vector processing output for the first iteration, showing the number and area of polygons in each classification.

Classification	Number of Polygons	Total Area in Class ($m^{2)}$
Bare	1,551	2,773,599
Bare/*Halodule* Mix	2,245	587,547
Bare/*Thalassia* Mix	8,856	1,041,989
Halodule	1,821	1,625,965
Mixed	122,001	17,331,652
MixedMono	3,974	2,227,158
No Clues	2,701	796,576
Ruppia	823	198,987
Syringodium	1	199
Thalassia	18	480,439
TOTALS	143,991	27,064,111

Table 2.6. Description of 'grassType' attributes.

Classification	Description:
Bare:	Devoid of any detectable submerged rooted vascular vegetation. The polygons classified as Bare contained only Learning Points that were classified as Bare. This was a final designation, as these polygons would not be included in the mask for the next iteration.
Bare/*Halodule* Mix:	This class of polygons contains *Halodule* Learning Points and at least 1 Bare learning point. (* 8 B100, 2 H100). This was a final designation, as these polygons would not be included in the mask for the next iteration. Final designation.
Bare/*Thalassia* Mix:	This class of polygons contains *Thalassia* Learning Points and at least one Bare learning Point. The class as a whole contains both *Thalassia* and Bare learning points, as well as learning points that were a combination of Bare and *Thalassia* (B50T50, B10T90). Final designation.
Mixed:	This class of polygons contains at least two different learning point classes. They may be mono-specific (1 H100, 1 T100) or they may be any number or combination of mono-specific, MixedMono, and Bare (* 4 H100, 1 T80H20, 2 T100, 1 B90T10, 1 B70T30). Polygons classified as 'Mixed' were used to generate the mask for the next iteration.
MixedMono:	This class of polygons contains only learning points that contained more than one species. (1 T80H20) would indicate that the class contained one learning point that was 80% covered with *Thalassia*, and 20% covered with *Halodule*. There may be several classes (MainSpecie) that have the 'grassType' 'MixedMono'. They would all be aggregated into one 'grassType' class. Final designation.
Halodule:	This class of polygons contains only learning points that were classified as *Halodule.* Final designation.
Thalassia:	This class of polygons contains only learning points that were classified as *Ruppia*. Final designation.
Ruppia:	This class of polygons contains only learning points that were classified as *Thalassia*. Final designation.
Syringodium:	This class of polygons contains only learning points that were classified as *Syringodium*. Final designation.
No Clues	This class of polygons contained no learning points, hence, gave no clue as to what 'grassType' it should be assigned to. Polygons classified as 'No Clues' were included in the mask for the next iteration. Intermediate designation.
Unclassified	Polygons classified as 'Unclassified' were used to generate the mask for the next iteration. These would be polygons that for some reason were not classified during the previous iteration. Intermediate designation.

The learning points used in the first iteration were buffered 3 m, and the buffers visually re-evaluated over a true-color image and any point buffer that was spatially ambiguous, for example a learning point buffer designated as being bare, but that appeared to be over a grassy area or very close to a grassy area, was eliminated. If the majority of the buffered area fell into a differently designated area, it was eliminated. The remaining buffers were merged with the 'Mixed' and 'No Clues' classes to form a new mask containing the polygon buffers around the learning points as well as the areas previously classified as 'Mixed' or 'No Clues'. The buffered areas allowed the re-inclusion of the previously used learning points in the ENVI classification workflow.

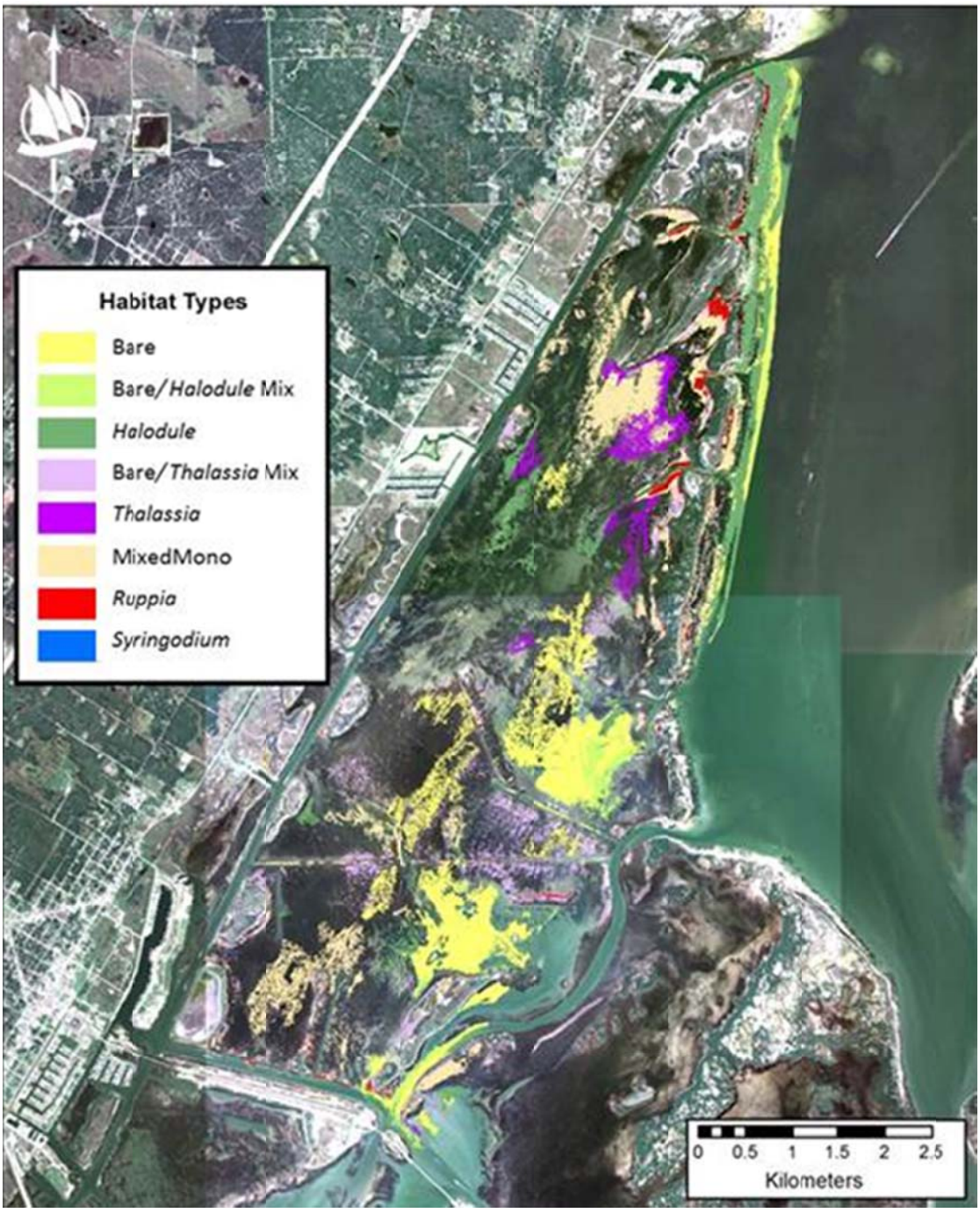

Figure 2.4. Classification of Redfish Bay benthic habitats after the first iteration with the 'Mixed' and 'No Clues' classes removed.

The second iteration

The original, corrected 5-band image and the newly created mask were then reprocessed in ENVI EX 4.8, producing ten classes of similar pixel values. By using only ten classes, it was more likely that pixels representing the same species would be classed together; the range of digital number values within each group would be larger within each individual group. The only areas which were being categorized were those that were previously classified as 'Mixed' or 'No Clues' and the areas around learning points that had been merged into the mask. The resulting categories were again aggregated into a minimum of 9 contiguous pixels, which were then exported as a shapefile. This shapefile was then opened in ArcGIS 10.0, and reclassified using the same process described for the previous iteration, based on the learning points, as shown in Figure 2.5. Table 2.7 shows the number and area of each classification of polygons.

Table 2.7. Classification results from the second iteration including the number of polygons and total areas found in each classification.

Classification	Number of Polygons	Total Area in Class (m^2)
Bare	21	363,346
Halodule	13	233,740
Mixed	94,133	14,893,124
MixedMono	17	190,640
No Clues	4,854	1,277,626
Ruppia	3	81
Syringodium	1	37,810
Thalassia	12	1,081,866
TOTALS	99,054	18,078,233

The retained classes from the first and second iterations were then merged. As in the first iteration, the ‘Mixed’ and ‘No Clues’ classifications were then merged with the learning point buffers (created earlier) and used to create the mask for the next iteration. Note that there were no ‘Unclassified’ classes during this iteration.

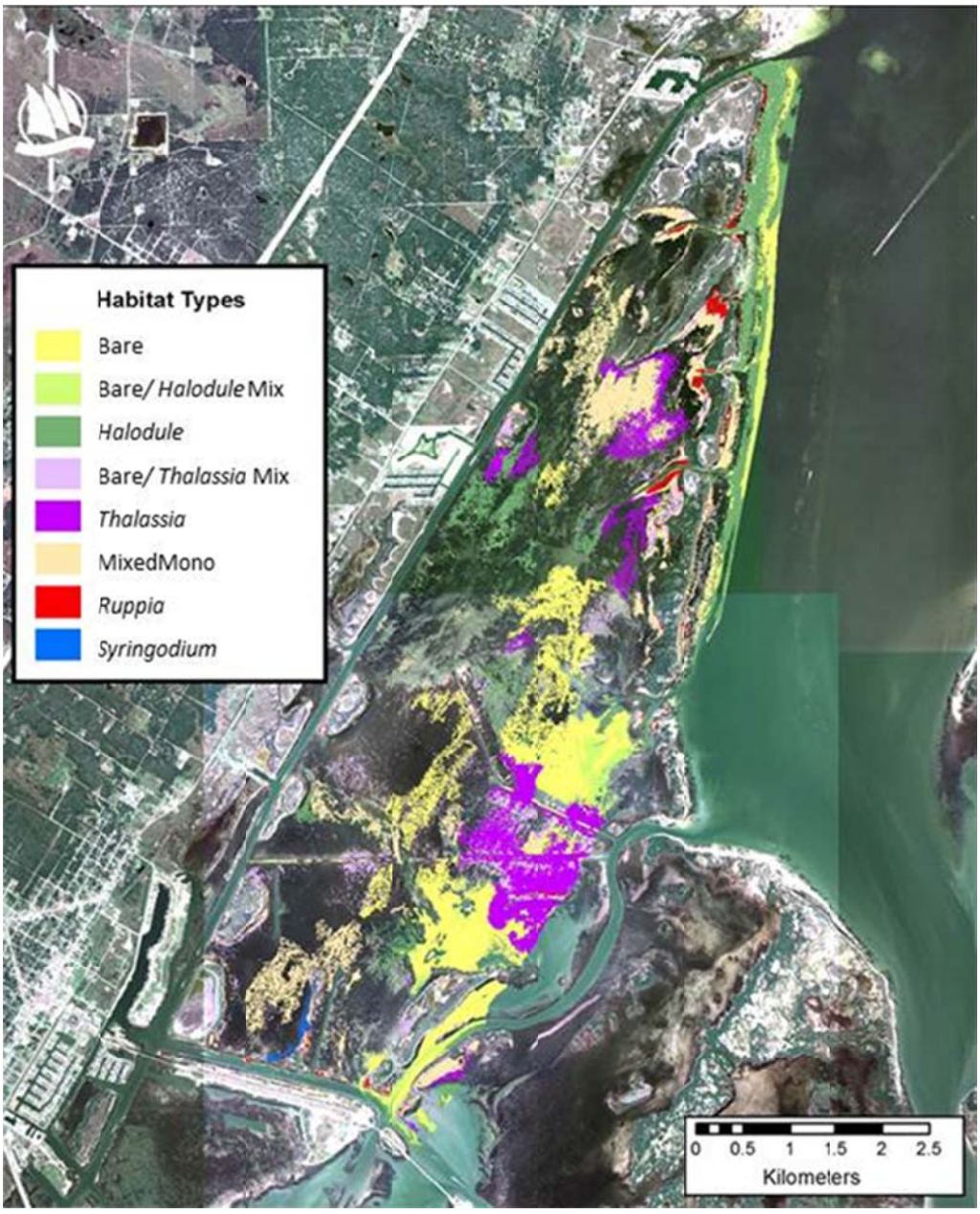

Figure 2.5. Classifications after the second iteration of processing, including results from both iterations, but omitting the ‘Mixed’ and ‘No Clues’ classifications.

The third iteration

For the third iteration, only 5 classes were created in ENVI EX. By decreasing the number of classes, the amount of variation within a class increases. After the image processing, the output shapefile was opened in ArcGIS. The same classification procedure was followed in ArcGIS as in the first two iterations, and all the monospecific polygons were retained and merged with previous outputs. The 'Mixed' and 'No Clues' polygons were used to create a mask for the fourth and final categorization iteration in ENVI. Table 2.8 shows the output from the third iteration. No map is shown because the difference between the second and third iterations is barely distinguishable at this scale.

Table 2.8. Classification results from the third iteration, including the number of polygons and area in each classification.

Classification	Number of Polygons	Total Area in Class (m^2)
Bare	13	384
Bare/*Thalassia* Mix	16,487	2,434,175
Halodule	14	4,534
Mixed	48,459	12,453,024
MixedMono	12	606
No Clues	1,372	403,536
Ruppia	1	801,940
Thalassia	10	66,620
TOTALS	66,368	16,164,819

The fourth iteration

For the fourth iteration, a 'supervised' classification was used. This classification method was chosen because the unsupervised method was not producing a substantial number of changes in classifications. The supervised method of classification puts each output segment or polygon into one of the user-specified classes based on user-defined training data. The polygon training set was developed by creating a 3 m buffer of a

selected subset of the learning points. Each pixel is classified based on the Minimum Distance Classification (MDC) function. The MDC uses the mean vectors of each training member, and calculates the Euclidean distance from the vector of each unknown pixel to the mean vector for each class. The like-classified pixels were then aggregated to a minimum grouping of 9 pixels, which were the exported as an ESRI polygon shapefile. The output shapefile was again opened in ArcGIS, and merged with the output from previous iterations. Figure 2.6 shows the final classification of seagrasses in the study area. Table 2.9 shows the final number of polygons within each class, as well as the areas in each classification, and the mean areas within each classification.

Table 2.9. Final number of polygons and sums of the area of each classification, as well as the mean area of polygons within each class.

Classification	Number of Polygons	Total Area in Class	Mean Area/Polygon (m^2)
Thalassia	22,038	4,976,130	225.80
Mixed	19,108	4,362,722	228.32
MixedMono	19,511	3,701,172	189.70
Halodule	13,968	3,608,193	258.32
Ruppia	12,656	3,585,130	283.28
Bare	2,954	3,537,991	1197.69
Bare/*Thalassia* Mix	25,343	3,476,164	137.16
Bare/*Halodule* Mix	2,245	587,547	261.71
Syringodium	2	38,009	19,004.50
TOTALS	117,825	27,873,058	2695.09

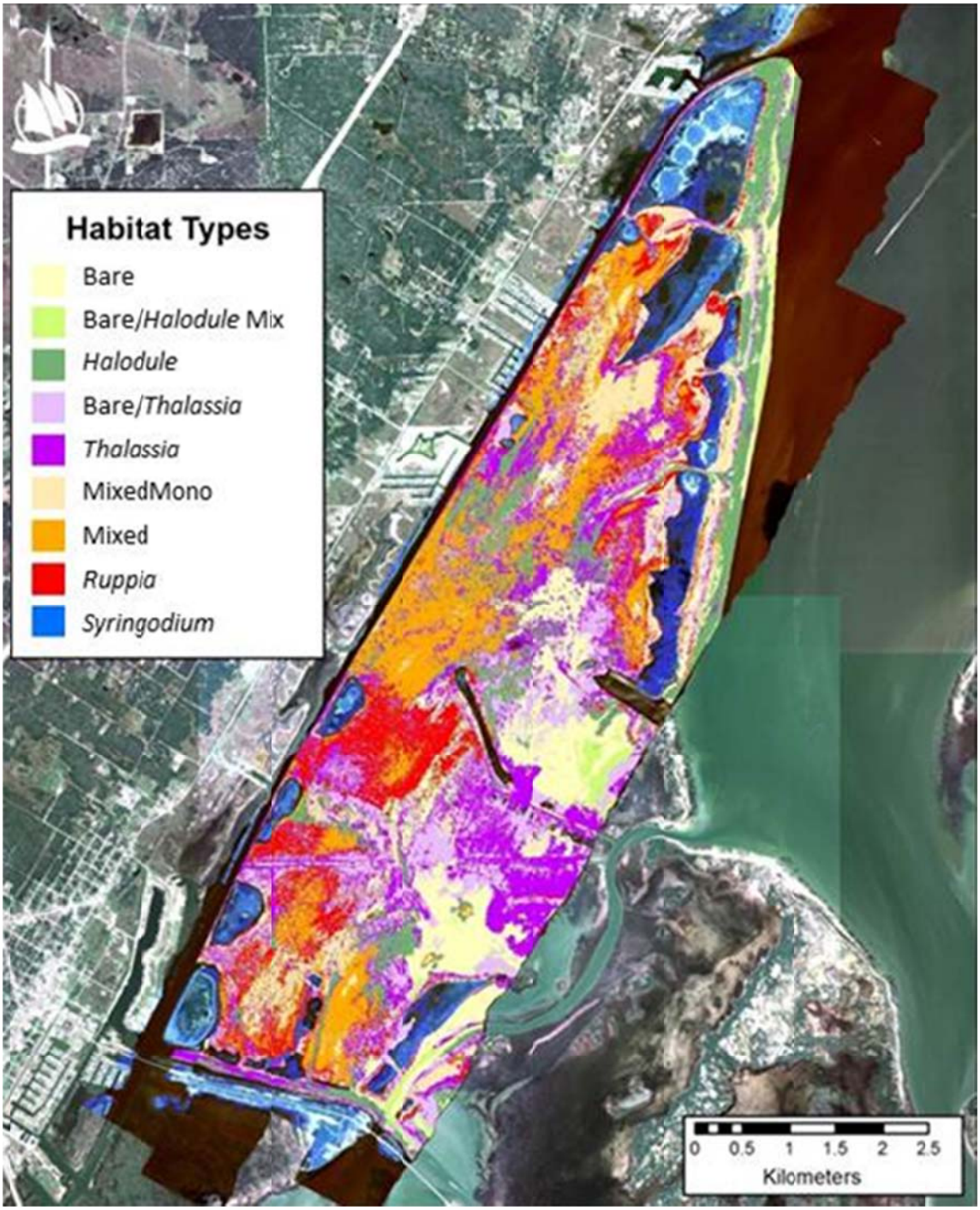

Figure 2.6. Final output from the classification of the benthic habitats in Redfish Bay, Texas.

RESULTS

The results from this study indicate that *Thalassia* covers the most area and has the greatest number of polygons, followed by Mixed, MixedMono, *Halodule*, *Ruppia*, Bare and *Syringodium*. However, if the 'Mixed' and 'MixedMono' classes are combined, the 'Mixed Class' would be the largest in both respects; likewise, if the 'Bare/*Thalassia*' and 'Bare/*Halodule*' classes are combined with the 'Bare' class, the 'Bare' class would be the second-largest class, and contain the second-largest number of polygons. Table 2.10 show the number of polygons for non-aggregated classes and those aggregated as described above, while Figure 2.7 shows the percentage of coverage in a pie chart for ease of visualization.

Table 2.10. Final number of polygons and the area of each class when the classes are combined as described in the text. The classes were aggregated thusly for the accuracy assessment.

Classification	Number of Polygons	Total Area (m^2) in Class	Mean Area/Polygon (m^2)
Mixed - MixedMono	38,619	8,063,894	208.81
Bare - Bare Mixed	30,542	7,601,702	248.89
Thalassia	22,038	4,976,130	225.80
Halodule	13,968	3,608,193	258.32
Ruppia	12,656	3,585,130	283.28
Syringodium	2	38,009	19,004.50
TOTALS	117,825	27,873,058	

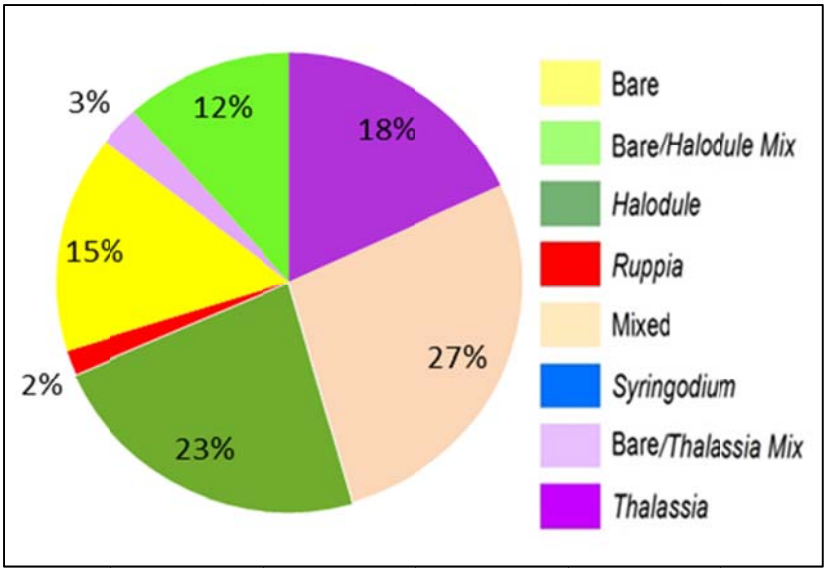

Figure 2.7. Percentage of coverage of the study area by each habitat class.

This dataset can be used to determine the Presence/Absence of seagrasses if the classes are aggregated to 'Bare' and 'Grass'. Doing so shows that there are 3,537,991 m^2 of bare areas, as before, and 24,335,067 m^2 of areas covered with grass; these numbers do not indicate, however, the density of grasses. Table 2.11 shows the results of that aggregation.

Table 2.11. Number of polygons, total area and mean area per polygon for bare and aggregated grass-covered areas.

Classification	Number of Polygons	Total Area in Class	Mean Area/Polygon (m^2)
Bare	2,954	3,537,991	1,197.69
Grass	114,871	24,335,067	211.85
TOTALS	117,825	27,873,058	

Accuracy assessment

To assess the accuracy of the output dataset, the points that had previously been reserved for accuracy assessment were intersected with the classified polygons from the final iteration. Each point was visually inspected, and an indication was inserted within

the database of whether or not the point was in agreement with the classification of the polygon that it fell within. By visually inspecting each accuracy point location, the observer can assure that there were no duplicate points, and note such phenomenon as the proximity of the accuracy point to a change in classification. If a point was in doubt, it was confirmed by comparison with the field notes. If the point was not in agreement with the polygon classification, the correct classification of the polygon was noted.

User's accuracy

A measure of commission error is obtained by dividing the total number of correctly identified areas by the total number of areas that were classified as being in that category (Strahler et al. 2006). This is known as the 'User's Accuracy' and indicates the reliability or the probability that an area on the output map actually represents what would be found at that site (Story and Congalton 1986). The results of this analysis indicate a 69.57% probability that an area mapped as 'Bare' would actually be found to be bare on the ground (or in this case, at the site). An area marked as *Halodule* or *Thalassia* has roughly a 40% probability of being correctly identified, while an area shown on the map to be 'Mixed' has a 22.58% chance of actually being mixed seagrasses and for areas marked as *Ruppia*, there is no chance of there actually being *Ruppia* at the site.

Table 2.12 shows the confusion matrix from the accuracy assessment.

Producer's accuracy

'Producer's Accuracy' is defined as a measure of the accuracy of a particular classification scheme, and shows the percentage of a particular class that can be correctly classified, and is a measure of *omission* error (Congalton 1991). Producer's accuracy is calculated by dividing the total number of correctly identified areas by the total number in the reference data (Strahler *et al.* 2006). The accuracy analysis indicates that 66.67% of the bare areas are correctly classified, 29.03% of the areas covered with *Halodule* are correctly classified, 46.15% of the areas covered with *Thalassia* are correctly classified, 0% of the areas containing *Ruppia* are correctly classified, and 23.33% of areas containing mixed species are correctly classified.

Table 2.12. Confusion matrix and accuracy assessment for the final output.

	Bare	*Halodule*	*Thalassia*	*Ruppia*	Mixed Mono/ Mixed
Bare	**16**	5	3	0	0
Halodule	2	**9**	5	3	12
Thalassia	1	3	**12**	2	8
Ruppia	0	0	1	**0**	4
MixedMono/Mixed	4	6	9	4	**7**

Producer's Accuracy		User's Accuracy	
Bare	66.67%	Bare	69.57%
Halodule	29.03%	*Halodule*	39.13%
Thalassia	46.15%	*Thalassia*	40.00%
Ruppia	0.00%	*Ruppia*	0.00%
MixedMono/Mixed	23.33%	MixedMono/Mixed	22.58%

Overall Accuracy	37.93%
Cohen's Kappa	0.2988

Overall accuracy

The overall accuracy of the map is obtained by dividing the sum of correct classifications by the sum of all the classifications, *n*. In this case, there were 116 classifications in the accuracy assessment, and of those, 44 were correctly classified giving us an overall accuracy of 37.93%.

Presence/Absence and accuracy assessments

"A pessimist sees the difficulty in every opportunity; an optimist sees the opportunity in every difficulty." ~ Sir Winston Churchill

As often happens in research, additional information may be gleaned from data, extending its value. This research can be used for quantifying the presence or absence of seagrasses in the study area. To do this, we aggregate the 'Grass' classes (*Halodule, Thalassia, Ruppia*, Mixed and MixedMono) into one single class, essentially producing a 'Presence/Absence' classification scheme. In the study area, 87% of the benthic habitat, 24,335,067 m^2, is classified as having some type of seagrass coverage, leaving 13%, or 3,537,991 m^2, uncovered or bare, including submerged oyster reefs.

Accuracy assessment for Presence/Absence classification

When the 'Grass' classifications are aggregated to examine presence/absence, a separate analysis of accuracies is needed. This accuracy assessment is performed using the same accuracy assessment points as before, with all grass classifications aggregated into a simple 'Grass' classification. As indicated in Table 2.13, the results are quite different from those using all the species-related classes. Producer's Accuracy values

were as follows: of the 24 assessment points classified as ‘Bare’, 16 (66.67%) were correctly classified, as before. However, of the 92 assessment points that had been previously classified according to species, 86 (93.5%) were correctly classified as ‘Grass’ after aggregation. User’s Accuracies were 72.7% for ‘Bare’ and 91.5% for ‘Grass’ classes. Overall accuracy for aggregated classification was 87.93%.

Table 2.13. Confusion matrix and accuracy assessment for aggregated ‘Grass’ classifications.

	Bare	Grass
Bare	16	8
Grass	6	86

Producer’s Accuracy		User’s Accuracy	
Bare	66.7%	Bare	72.7%
Grass	93.5%	Grass	91.5%
Overall Accuracy	87.93%		
Cohen’s Kappa	.6206		

Cohen’s Kappa Coefficient

The Producer’s and User’s accuracy assessment methods above have been occasionally criticized for the possibility that some cases may have been correctly classified merely by chance. Cohen’s *Kappa* Coefficient (Cohen 1960) is suggested as an additional index of classification accuracy that compensates for chance agreement and may be used to calculate a variance term which may be used in the statistical testing for significance of the difference between two coefficients (Foody 2002). *Kappa* is calculated by subtracting the hypothetical probability of a chance agreement (of two observations) from the relative observed agreement, and yields a number between 0 and

1. A zero would indicate that accuracy in classification was merely coincidental, while a one indicates that there is no probability that there is a chance agreement (Strahler *et al.* 2006).

As with most statistical procedures, there are some assumptions and conditions that must be met. Cohen's Kappa Coefficient of Agreement supposes that the units are independent of one another, the categories are mutually exclusive and exhaustive, and that the selection (judges) operate independently (Cohen 1960). The accuracy assessments above (see Table 2.12 and Table 2.13) meet those presumptions at least in theory; *Halodule* cannot be *Thalassia*, and a polygon classified as MixedMono cannot be classified simultaneously as either.

The Cohen's *Kappa* Coefficient calculated for the accuracy assessment matrices indicates a fair amount of chance agreement for the final output of the classification by species, the least accurate of the two, is possible, and a lesser probability of chance agreement in the classification of aggregated grasses and bare subsurface.

DISCUSSION

This project demonstrates that hyperspectral imagery can be used successfully to discriminate between species of seagrass in optically shallow waters. While single iteration classification techniques have traditionally been used for terrestrial classification schemes, using multiple iterations to distill information from hyperspectral imagery can improve thematic accuracy. As techniques are improved and methods developed, such as the water depth correction developed by Cho (Cho and Lu 2010), hyperspectral imagery will be a valuable tool in the resource manager's toolbox.

Likewise, hyperspectral imagery is useful and highly accurate for determining presence/absence of seagrass in large spatial areas such as Redfish Bay. Previous studies (Peneva *et al.* 2008) conducted off Horn Island, Mississippi, had achieved accuracies as high as 89% from a variety of supervised classification techniques including Spectral Angle Mapping (SAM), Maximum Likelihood (ML) and Minimum Distance to Mean (MDM). Peneva (2008) noted that different classification techniques produced better results depending on depth, water turbidity and variability of intensity for bottom types. The methods described for this study employ a variety of both supervised and unsupervised techniques, and allow a choice of classification methods at each iteration based on the highest output accuracy. The results indicate that having a diverse range of techniques available enhances the accuracy of the analysis.

Field work for this study was conducted by visiting a series of randomly selected field points, documenting the type and density of coverage, and the depth. A similar study was being conducted coincidentally and almost simultaneously in the Eastern Banks off Moreton Bay, Australia, by a group of highly respected remote sensing experts (Phinn *et al.* 2008), comparing a variety of aerial and satellite platforms. The Australian study employed a series of 100 m photo transects, with transect sites chosen to cover the range of species and densities, and adjusted so that they would be over gradients or boundaries in seagrass coverage or densities. Digital photographs were then taken at 2 m intervals along the transect line, and positioned 1 m above the benthos, which produced a digital image with approximately 1 m x 1 m field of view. Each photo was then analyzed by placing 24 points on each photo in a regular grid, and entering species or bottom type for each point into a database, and coverage was then determined by the percentage of

those 24 points per photo which contained seagrass. Coordinates for each photo were then estimated, and that data assigned to that referenced point. This tedious process was undertaken to "take into account the positional accuracy of the GPS measurements (at least +/- 5.0 m) and mis-registration of the image data" (Phinn *et al.* 2008).

The study described in this paper and that conducted in Australia produced comparable accuracy levels for similar imagery types. However, the methodology employed for the Redfish Bay study field work was less labor intensive. Both studies were limited by the spatial inaccuracies within the imagery. Future studies should concentrate on methods to reduce those inaccuracies, as well as restrain the costs of field research.

Future studies should follow the guidelines found in 'Guidance For Benthic Habitat Mapping: An Aerial Photographic Approach' (Finkbeiner *et al.* 2001). In addition to these guidelines, several other caveats should guide attempts to use hyperspectral imagery to distinguish seagrass species in coastal estuarine environments:

1. Obtain a very good bathymetric data set for the study area. This should be done before the fieldwork is attempted, as it will be critical in establishing accessibility of field points, and necessary to verify that the randomly selected sampling points cover the range of depths well.

2. Timing of both the aerial acquisition and fieldwork are critical to the success of this type of mission. In addition to calm seas, light winds and cloud-free skies, clear water and the minimum of epibiotic fouling are essential. Minimum fouling

usually occurs in late spring or early summer; unfortunately, this is also one of the most unpredictable seasons, as far as clear, calm water are concerned.

3. If at all possible, a spectrometer should be used to capture the spectral readings at each field site. Although this will add some valuable time to the field portion of the project, the information gained should prove well worth the effort.

4. Select 50% more field sites than are estimated to be necessary. A lack of suitable field sites is likely to be problematic.

5. Copious and accurate field notes are a must. Note the amount of macroalgae, drift algae, wrack or other confounding influences. Note the amount of sediment visible for patchy areas. Notes should accurately reflect what will be visible in the imagery; decide how to classify an area that is 100% *Halodule* but 50% coverage before going to the field.

CHAPTER III: IDENTIFYING SPECTRAL DIFFERENCES IN SEAGRASS SPECIES

ABSTRACT

In order to determine effective hyperspectral imagery bands for species differentiation, spectral reflectance signatures of two species of seagrass, *Thalassia testudinum* and *Halodule wrightii*, were collected using a portable spectrometer at three positions *in situ*: just above the surface/water interface, directly below the surface/water interface, and at the canopy level.

These signatures were imported into Microsoft Excel, separated into worksheets containing a single species from a single position (*i.e.*: *Halodule* at the surface, *Thalassia* at the canopy, etc.), and a depth correction algorithm applied. Each of these data sets were then normalized using a maximum normalization technique, and a Multiplicative Scatter Correction was applied.

The mathematical means for these spectral curves were compared by collection position. Results for this analysis show that the spectral signatures of these two seagrasses are distinct at all collection levels. However, large variances were noted in the subsurface and canopy spectral curves. Recommendations for band selections were made, and it is noted that these recommendations were valid for this particular site under these particular conditions. Final recommendations include the collection and analysis of spectral data at the time of imagery collection. This method of *in situ* spectral collection and comparison provides valuable insight into proper band selection for subaquatic vegetation analysis and species discrimination.

INTRODUCTION

Hyperspectral imaging has been used for a variety of terrestrial classification, with remarkable results (Tamilarasan *et al.* 1983, Zomer *et al.* 2009, Xie *et al.* 2011). Land use/land cover, species differentiation, fire susceptibility modeling, invasive species detection, and wetlands vegetation mapping all have been successfully mapped using hyperspectral imagery (Hirano *et al.* 2003).

Hyperspectral imaging has also been used in aquatic environments for a variety of purposes, at a variety of scales, and with varying results. Methods were developed for using hyperspectral imagery to map coral reef features and discriminate healthy from diseased corals as early as 2000 (Holden and LeDrew 2000). Researchers have successfully detected harmful algal blooms (HAB) from shipside (Craig *et al.* 2006), as well as from satellite platforms such as the SeaWiFS (Sea-viewing Wide Field-of-view Sensor) (Tang *et al.* 2003).

Researchers have examined the use of hyperspectral imagery to detect the presence or absence of seagrass (Barillé *et al.* 2010, Guimarães *et al.* 2012), as well as attempt to differentiate between species (Wabnitz *et al.* 2008, Cho and Lu 2010). This project examines the effect of the water column on the spectral signature of the seagrass canopy (Rundquist 2001). The rationale behind this research is simple: the effects of the atmosphere, which are widely recognized, are virtually the same whether imaging the terrestrial or the aquatic environment (Kutser *et al.* 2006, Gao *et al.* 2009). Air - water interface influences can be ephemeral, varying with the wind, clouds and other parameters over very short times, even a matter of minutes, and can easily vary within a single image. What happens below the water surface is also of interest. While subsurface

conditions can be somewhat ephemeral and can be influenced by spatially restricted events, such as a boat passing through the area, these events generally are more consistent throughout an area and last longer than the time it takes to acquire imagery, as compared to the lifetime of an individual cloud.

This research seeks to confirm that, without the effects of atmospheric distortion and surface influences, seagrasses, particularly *Halodule wrightii* and *Thalassia testudinum*, are spectrally distinct *in situ*, and as observed through the water column.

METHODS

In June of 2012, we used a portable spectrometer to capture spectral signatures of seagrasses *in situ* from three positions: above the surface/water interface, just below the surface/water interface, and just above the canopy. These signatures were collected above monotypic stands of *Halodule wrightii* and *Thalassia testudinum* in Redfish Bay, in the Coastal Bend area of Texas.

Study area

Redfish Bay is a shallow estuary located between Aransas Pass and Port Aransas, Texas, and extends almost to Rockport Texas to the north, and is typical of many of the dynamic grass flats and inland tidal bays found along the Texas coast. The area is dry sub-humid (Kornicker 1964), and frequented by hurricanes and tropical storms (Oppenheimer 1963). The maximum depth of Redfish Bay is around 2 m, with the average depth being .75 m. Bottom sediment types vary considerably.

Data acquisition

Portable spectrometers are able to capture the characteristic spectral signatures of seagrasses. For this research, we used an Ocean Optics Jaz Modular Sensing Suite, a highly portable, expandable spectrometer with water-resistant sensing probes. The specifications for this spectrometer are shown in Table 3.1. This research examines the light returning from the canopy of different species of seagrass, from above the water surface, just below the surface and at the canopy level. Figure 3.1 graphically depicts the contributions to total upwelling, as well as other vectors that radiance (light) travels. By holding the sensing probe just below the surface of the water, the effects of the surface reflection, shown as L_r in Figure 3.1, are eliminated from the resulting spectral curve. The effects of scattering in the water column are determined by examining the differences between the response from the canopy and that obtained from just below the surface. Samples were acquired, *in situ,* for the range of 190 to 1029 nm within 4 hours of solar maximum with a sensor having a fore optic with a 25º Field of View (FOV), and using a +/- 99% white Spectralon plate as a reflectance reference. Unlike the methods described by Fyfe (2001) and others, these samples were taken in place, from either just above the water surface, just below the water/surface interface (see Figure 3.2), and just above the canopy level. Figure 3.3 shows the distribution of depths of the sampling effort.

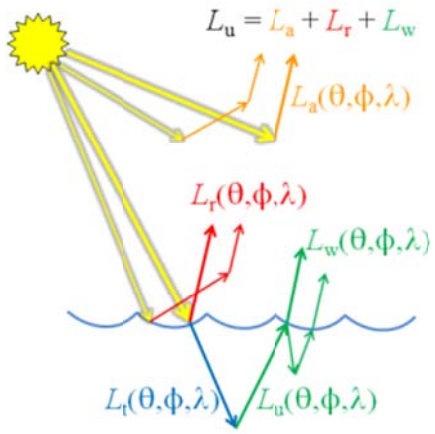

Figure 3.1. Contributions to the total upwelling radiance above the sea surface, (L_u). The sun's unscattered beams are shown as yellow arrows; orange arrows depict the atmospheric path radiance (L_a); red is surface-reflected radiance (L_r) is depicted with red arrows; water-leaving radiance (L_w) is depicted with green arrows. The upwelling radiance (L_u) is depicted with the green arrows. Thick arrows illustrate single-scattering contributions; thin arrows represent multiple scattering contributions. Theta (θ) represents the nadir angle, while phi (φ) represents the azimuthal angle and lambda (λ) represents the wavelength. Adapted from Ocean Optics Web Book at http://alturl.com/w2zon.

Figure 3.2. Photographs of seagrass, taken from the water surface (left), and the subsurface, (right).

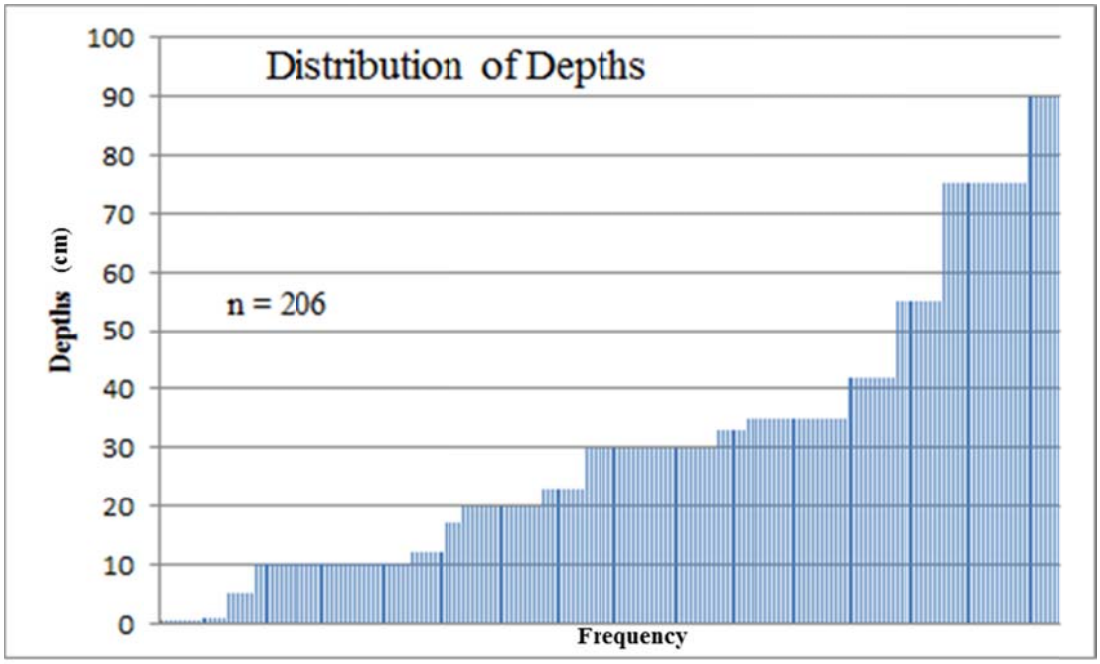

Figure 3.3. Distribution of depths of recorded spectral readings.

Table 3.1. Specification sheet for the Jaz Modular Spectrometer. Adapted from Ocean Optics Jaz Modular Spectroscopy Catalog at http://www.oceanoptics.com/catalog/Ocean_Optics_Jaz.pdf.

Selected Jaz Spectrometer Specifications	
Wavelength range	Grating dependent (extended-range grating available for 200-1025 nm coverage)
Optical resolution	~0.3-10.0 nm FWHM
Signal-to-noise ratio	250:1 (at full signal)
A/D resolution	16 bit
Dark noise	50 RMS counts
Dynamic range	8.5 x 107 (system); 1300:1 for a single acquisition
Integration time	870 ìs to 65 seconds (20 s typical maximum)
Stray light	<0.05% at 600 nm; <0.10% at 435 nm
Sensitivity	75 photons/count at 400 nm; 41 photons/count at 600 nm
Fiber optic connector	SMA 905 to 0.22 numerical aperture optical fiber
Electronics connector	19-pin MHDMI connector; use ADP-MHDMI-RS232 adapter to interface to RS-232
Channels supported	Up to 8 spectrometers
OEM integration supported	Yes
Inputs/Outputs	4 onboard digital user-programmable GPIOs

The spectrometer module requires a Reflectance Standard Reference (R), obtained by sensing the reflected light from a Spectralon panel, which is then considered the maximum amount of light available. A dark reference standard (D), the minimum amount of light available, is also recorded. R and D are stored within the Jaz unit, and when a signal (S) is recorded, R, D, and S are recorded in a single data file, along with the wavelength (Table 3.2). Once the spectrometer is turned off or another mode is selected, the current reference and dark (R and D) standards are discarded, and new ones are required for the next measurement.

Data is stored within the Jaz unit on a removable SD (Secure Digital) memory card in delimited text format and may be viewed in an Excel Spreadsheet, as in Table 3.2. The data may also be viewed within Ocean Optic's proprietary SpectraSuite software, and the data files may be opened in an Excel spreadsheet for further analysis.

From the data table, Percent Reflectivity for each wavelength (R_λ) can be calculated by dividing the reflected radiance (S) at each λ by the reflectance standard reference (RSR), and multiplying by 100:

$$R_\lambda = S/RSR * 100 \quad (3.1).$$

Location data, sample number and type, date, time and depth were recorded within the Excel datasheet. The data was segregated by sensor position: above surface (SURF), subsurface (SUBS) or canopy (CAN). Spectra were then further separated by species. Spectra for each species were then normalized and their standard deviations calculated and plotted.

Table 3.2. A typical data file as collected with the Jaz Spectrometer reveals the parameters spectra acquisition, as well as time, date, wavelength (W), dark (D) and reference readings (R), collected signal (S), and processed (P) signal.

Jaz Data File				
Date: Sat Jun 09 10:53:39 2012				
User: jaz				
Dark Spectrum Present: Yes				
Reference Spectrum Present: Yes				
Processed Spectrum Present: Yes				
Spectrometers: JAZA1552				
Integration Time (usec): 35000 (JAZA1552)				
Spectra Averaged: 1 (JAZA1552)				
Boxcar Smoothing: 0 (JAZA1552)				
Correct for Electrical Dark: No (JAZA1552)				
Strobe/Lamp Enabled: Yes (JAZA1552)				
Correct for Detector Non-linearity: No (JAZA1552)				
Correct for Stray Light: No (JAZA1552)				
Number of Pixels in Processed Spectrum: 2048				
>>>>>Begin Processed Spectral Data<<<<<				
W	**D**	**R**	**S**	**P**
190.2256	521.5109	722.2695	653.0424	65.51724
190.6828	625.3516	671.503	655.35	65.00005
192.054	673.8105	722.2695	696.8863	47.61913
…				

Data manipulation

Figure 3.4 shows the mean spectral values for *Thalassia* and *Halodule* from all three positions, as well as their respective standard deviations. Figure 3.5 and Figure 3.6 show the above-surface spectral curves for each species type before normalization.

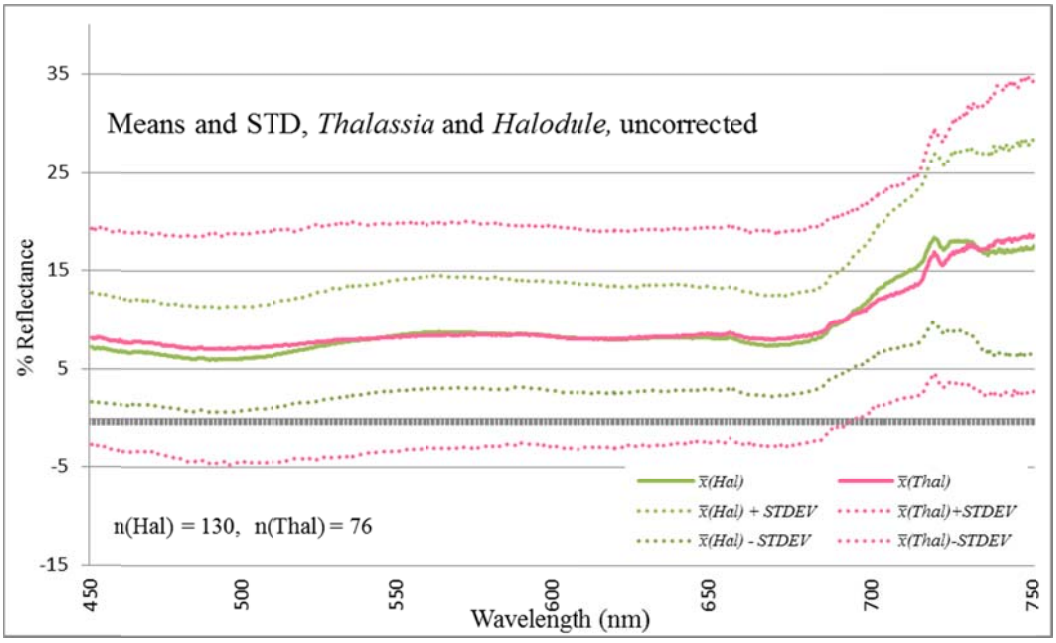

Figure 3.4. Mean reflectance values for both *Thalassia* and *Halodule* of the entire dataset. Note that this is before applying normalization and Multiplicative Scatter Correction (MSC). Also note that the standard deviations for *Thalassia* envelop those for *Halodule*.

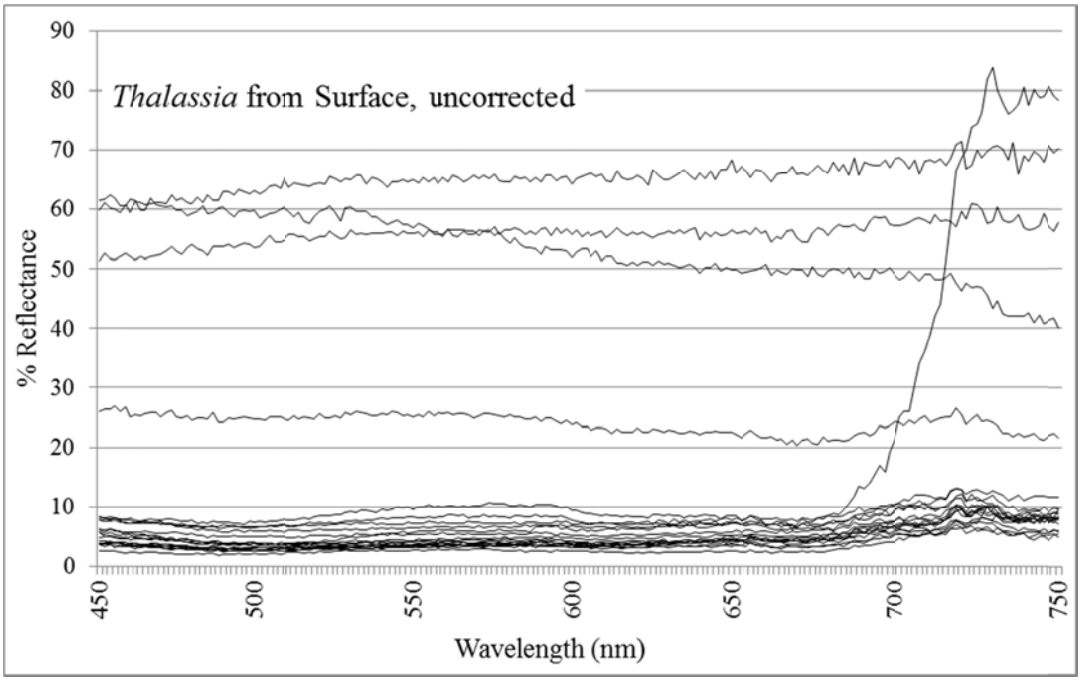

Figure 3.5. *Thalassia* reflectance captured from above the surface of the water, before corrections are applied

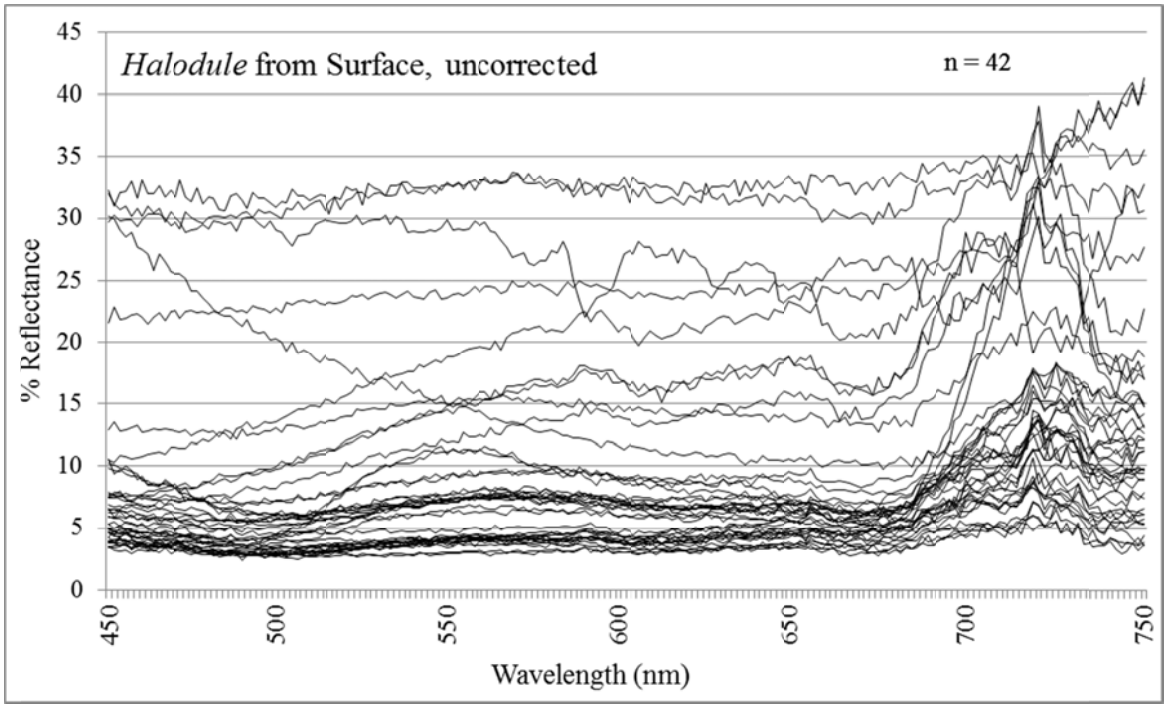

Figure 3.6. *Halodule* reflectance captured from above the water surface, before corrections are applied.

Figure 3.7 shows the subsurface reflectance curves for *Thalassia*. Figure 3.8 shows the same spectra, after normalization and Multiplicative Scatter Correction (MSC). MSC is a transformation method used to compensate for additive and/or multiplicative effects in spectral data. It has also been successfully used to adjust for path length problems, offset shifts, and interference. It removes the effects of amplification and offset, which can otherwise dominate the information in the data table, as shown in Figure 3.9. Offset is a type of noise and refers to an undesired increase or variability in amplitude along an entire spectral curve (Ganssle 1990). MSC performs two simple transformations by calculating two correction coefficients from regression of each individual spectrum onto the average spectrum. The first coefficient, a, is the intercept (offset) and coefficient b is the slope of this regression line.

The equation used to perform MSC is:

$$Mnew(i,k) = (M(i,k) - a)/b \quad (3.2)$$

where M is the Matrix to be corrected, *i* is the *i*th element in the *k*th column of M, a is the coefficient for the intercept and b is the coefficient for the slope of the regression line.

Before performing the MSC, the data must be normalized. These matrices were normalized using the maximum normalization equation, which divides each row by its maximum absolute value, as expressed in Equation 3.3:

$$X(i,k) = X(i,k)/ \max(|X(i,)|) \quad (3.3).$$

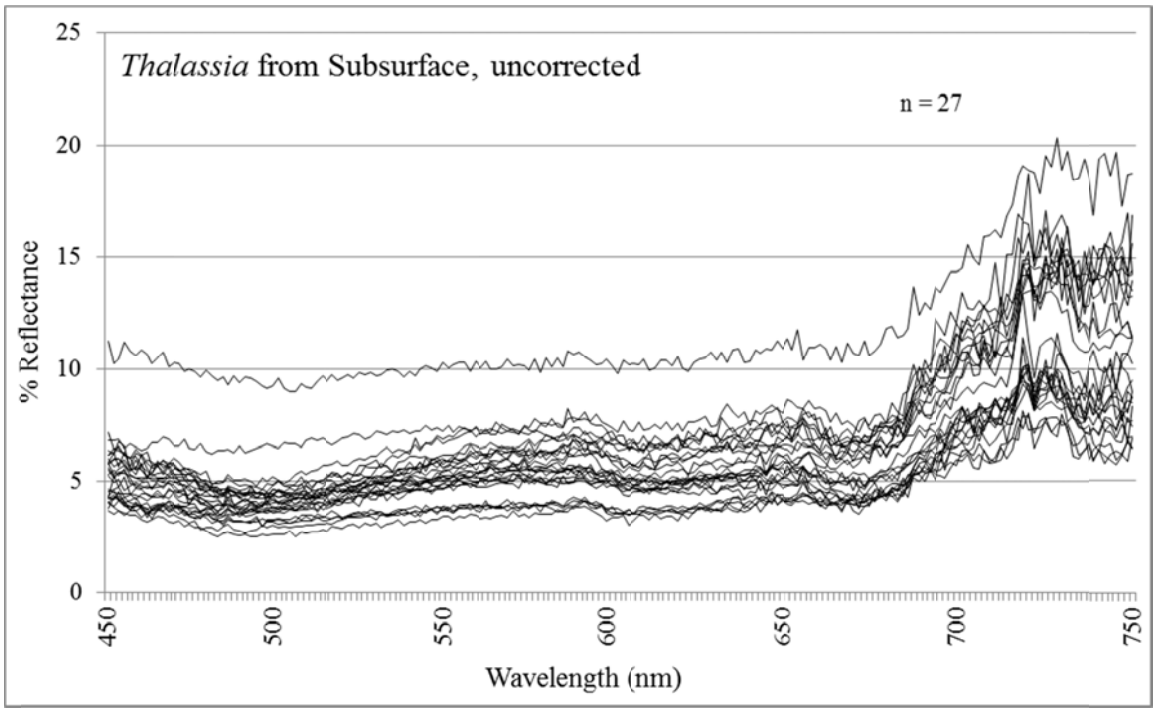

Figure 3.7. Spectral curves from *Thalassia*, captured from below the water surface.

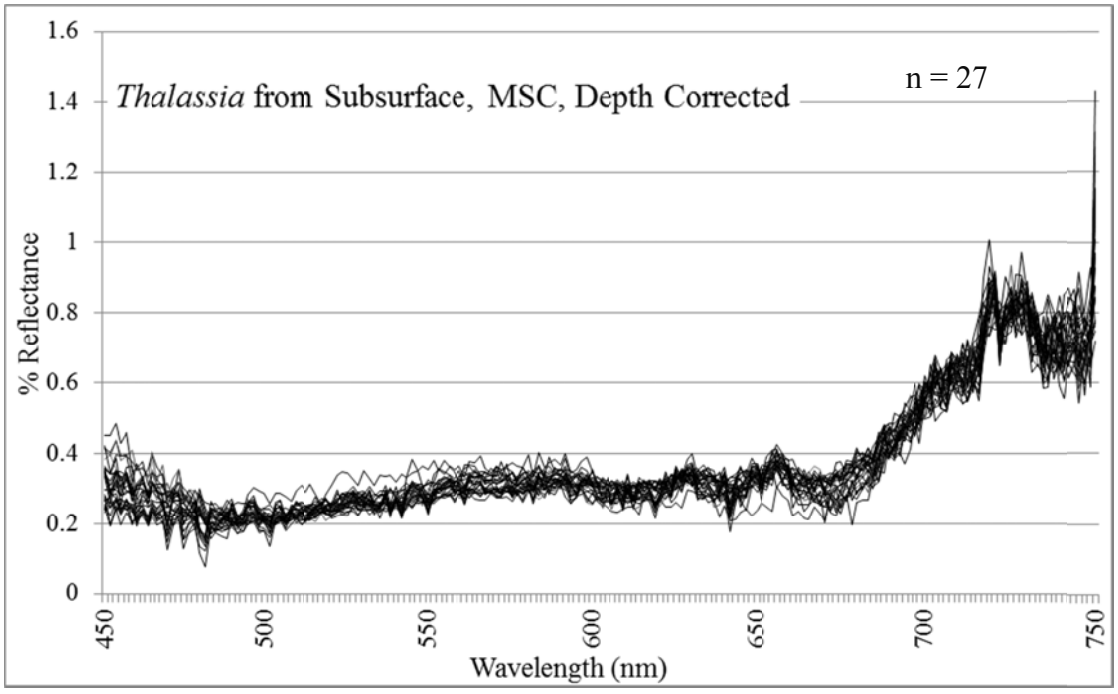

Figure 3.8. Reflectance curves for *Thalassia* have been normalized and the MSC applied.

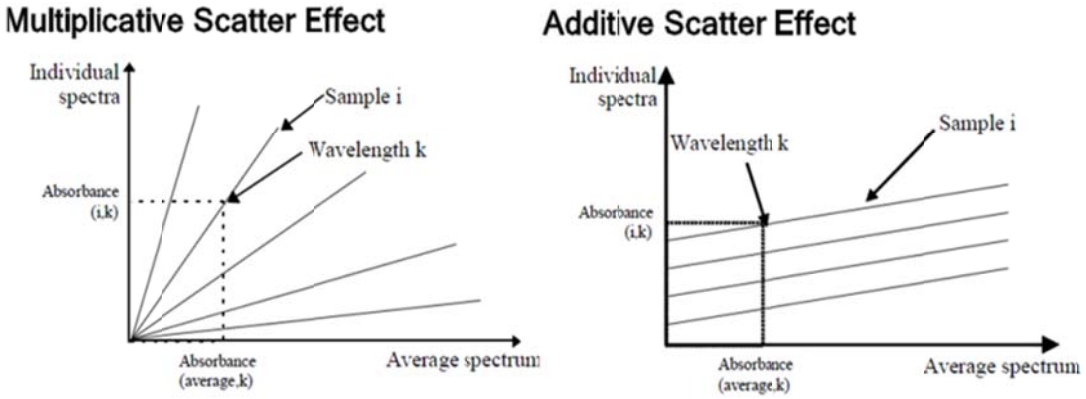

Figure 3.9. The effects of multiplicative and additive scatter. These effects are removed using The Unscrambler Multiplicative Scatter Correction utility.

Similar plots were created for each species (*Thalassia* and *Halodule*), before and after normalization, as captured from just below the surface and from just above the canopy. These plots are shown in Figure 3.10 through Figure 3.14.

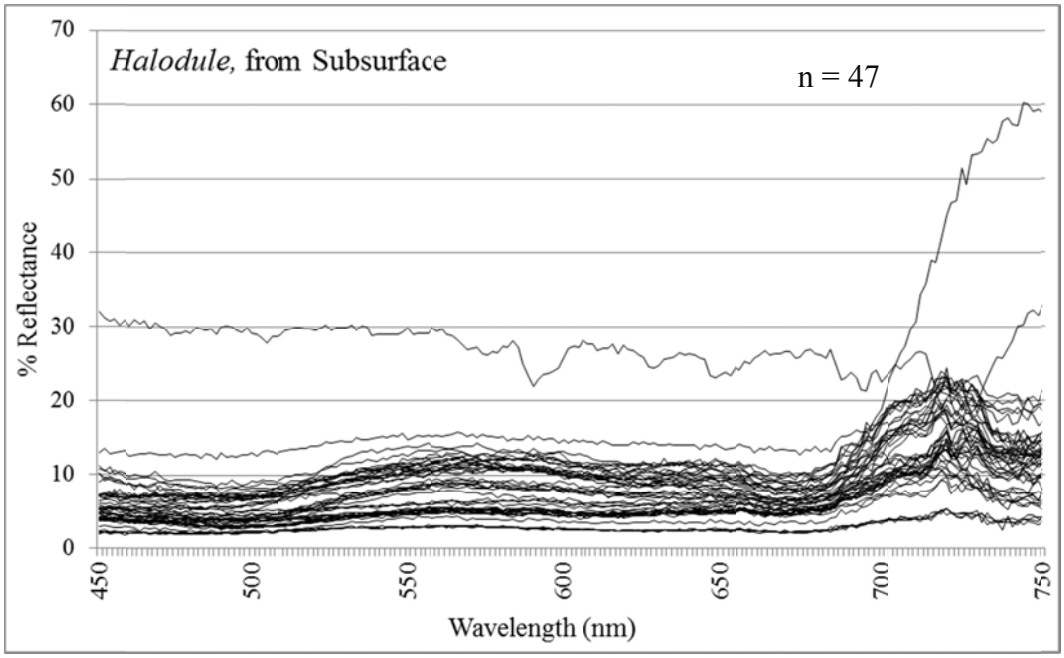

Figure 3.10. The spectral curves of *Halodule*, captured from just below the surface.

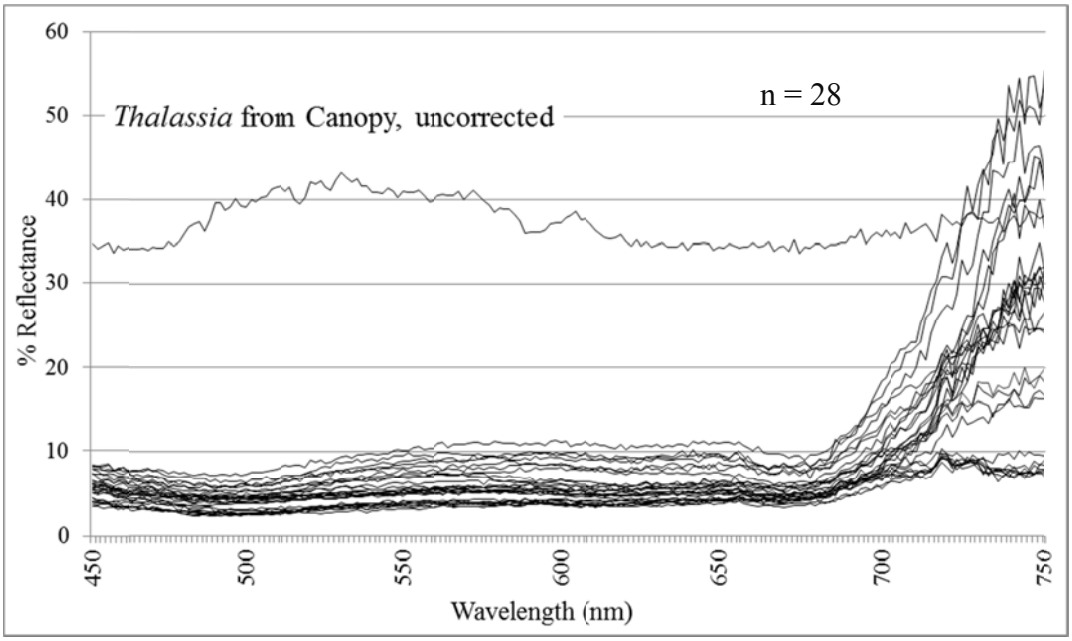

Figure 3.11. Spectra from *Thalassia*, captured at canopy level.

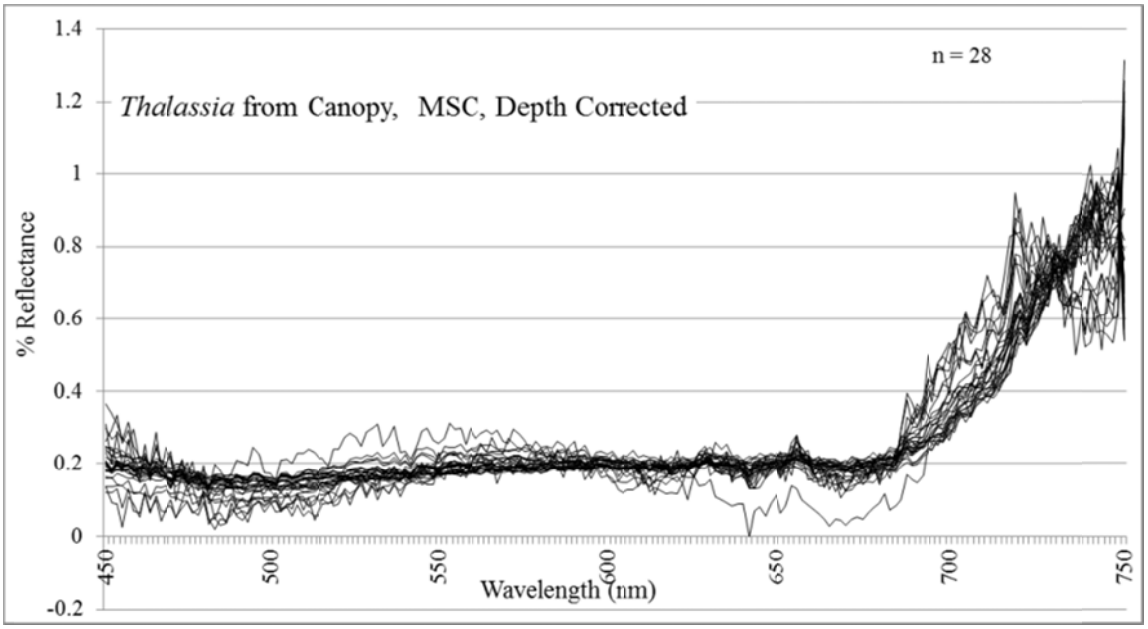

Figure 3.12. *Thalassia* spectra, captured at canopy level, and normalized.

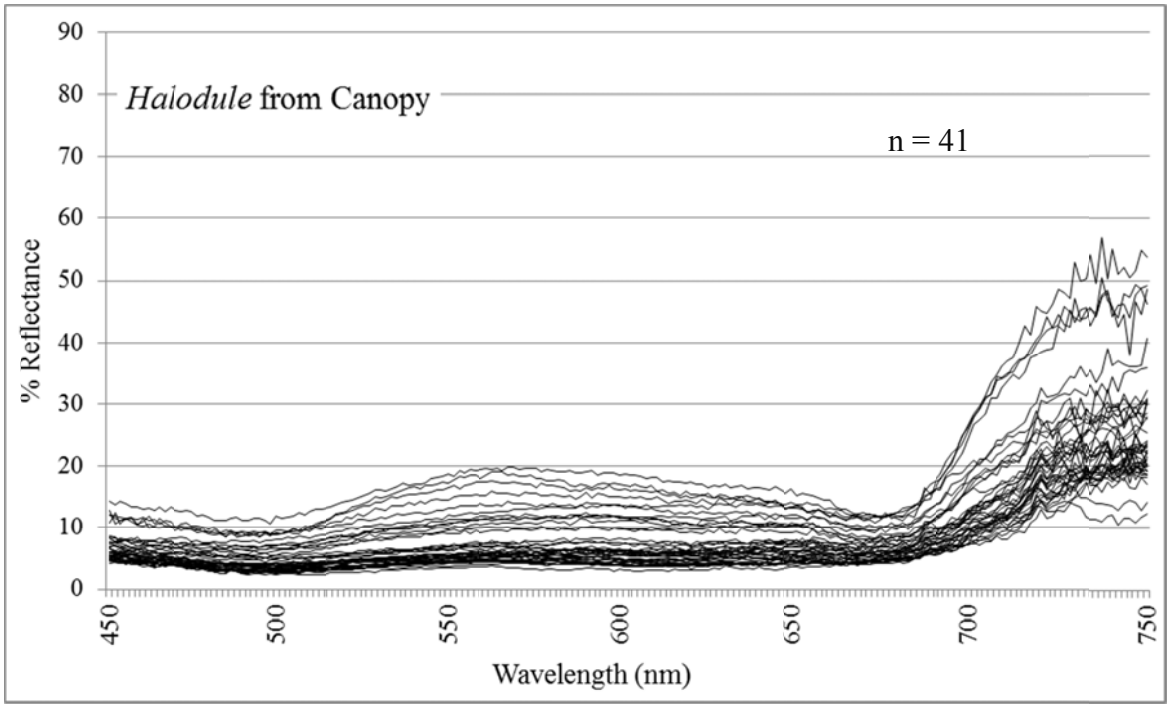

Figure 3.13. *Halodule* spectra, captured at canopy level.

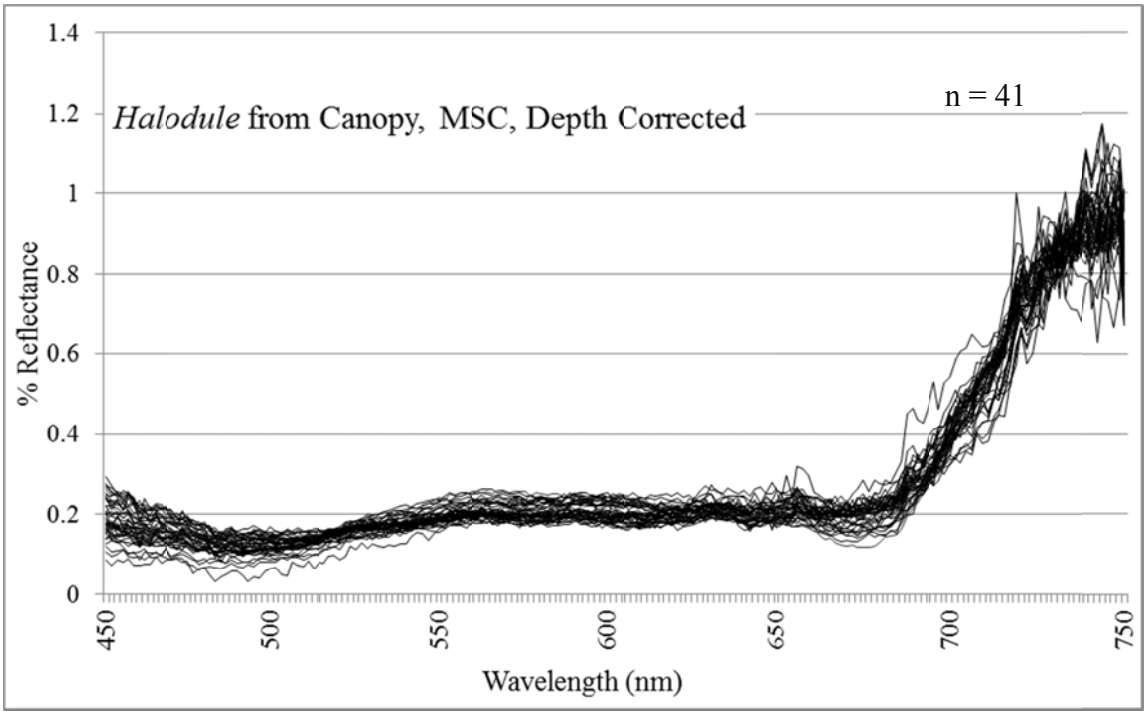

Figure 3.14. *Halodule* spectra, captured at canopy level, and corrected for depth and MSC.

After the spectra were normalized, mean values, standard deviations, and mean plus and minus one standard deviation for each wavelength were calculated, by species, at each level of collection. These are plotted in Figure 3.15 through Figure 3.17.

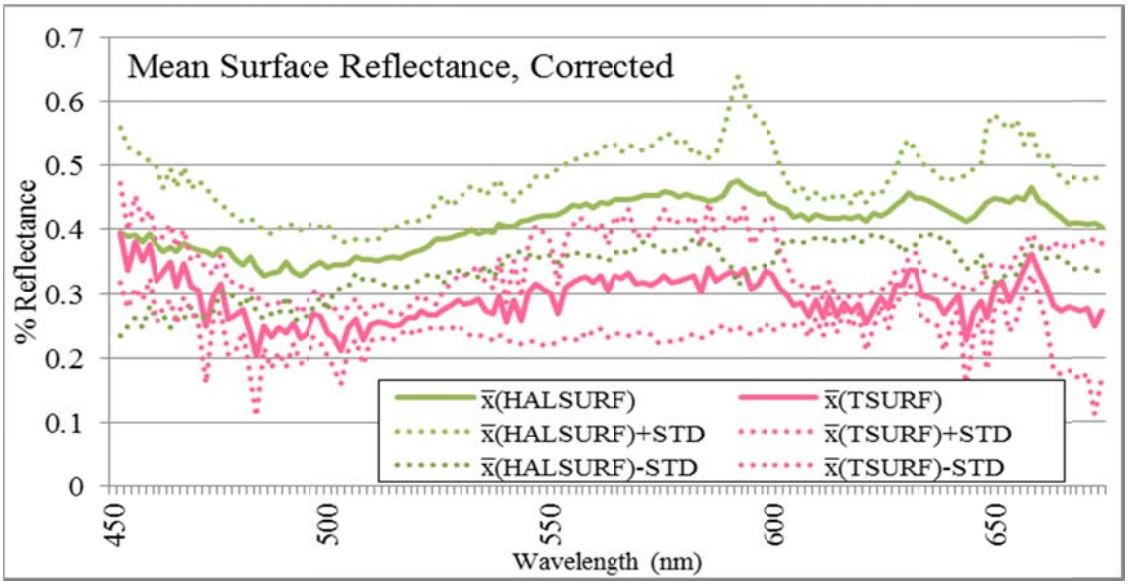

Figure 3.15. Mean, +/- STD of *Thalassia* and *Halodule* from Surface, Normalized and MSC.

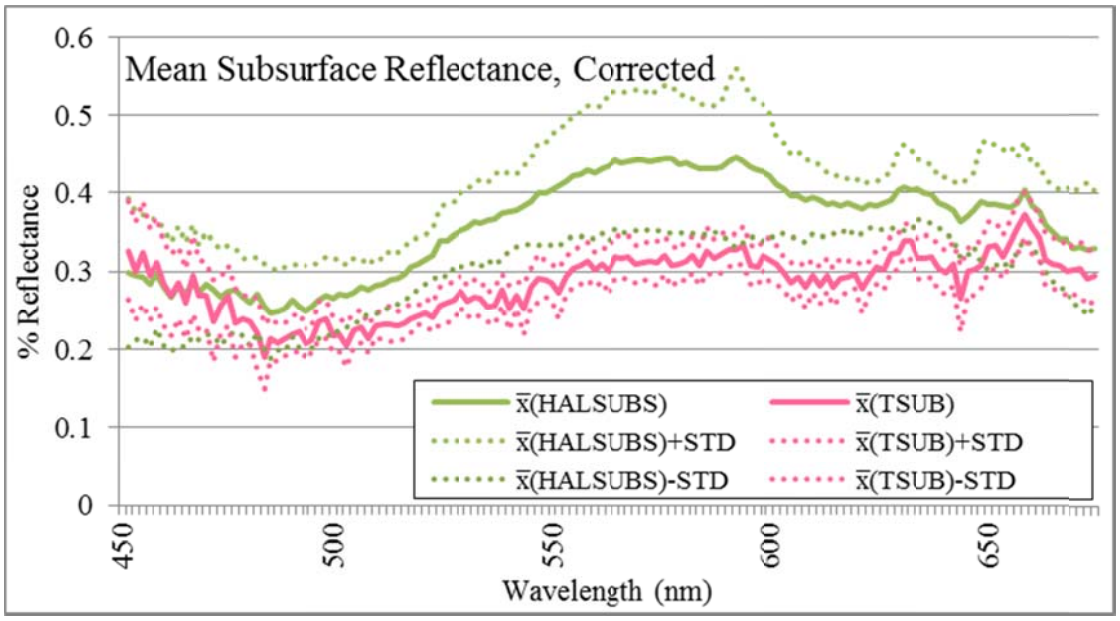

Figure 3.16. Mean, +/- STD of *Thalassia* and *Halodule*, normalized and MSC, from the subsurface.

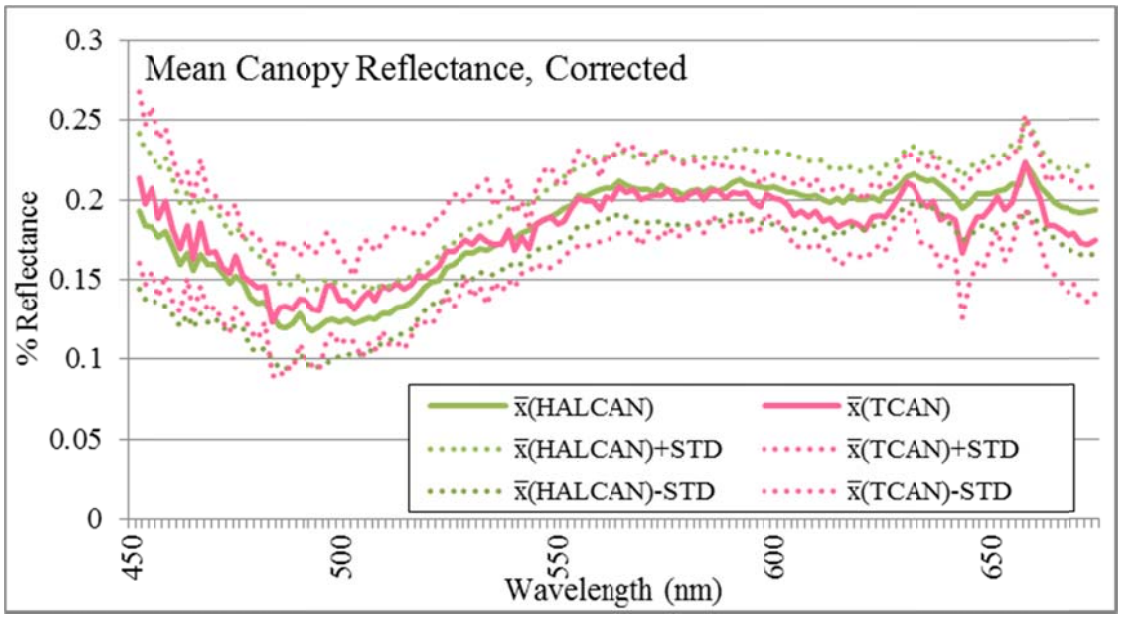

Figure 3.17. Mean, +/- STD of *Thalassia* and *Halodule*, measured at the canopy, normalized and MSC.

Once these means and standard deviations were established for each species at each sensing position, they were then compared and plotted.

DISCUSSION

In her study of Australian seagrasses, Fyfe (2003) examined leaf samples of three species of seagrass found in several estuaries in southeastern Australia. She identified several key wavelengths where spectral signatures had no overlap between the three species of seagrasses. These spectral differences are attributed to differing proportions of red, orange, yellow and brown carotenoids (Fyfe and Dekker 2001). For that study, the green reflectance peak, found at 540-560 nm, and the red absorption trough, around 670-680 nm, allowed separation of the grasses *Posidonia australis, Halophila ovalis* and *Zostera capricorni* based on chlorophyll content (Figure 3.18). These separations were evident regardless of epibiont coverage, which can include microalgae, juvenile macroalgae, and sessile invertebrates. A peak in reflectance observed between 560 and 670 nm are attributed to those epibionts. It is important to note that these leaf samples were brought to the surface, rather than sampled through the water column.

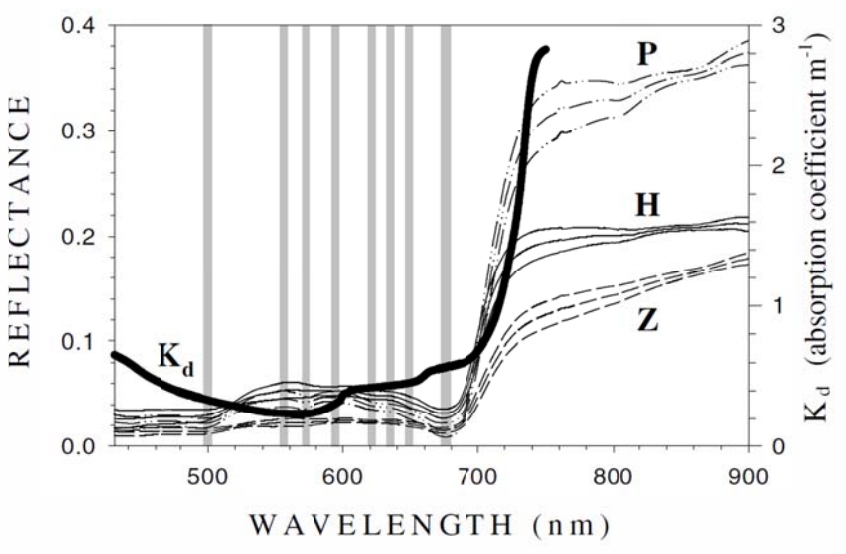

Figure 3.18. Wavebands, marked in grey, that are recommended for discriminating between *Posidonia australis* (P), *Halophila ovalis* (H) and *Zostera capricorni* (Z), from Fyfe and Dekker (2001). K_d is the absorption coefficient.

Thorhaug *et al.* (2007) compared *Thalassia*, *Halodule* and *Syringodium* in their study, along with several species of siphonaceous macroalgae and detected small differences in reflection between the three seagrasses in the 500 – 530 nm and 680 – 720 nm ranges, as shown in Figure 3.19. Thorhaug's samples were brought into the laboratory alive and rooted, and scans were carried out under controlled low-light conditions with plants in various incubation treatments, and at live, senescing and dead stages. Samples were brought to the surface for scanning.

Both Thorhaug and Fyfe converted scans to percent reflectance, then calculated the mean percent reflectance as the mean of the percent reflectance at each wavelength across all samples of a particular species (Fyfe and Dekker 2001, Thorhaug *et al.* 2007).

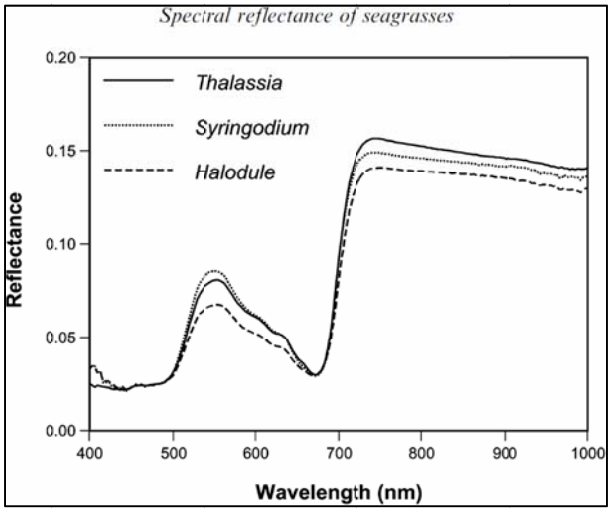

Figure 3.19. Reflectance in the 400 – 1000 nm range of individual blades of *Thalassia testudinum, Syringodium filiforme* and *Halodule wrightii* (Thorhaug *et al.* 2007).

The methods for this project followed similar procedures to the Thorhaug and Fyfe research. One major difference between this project and earlier studies is that the spectra in this project were collected *in situ* and through the water column. As shown in Figure 3.15 through Figure 3.18 (surface, subsurface and canopy), a clear separation of

the means is apparent, however, measurements at the canopy level show only a slight separation, and standard deviations between the two species overlap almost continuously. At the subsurface level, there is a good separation between the means between 515 and 620 nm, but again, the standard deviation for the *Halodule* measurements overlaps the mean and higher standard deviation of the *Thalassia* measurements in this range. At the surface level, the separation between species is much more apparent and there is no overlap of the standard deviations in the range between 490 nm to around 660 nm. Figure 3.20 shows the difference between the means of the surface-captured reflectance between these two species, after the spectral values are normalized and a MSC is applied, as well as the mean standard deviations for *Thalassia* and *Halodule*.

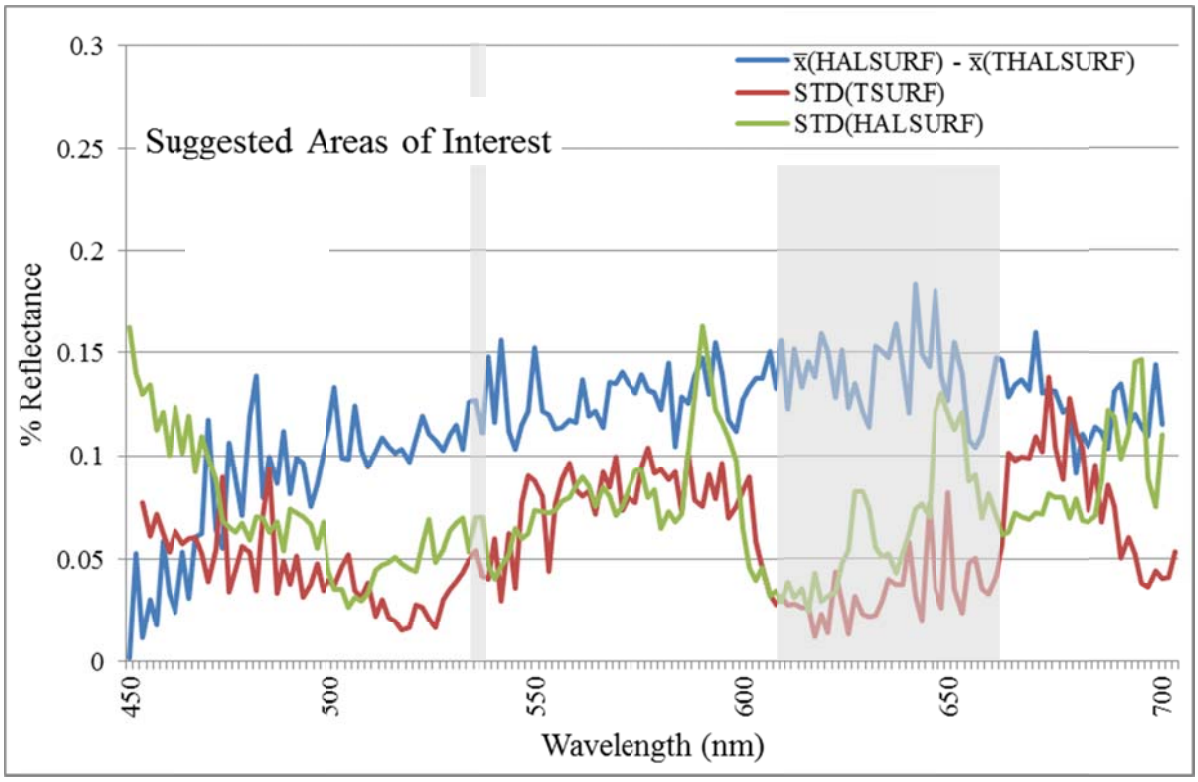

Figure 3.20. Suggested areas for band selection are between 600 – 660 nm, as well as 535 nm. These areas are selected because there is a useable amount of difference between the species but little variation within the species from surface collected data.

This research examined differences in reflectance value for two species of seagrass, *Thalassia* and *Halodule*, which are dominant in estuarine water bodies in Texas. Spectral signals were collected at three positions: at the canopy level, just below the water surface, and just above the surface/water interface. These signals were collected as reflected radiance, converted to reflectance, normalized, and corrected for scatter. The mean values and standard deviation were calculated for each species at each level of collection. Figure 3.16 through Figure 3.18 show the means and standard deviations for each species at each level of collection. Each collection level has a detectable difference between mean responses, but only those collected at the above-surface level showed a significant difference in means and exhibited small enough standard deviations to avoid overlapping the means of the other species. This condition persisted throughout the range from approximately 515 and 660 nm.

Figure 3.20 shows the difference between surface-collected mean values of *Halodule* and *Thalassia* spectra after normalizing and applying an MSC. The standard deviations for each species are also shown. Between 500 nm and 700 nm, there is about a 10% difference in normalized spectral values. Both *Halodule and Thalassia* spectra standard deviations remain consistently below 10%.

The results from this research indicate that a better separation of species can be obtained from above the surface than below the surface/water interface. While this seems rather perplexing, it is perhaps a matter of the signals measured at the canopy reflecting from individual leafs rather than a coalesced background of leaves, as sensed from above the surface/water interface. Although the above-surface images were taken within millimeters of the surface, and all the sites were under 1 m depth, given the rather small

aperture of the sensor, and a FOV of 25º, this explanation seems quite possible. As seen in Figure 3.21 and noted by Thorhaug, there can be substantial variation in seagrass blades, depending on numerous factors including epiphyte coverage, stage of senescence or morbidity (Thorhaug *et al.* 2007). Figure 3.22 shows the spectral responses of *Thalassia* in three different states of morbidity.

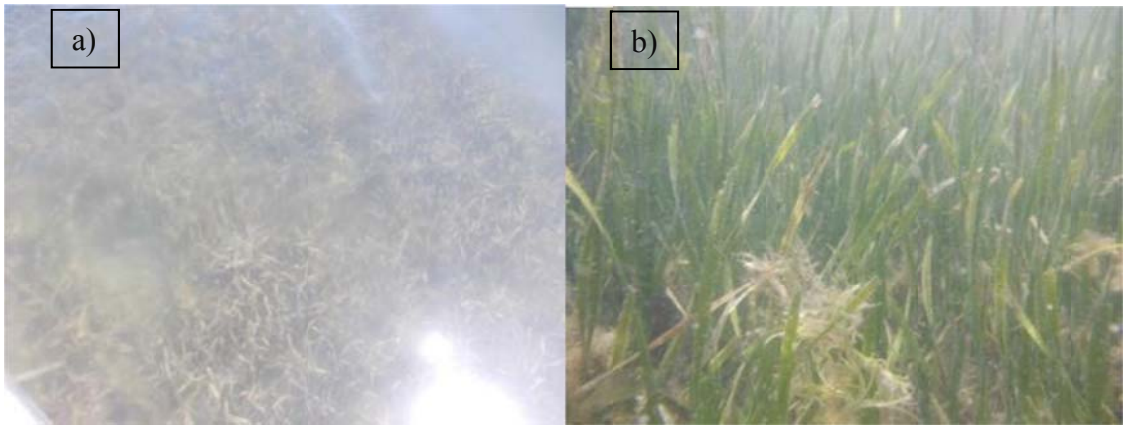

Figure 3.21. Seagrass photographs from a) above the surface and b) below the surface.

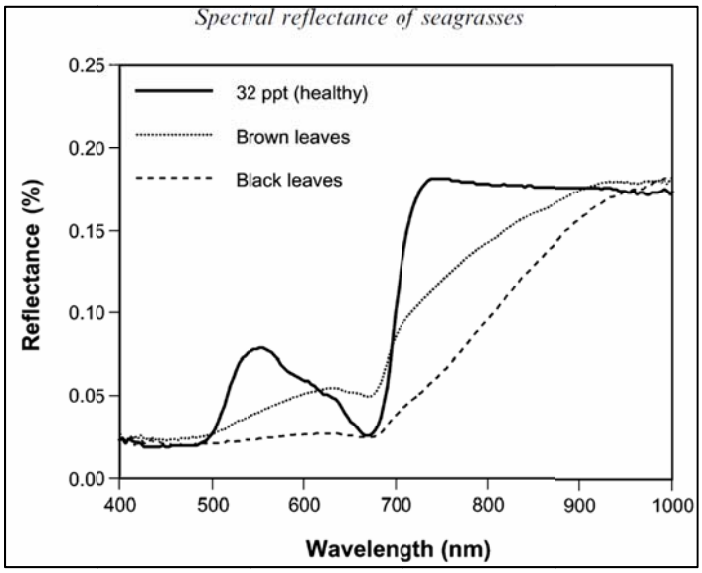

Figure 3.22. Three different spectral responses from *Thalassia testudinum* blades: Healthy blades with 32 ppt chlorophyll, yellowing and brown mottled leaves which were losing their pigments, and black leaves which were dead. From Thorhaug et al. (2007).

As the sensor is moved farther from the individual leaves, the spectral responses coalesce to return one ‘averaged’ signal, and minor changes in ‘color’ or shadow are melded into a single response. This also helps explain why areas with a high degree of macroalgae will still be classified as seagrass because the seagrass signal is dominant, and the macroalgal signals either aren’t strong enough for detection or occur in different locations along the visible spectrum.

This research demonstrates that the seagrass species *Thalassia testudinum* and *Halodule wrightii* have distinct spectral signals and that the differences in spectral signature are detectable using hyperspectral sensors and advanced processing techniques.

CHAPTER IV: HYPERSPECTRAL DISCRIMINATION OF BENTHIC HABITAT TYPES: TAKE DEUX

ABSTRACT

Hyperspectral imagery of Redfish Bay on the Texas coast was classified for seagrass species using a band selection determined by *in situ* spectral sampling and the application of spectral water depth corrections. An iterative classification scheme was used. Three iterations included unsupervised classifications and field site classification matching, and the fourth iteration employed a supervised classification with the Maximum Likelihood procedure. Results showed an increase in accuracy from similar studies using other band combination recommendations found in recent literature, developed empirically and with other methods of *in situ* sampling. Kappa Coefficients indicate that the results are not due to a chance occurrence.

The methods employed in this study allow flexibility in classification methods used at each iteration, and employ depth corrections that were previously unavailable.

INTRODUCTION

In 2008, as part of a National Oceanic and Atmospheric Administration (NOAA) Environmental Cooperative Science Center (ECSC) funded project, hyperspectral imagery was collected over Redfish Bay, Texas. The 63 hyperspectral bands were collected with an AISA Eagle imaging spectrometer aboard a specially modified Piper Saratoga aircraft.

Redfish Bay is in the Texas Coastal Bend area and is part of the Mission-Aransas National Estuarine Research Reserve (MANERR). Data collection was performed with

several goals in mind, including mapping the seagrasses and benthic habitats of Redfish Bay, mapping and analyzing the invasive black mangroves, and mapping the marsh vegetation at Aransas National Wildlife Refuge, to the north of the MANERR. This set of collaborative projects is designed to increase knowledge of these habitats, while providing research and cooperative study opportunities in geospatial technologies to a diverse group of students from a wide area.

Hyperspectral imagery has previously been used to map benthic and wetland habitats. Mumby *et al.* (1998) used hyperspectral sensors (Landsat MSS, Landsat TM, SPOT-XS and SPOT Pan, and CASI) to discriminate between coral reef species and seagrasses in the Turks and Caicos Islands, British West Indies. Fyfe and Dekker (2001) determined that 3 species of seagrasses found in southeastern Australia were spectrally distinct, regardless of whether they had epiphytic coverage. Peneva *et al.* (2008) were successful in determining seagrass distribution and coverage of seagrasses around Horn Island, MS. Phinn *et al.* (2008) mapped seagrass species, cover and biomass in Moreton Bay in Australia.

Cho *et al.* and Fyfe have both published recommendations for band selections to be used to discriminate between seagrass species (Fyfe and Dekker 2001, Fyfe 2004, Cho and Lu 2010). Cho developed these recommendations based on laboratory tank studies, while Fyfe took spectral readings *in situ*, using species found in Australian estuaries. Cho and Lu (2010) devised a depth correction algorithm to correct for absorption and scattering within the water column. In Chapter II, a study in which this correction was applied using a default value of 60 cm depth to hyperspectral images is described, in which accuracy improvements in mapping Redfish Bay seagrasses are noted (Cho *et al.*

2012). In that study, Cho's band recommendations were also adopted because they were believed to be ideally suited for the species of seagrasses found in the Redfish Bay estuary.

Subsequent *in situ* spectral sampling and analysis during 2012 indicated that certain bands may be more effective in discriminating seagrass species found in Redfish Bay than those spectral bands previously suggested by Fyfe or Cho. Chapter III describes details on the processing and analysis of the spectral samples collected with the Jaz Spectrometer, Chapter II details the original image analysis. This chapter will discuss the reprocessing of the images, using the band selection developed in Chapter III. This chapter presents these new findings and compares the results of earlier studies with those using spectral bands suggested as a result of the 2012 studies.

METHODS

Hyperspectral imagery was collected in the Redfish Bay study area during October 2008, and delivered as a georectified, atmospherically corrected data set in November 2008. The data set contained 9 images, which were approximately 1 km wide and 8-14 km long. These images were mosaicked into one single image for processing.

Study area

Redfish Bay is a shallow estuarine bay located between Aransas Pass and Port Aransas, Texas, in an area known as the Texas Coastal Bend. The study area portion of Redfish Bay is bounded by the Aransas Channel on the south, Corpus Christi Bayou on the east, the Lydia Ann channel on the north, and the Gulf Intracoastal Waterway on the west. Redfish Bay is an integral part of the Mission-Aransas National Research Reserve,

and has been designated as a state scientific area by Texas Parks and Wildlife Department. Figure 4.1 shows many of the features of Redfish Bay, and there is a more complete description in Chapters I and II.

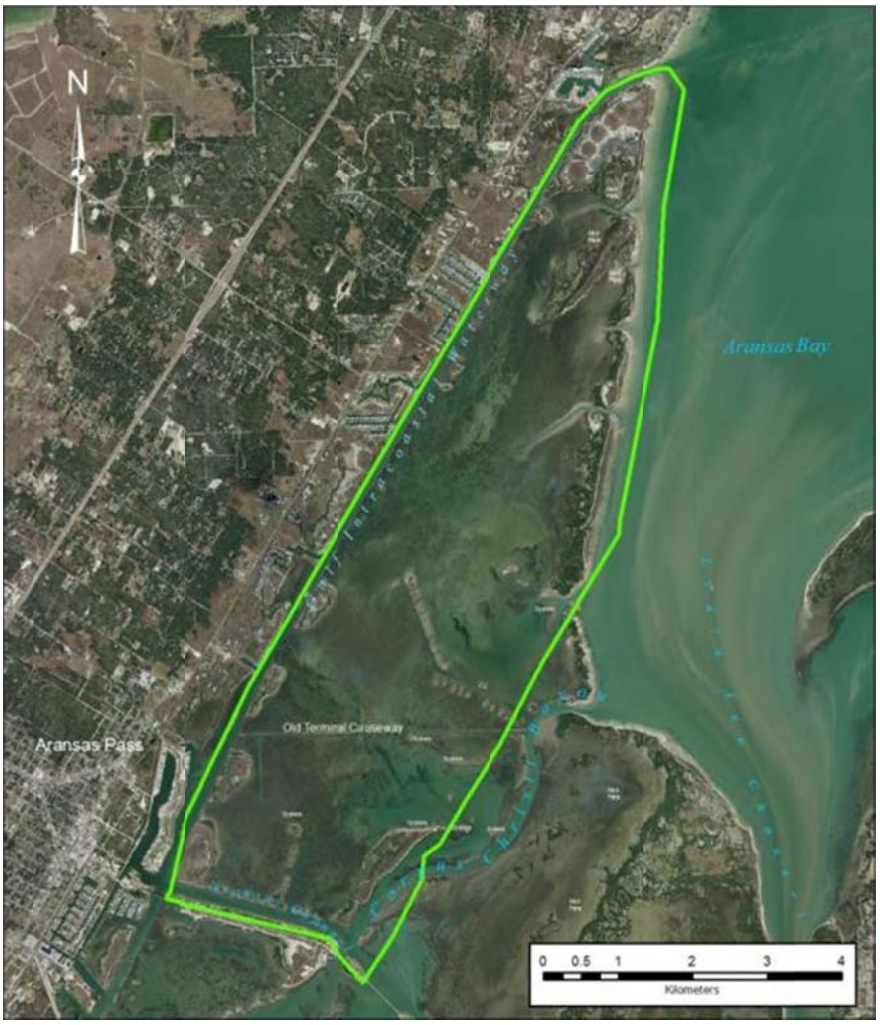

Figure 4.1. The study area, the northern part of Redfish Bay, in the Coastal Bend Area of Texas. This shallow estuarine bay is located within the Mission-Aransas National Estuarine Research Reserve, and is bounded by the Aransas ship channel, the Gulf Intracoastal Waterway, Corpus Christi Bayou and Lydia Ann channel.

Field data

Three hundred locations were randomly selected within Redfish Bay as field sites. Each of these sites was visited in July 2008, and the presence or absence of seagrass, species present, and their approximate percent coverage and water depth, were recorded

in a field book. These details were then transcribed into an Excel 2003 spreadsheet and subsequently imported into an ESRI ARCGIS point vector shapefile. Locations were then randomly split into working data and accuracy assessment data categories using a random binary number generator.

In addition to the original field work, spectral signatures were collected in June 2012. These signatures were collected over monotypic areas with 100% seagrass coverage. Sensor positions for collection were at the top of the canopy, just below the water surface, and just above the water surface, as shown in Figure 4.2. Chapter III describes the collection process and the collected data in detail. Analysis of that data indicated that certain bands were well suited for species separation.

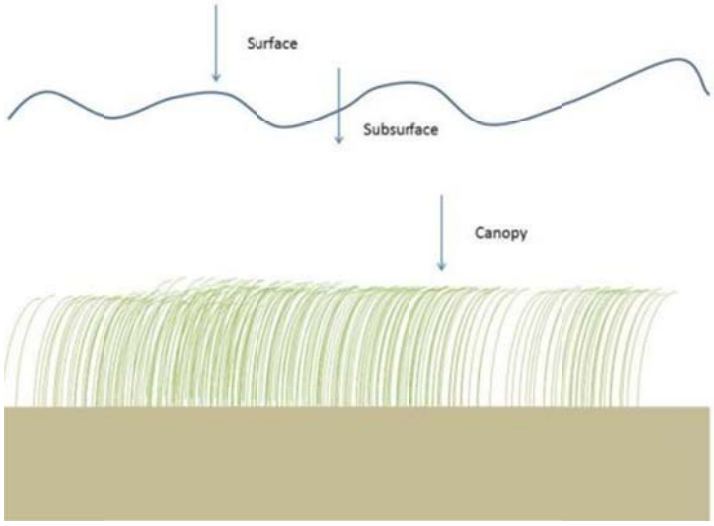

Figure 4.2. Three capture levels of spectral readings: surface, subsurface, and canopy. At each level, new reference and dark standard signals were collected. In shallow locations, the canopy and subsurface readings were often the same.

Acquired data

Hyperspectral imagery was collected over Redfish Bay in October 2008, and delivered as atmospherically corrected, georeferenced digital images in mid-November, 2008. These images have 63 bands, of approximately 10 nm bandwidth each. These images were acquired using an Airborne Imaging Spectroradiometer for Applications (AISA) Eagle Hyperspectral sensor, developed in Finland by SPECIM Spectral Imaging Ltd. The AISA sensor is mounted in a specially modified Piper Saratoga aircraft owned and operated by the Center for Advanced Land Management Information Technologies (CALMIT), in cooperation with the University of Nebraska-Lincoln. Table 4.1 shows several pertinent specifications for the sensor. Chapter II contains a detailed description of the collection system.

Table 4.1. Specifications for the Airborne Imaging Spectroradiometer for Applications (AISA) Eagle Hyperspectral sensor and is adapted from Bertels *et al.* (2005).

Characteristic	Value
Field of view (FOV)	39.7º
Instantaneous field of view (IFOV)	0.039 º
Spatial resolution	0.5 - 10 m
Spectral range	400 - 970 nm
Spectral channels	max. 244
Spectral sampling interval	2.3 nm
Spectral resolution (FWHM)	2.9 nm
Dynamic range	12 bits (4096)

The images were delivered in mid-November 2008, on a portable hard drive. The Redfish Bay collection contained 13 images, each with 63 bands and approximately 1 km wide and 8 – 14 km long. Of these 13 images, 9 were selected for further processing.

These 9 images were then mosaicked into a single image containing 63 bands, as described in Chapter II.

Image processing

Bands 16 (535.61 nm), 23 (600.58 nm), 25 (619.39 nm), 27 (638.19 nm) and 29 (656.49 nm) were selected, based on results of the field spectra analysis described in Chapter III, and depicted in Figure 4.3. These bands were separated from the larger image set. Coefficients for water absorption and water scattering were calculated for each wavelength from data supplied by Cho (personal e-mail communications, 2012). A bathymetry layer was created from multiple data sources, including field measurements, existing bathymetry point data, fishing maps and other sources. The depth raster shown in Figure 4.4 was re-sampled to match the 1 m pixel size of the imagery. This bathymetry layer was then reclassified to the R_w and A_w coefficients at each depth to be used in the algorithm developed by Cho and Lu (2010).

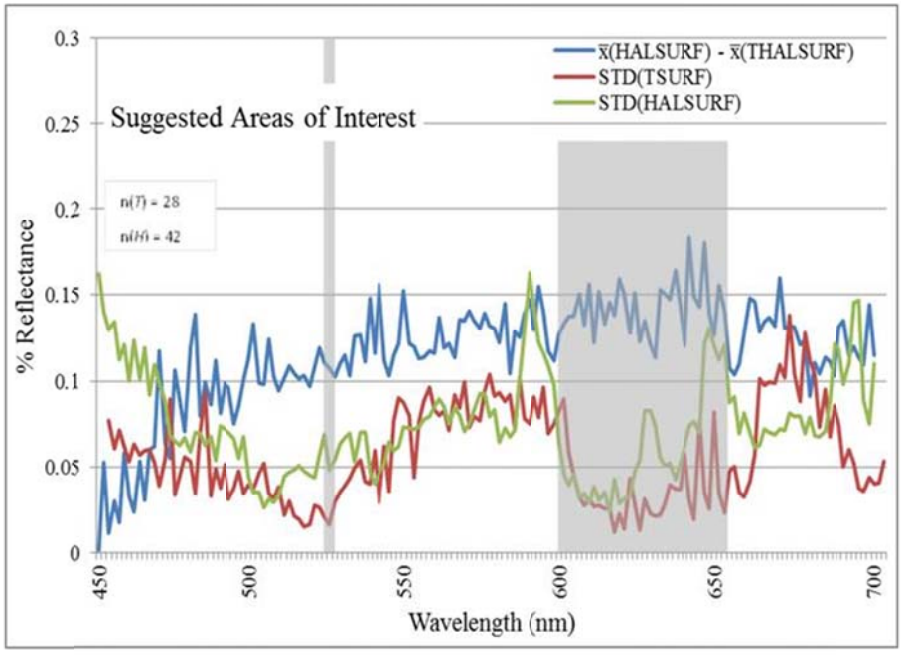

Figure 4.3. Suggested areas for band selection between 600 – 660 nm, as well as 535 nm for a reference point where there is little difference between the bands. These areas are selected because there is a useable amount of difference between the species at wavelengths where there is not large amounts of variation within the species. Details of the analysis are presented in Chapter III.

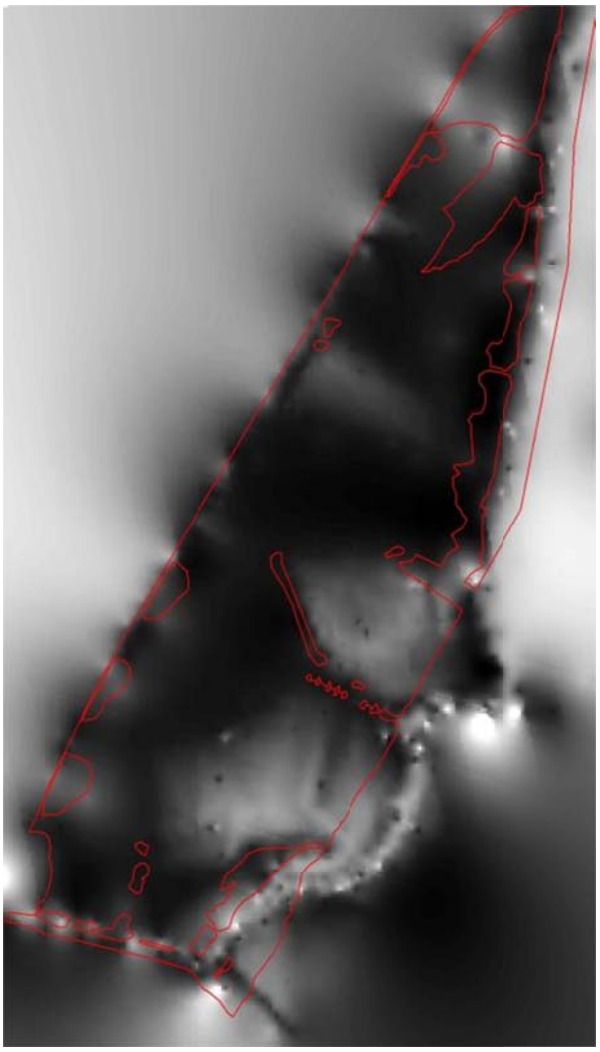

Figure 4.4. Depth raster (bathymetry) of Redfish Bay derived from multiple sources. Areas outside of the study area or on land were masked during the process.

Cho's depth correction algorithm (Equation 4.1) was then applied to each of the 5 bands, to correct for depth attenuation:

$$(R + 14 - R_w) / (1 - A_w/200)^2 \quad (4.1)$$

where R is the reflectance value, the pixel value found in each band pixel, expressed as a percentage, R_w is the water scattering coefficient for the depth found in the bathymetry raster, and A_w is the water absorption coefficient for the depth found in the bathymetry raster. After corrections, the bands were re-stacked and opened in ENVI 5.0 for classification using ENVI's classification workflow.

The first step in the ENVI process is to specify the image being processed and any mask to be used. A mask specifies that area which is to be analyzed, and conversely, the areas to be omitted from analysis. The mask for this iteration eliminates processing of land areas within the study area. In future iterations, the mask will reduce the analysis to only areas which are to be reprocessed.

The workflow in ENVI categorizes pixels within the image into groups of pixels with similar characteristics. For the first iteration, 25 categories were created, each having similar pixel values. These categories were then aggregated into polygons with a minimum of 9 pixels (9 m^2). These categorized polygons were then exported as ESRI shapefiles.

Vector processing

The polygons generated in ENVI version 5 are categorized as 'Class 1', 'Class 2', through 'Class 25'. Each of these categories represents groups of pixels with similar pixel digital numbers, with no association to species types. To derive species types from these classes, the polygons are reclassified in ESRI's ArcGIS 10.0. Each class is attributed with the learning points that fall within the polygons of that class. A custom process was created that selects all the learning points that fell within a selected class, and then selects all the polygons that contain those learning points. Each selected polygon was then

attributed with the codes for learning points that fell within them, and then with the species names or descriptive note, as shown in Table 4.2. Asterisks indicate that an attribute has been derived, based on the learning points that fell within other polygons within the same class. The entire class was then selected and attributed with a list of all the codes that fell within that class, and then the species code or descriptive note. This process was repeated for the next class, until all the classes of polygons were processed and attributed.

Table 4.2. Attribute table with classification data for Redfish Bay. Asterisks denote a derived classification.

CLASS_NAME	AREA	MainSpecie	grassType
Class 1	47	1 H100	*Halodule*
Class 1	150,020	1 H75T25	MixedMono
Class 1	4,687	* 1 H100, 1 H75T25	Mixed
…	…	…	…
Class 2	12	* 1 B100, 3 H100, 1 T100, 1 T50S50, 1	Mixed
…	…	…	

After all the classes were attributed thusly, the ‘Mixed’ and ‘No Clues’ categories were removed, and used to create a mask for the next iteration.

The second iteration

A set of training points was selected and buffered. Buffering refers to a process that creates a polygon of a specified width that surrounds the location of the training point. The polygons created in the first iteration that were classed as ‘Mixed’ or ‘No Clues’ were removed from the first iteration output. The buffers from the training points and the removed classes were merged to create a mask for the second iteration. This mask

was opened in ENVI along with the corrected 5-band image. The classification workflow was again initiated, and the masked area of the image was categorized into 10 categories of similar pixels, which were then aggregated into groups of 9 or more contiguous pixels, similar to the process described in Chapter II.

The third iteration

The 'Mixed and 'No Clues' classes from the second iteration formed the mask for the third iteration, along with the buffered learning point polygons. These were again processed in ENVI 5.0, which created categories of like pixel values and then assigned to one of five output categories, which were then aggregated to minimum groupings of 9 contiguous pixels. These were exported as an ESRI shapefile, which were then reclassified using the learning points, as described above.

The fourth iteration

A mask formed from the 'Mixed' and 'No Clues' classes from the third iteration was applied to the classification workflow within ENVI 5.0 to the same depth-corrected image. In this iteration, a supervised classification was selected, using a training data set developed previously and described in Chapter II. The supervised classification, using the 'Most Likely' classification algorithm, classed each polygon as being either 'Bare', '*Halodule'*, '*Ruppia'*, '*Thalassia'*, MixedMono, or 'Unclassified', to match those of the training data set. Since the unclassified category was 'Mixed' before the last iteration, it will be returned to a 'Mixed' category.

RESULTS

Figure 4.5 shows the classified polygons from the first iteration, and Table 4.3 shows the area and number of polygons in each class. Figure 4.6 shows the polygons from the first and second iterations. Table 4.4 shows the combined results of iterations one and two. Figure 4.7 shows the polygon output from the third iteration of processing. Table 4.5 shows the combined number and area of polygons. Table 4.7, from Chapter II, shows the final output from that previous processing, while the final output polygons from this chapter are mapped in Figure 4.8. The number of polygons and area of each class may be found in Table 4.6 and represents the final results of the processing from this chapter. Table 4.8 below shows the differences between those two tables. There are approximately 17,265 more *Thalassia* polygons in the processing from Chapter IV, 5,183 fewer 'Mixed' polygons, 12,034 more polygons classified as 'MixedMono', 19,241 more polygons classified as *Halodule*, 5,219 fewer classified as *Ruppia*, 3,528 more classified as 'Bare', 24,158 fewer classified as 'Bare/*Thalassia* Mix', 26,890 more classified as 'Bare/*Halodule* Mix', and one less polygon classified as *Syringodium*.

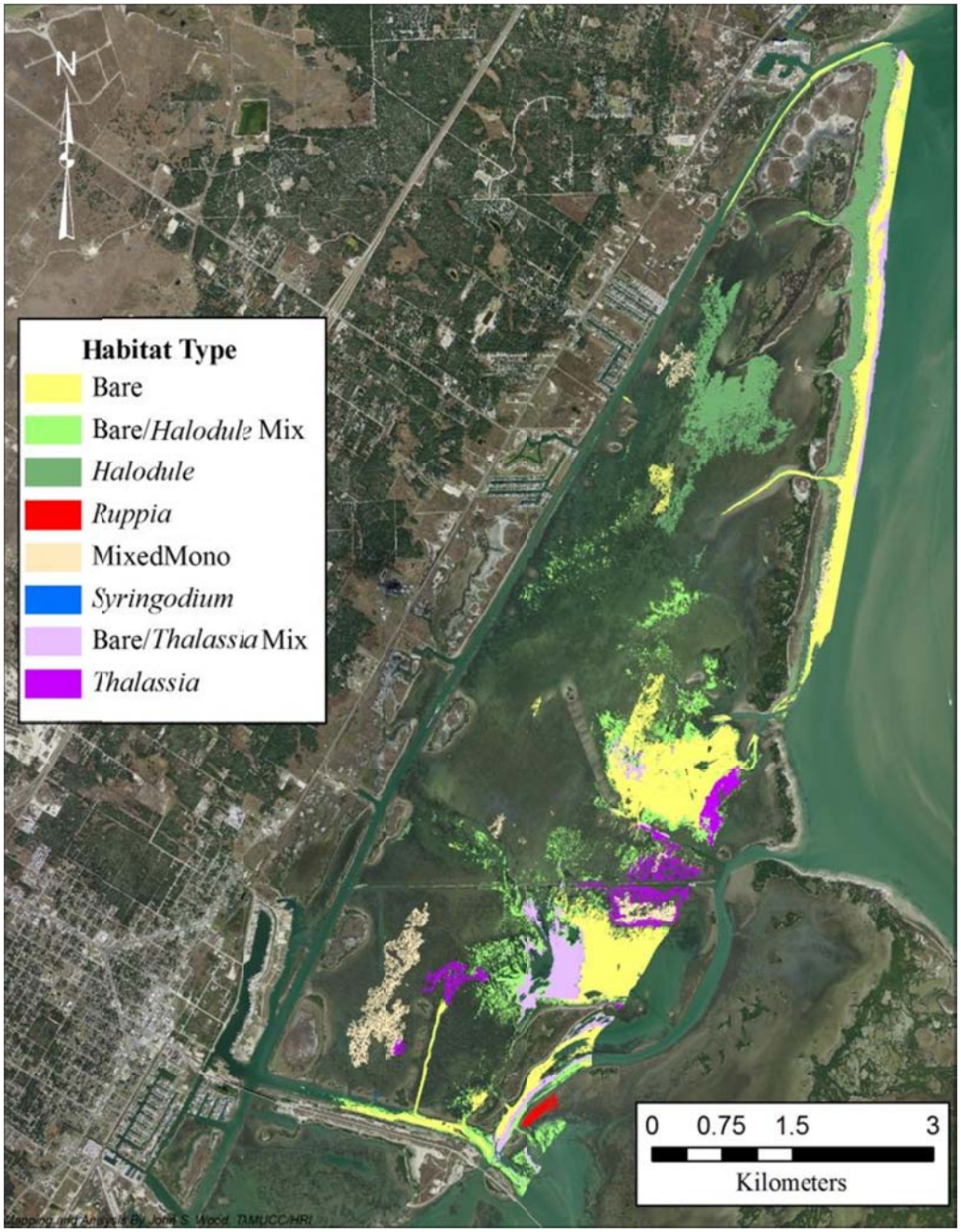

Figure 4.5. Results from first iteration. The 'Mixed' and 'No Clues' classes have been removed.

Table 4.3. Results from the first iteration. The number of polygons in the 'Mixed' and 'No Clues' Classes were unavailable.

Classification	Number of Polygons	Total Area in Class (m^2)
Bare	766	2,797,248
Bare/*Halodule* Mix	7,302	1,327,681
Bare/*Thalassia* Mix	1,185	767,466
Halodule	629	1,553,438
Mixed		19,528,531
MixedMono	28	527,852
No Clues		89,608
Ruppia	5	40,667
Syringodium	1	1,042
Thalassia	18	409,374
TOTALS	N/A	27,042,907

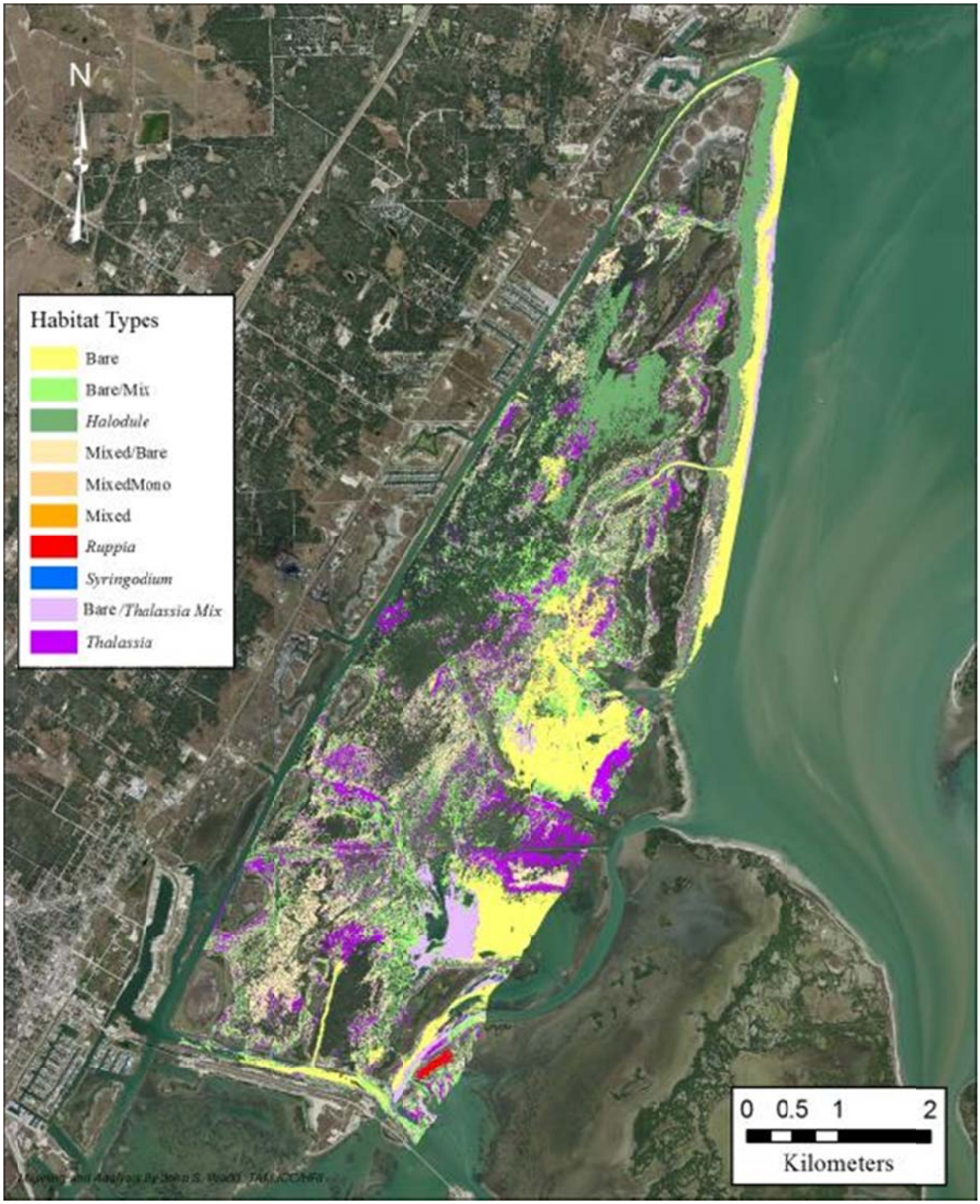

Figure 4.6. Output polygons from the second iteration. The 'Mixed' and 'No Clues' classes have been removed.

Table 4.4. Combined results of iterations 1 and 2, showing total areas and numbers of polygons.

Classification	Number of Polygons	Total Area in Class (m^2)
Bare	769	3,193,578
Bare/*Halodule* Mix	29,135	3,115,812
Bare/*Thalassia* Mix	1,185	767,466
Halodule	20,496	3,288,339
MixedMono	18,915	2,829,819
Ruppia	6	41,449
Syringodium	1	1,042
Thalassia	18,658	2,488,805
TOTALS	89,165	15,726,310

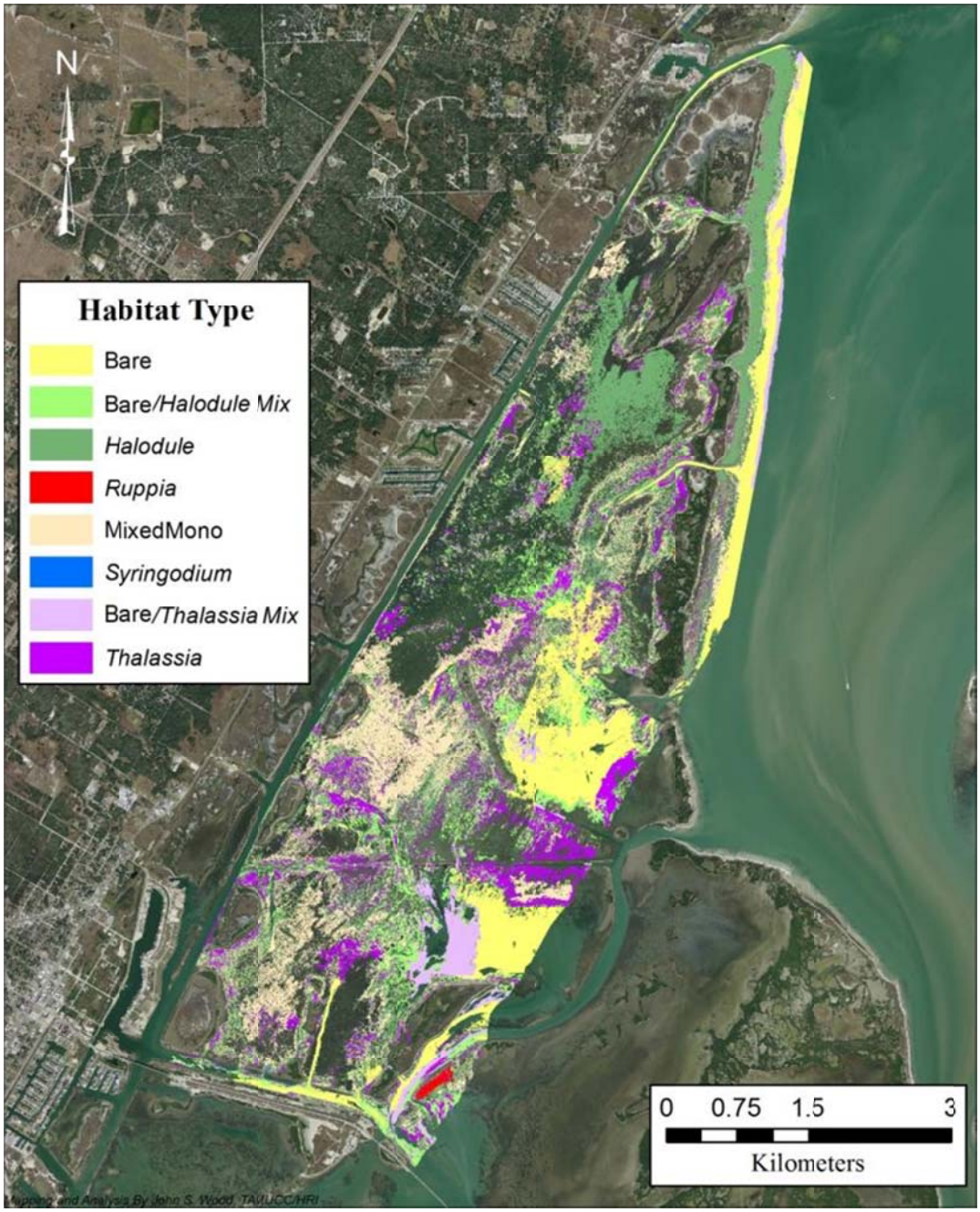

Figure 4.7. The output from the third iteration of reprocessing.

Table 4.5. Combined output from the first three iterations.

Classification	Number of Polygons	Total Area in Class
Bare	773	3,195,229
Bare/*Halodule* Mix	29,135	3,115,812
Bare/*Thalassia* Mix	1,185	767,466
Halodule	20,505	3,305,144
MixedMono	18,925	3,583,676
Ruppia	7	41,478
Syringodium	1	1,042
Thalassia	18,661	2,489,748
TOTALS	89,192	16,499,595

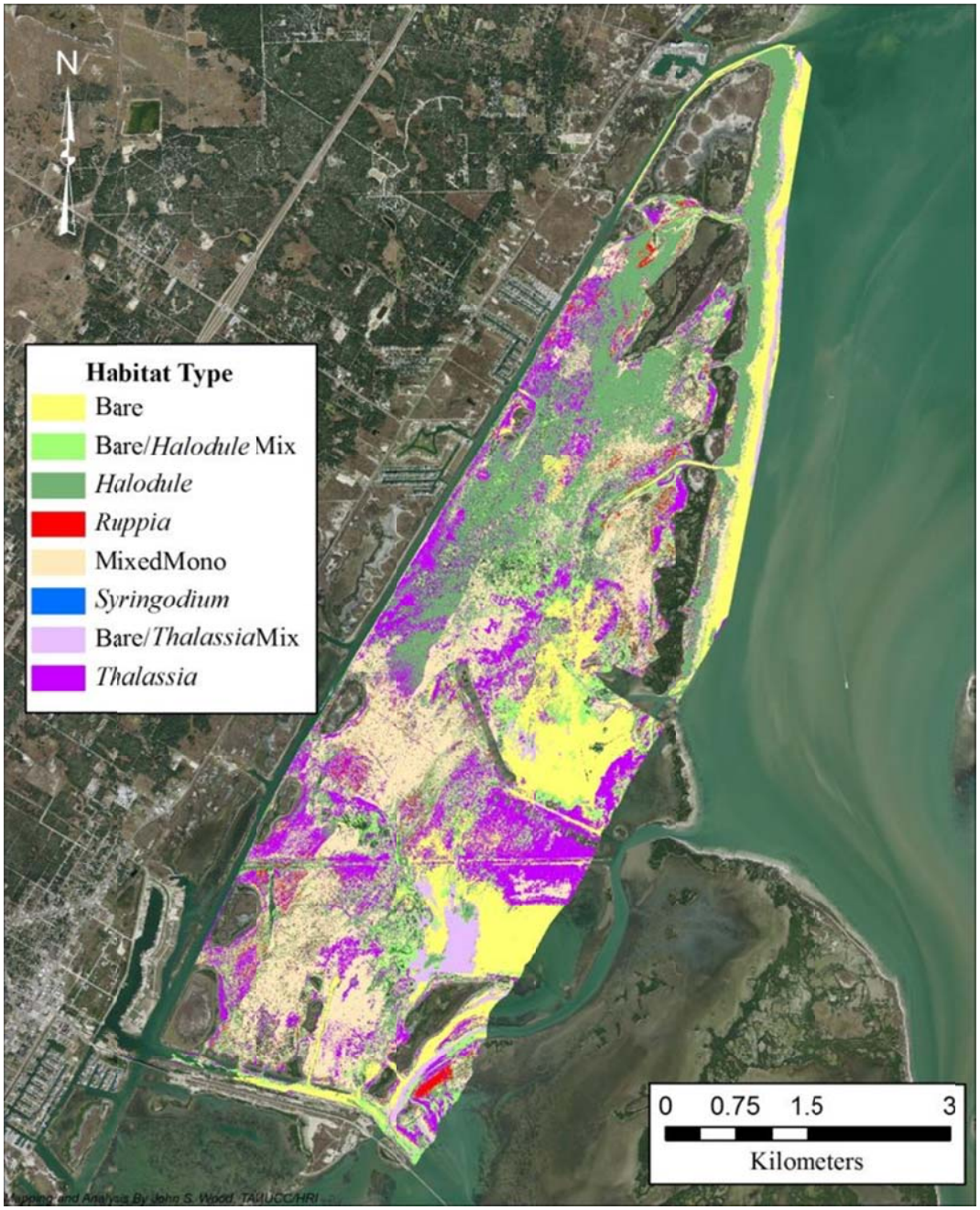

Figure 4.8. The final output from reprocessing using a depth correction and improved band selection.

Table 4.6. Results of iterations 1-4, with area and number of polygons found in each class. These are the final results of the reprocessing.

Classification	Number of Polygons	Total Area in Class (m^2)	Mean Area/Polygon (m^2)
Thalassia	39,303	4,857,068	123.5
Mixed	13,925	1,350,628	96.99
MixedMono	31,545	6,016,575	190.73
Halodule	33,209	6,125,249	184.445
Ruppia	7,437	462,619	62.205
Bare	6,482	4,120,545	635.6904
Bare/*Thalassia* Mix	1,185	767,466	647.6506
Bare/*Halodule* Mix	29,135	3,115,812	106.944
Syringodium	1	1,042	1042
TOTALS	162,222	26,817,004	165.31

Table 4.7. The final number of polygons and the area of each classification from the final iteration in the first set of processing from Chapter II.

Classification	Number of Polygons	Total Area in Class (m^2)	Mean Area/Polygon (m^2)
Thalassia	22,038	4,976,130	225.80
Mixed	19,108	4,362,722	228.32
MixedMono	19,511	3,701,172	189.70
Halodule	13,968	3,608,193	258.32
Ruppia	12,656	3,585,130	283.28
Bare	2,954	3,537,991	1197.69
Bare/*Thalassia* Mix	25,343	3,476,164	137.16
Bare/*Halodule* Mix	2,245	587,547	261.71
Syringodium	2	38,009	19,004.50
TOTALS	117,825	27,873,058	21,786.48

Table 4.8. The differences in areas and number of polygons between the classifications in Chapter II and Chapter IV. Results from Chapter II were subtracted from those from Chapter IV.

Classification	Number of Polygons	Total Area in Class	Mean Area/Polygon (m^2)
Thalassia	17,265	-119,062	-102
Mixed	-5,183	-3,012,094	-131
MixedMono	12,034	2,315,403	1
Halodule	19,241	2,517,056	-74
Ruppia	-5,219	-3,122,511	-221
Bare	3,528	582,554	-562
Bare/*Thalassia* Mix	-24,158	-2,708,698	510
Bare/*Halodule* Mix	26,890	2,528,265	-155
Syringodium	-1	-36,967	-17,963

There are also major differences in the area within each class, with the largest declines in the areas classified as *Ruppia*, with 312 fewer hectares, 'Mixed' with 300

fewer hectares, 'Bare/*Thalassia* Mix' with 270 fewer hectares. Increases were noted in the areas of 'MixedMono' classification, with 232 more hectares than previous, *Halodule* with 252 more hectares, and 'Bare/*Halodule* Mix', with 252 more hectares.

Figure 4.9 shows the proportions of coverage by each class from Chapter IV, while Figure 4.10 shows the proportions from the classification performed in Chapter II for comparison.

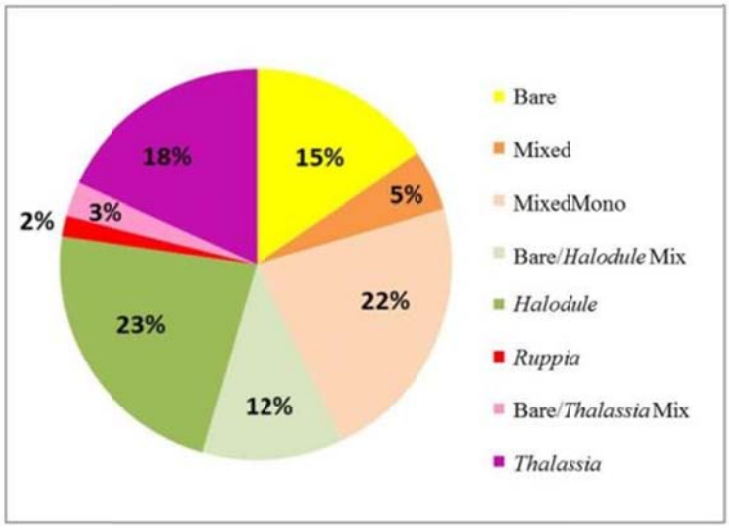

Figure 4.9. The benthic habitat makeup of Redfish Bay, Texas.

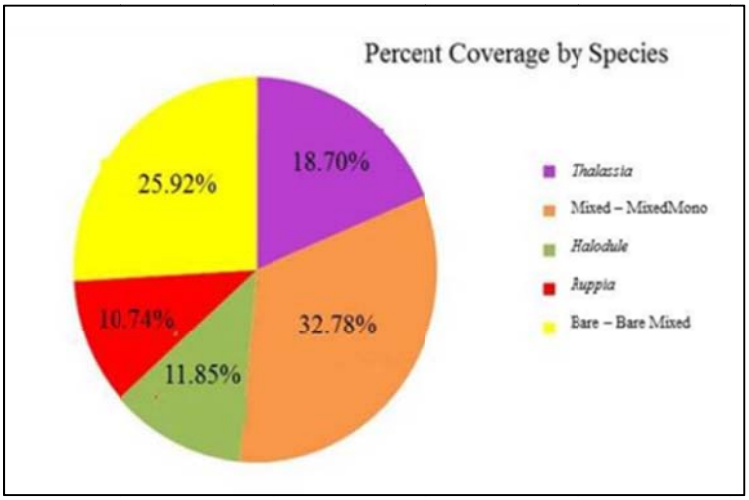

Figure 4.10. Benthic habitat proportions from Chapter II.

The accuracy assessment for the final iteration of this processing, shown in Table 4.9, shows a substantial improvement from the methods used in Chapter II. The overall accuracy improved from 38% to approximately 57%. Producer's accuracy for the 'Bare' class increased from 66.67% to 73.08%, for *Halodule*, the increase was from 29% to 63.89%. The accuracy for *Thalassia* actually decreased from 46.15% to 45.83%, while accuracy for the 'MixedMono' class increased from 23.33% to 47.37%. User's accuracies also show a dramatic increase in all classes except 'Bare', which decreased from almost 70% to 66%. *Halodule* accuracy went up from 39% to 64%, *Thalassia* accuracy increased from 40% to 55%, and 'MixedMono' increased from 22.58% to 39%. The Kappa Coefficient also increased, from 0.2988 to 0.4459, providing another indication that there is an even less likelihood that an area was classified correctly by chance agreement only.

When the 'Grass' classes are aggregated to calculate Presence/Absence as in Chapter II, very little difference in Accuracy Assessment is noted. The overall accuracy actually decreased from 87.93% to 86.11%, while the User's accuracy for the 'Bare' class increased from 72.7% to 73.08%, and the 'Grass' class User's accuracy decreased from 91.5% to 90.24%. Producer's accuracies increased from 66.7% for the 'Bare' class to 70.4%, while the 'Grass' class Producer's accuracy decreased from 93.5% to 91.4%. Kappa Coefficient for this calculation is 0.641, a very slight increase from the .6206 obtained in Chapter II.

Table 4.9. Confusion matrix details the accuracy assessment for the classifications generated using the improved band selection and water depth corrections using a depth raster.

Accuracy Assessment and Confusion Matrix

	Bare	*Halodule*	*Ruppia*	*Thalassia*	MixedMono	
Bare	19	3	0	1	3	73%
Halodule	2	24	0	4	6	63%
Ruppia	0	1	0	0	2	0%
Thalassia	3	5	0	12	4	50%
MixedMono	3	3	1	4	8	42%
	70%	67%	0%	57%	35%	57%

Producer's Accuracy		**User's Accuracy**	
Bare	73%	Bare	70%
Halodule	63%	*Halodule*	67%
Ruppia	0%	*Ruppia*	0%
Thalassia	50%	*Thalassia*	57%
MixedMono	42%	MixedMono	35%
Overall Accuracy	57%		
Kappa Coefficient	.4459		

CONCLUSIONS

The addition of a depth (bathymetric) raster and application of a depth correction combined with band selection based on *in situ* spectral sampling greatly improved the accuracy of benthic habitat classification using hyperspectral imagery. These findings concur with those of Fyfe and Dekker (2001). However, the specific wavelengths recommended by Fyfe are different than those used in this research. Therefore, it is highly recommended that future seagrass mapping efforts using hyperspectral imagery

include not only extensive field site visits, but also include the extensive use of portable spectrometer data collection and analysis of that data to determine the best bands for the species of seagrasses that may be present.

Lee (2003) extolls the virtues of the fusion of complementary data sets, such as hyperspectral imagery and bathymetry, in benthic habitat mapping research. Lee used airborne laser bathymetry in conjunction with hyperspectral imaging, as did Lyzenga (1985). Lee points out that such fusion comes with its own set of problems; there are varying levels of abstraction at which the fusion may take place, and data sets must be registered with each other and brought to a common scale or resolution. There are also limits to which this fusion is applicable. Lee uses the term Maximum Surveyable Depth (MSD), describing the maximum depth at which existing mapping standards can be met. According to Lee, the MSD for Airborne Lidar Bathymetry (ALB) can range from 50 m in clear waters to 10 m in murky waters, or usually two to three times the Secchi depth. Wang and Philpot (2007) concur with Lee, but point out one critical factor: there is also a minimum depth at which ALB is capable of capturing accurate measurements – stated at 1.5 m. Since the study area average depth is less than 1.5 m, and the maximum natural depth is around 2 m, ALB may not be suitable for fusion into the hyperspectral image processing. Bachmann (2008) states that at less than 2 m, ALB systems do not provide reliable depth retrieval.

So, depth measurements (bathymetry) are critical to accurately discriminating species of SAV using hyperspectral imagery, but ALB measurements aren't reliable under 2 m, the depth where seagrass is found in these shallow bays systems. But there is good news: scientists with the U.S. Army Engineer Research and Development Center

are developing an integrated hyperspectral imaging/lidar collecting system, capable of +/- 30 cm vertical accuracy with a 4 m spot spacing. While this is still not quite accurate enough to take full advantage of the depth correction algorithm developed by Cho (2010), this is a sign that improved technology available in the near future may do just that.

This research demonstrates that increases in accuracy of benthic habitat mapping are achievable by using depth corrections and site specific band selection. While depth corrections described in Chapter II were calculated using an approximation of depth, an average 65 cm, calculations in this chapter were accomplished using a bathymetry developed from various sources of varying and unverifiable accuracy. Therefore, it is difficult to determine which factor – depth corrections or site specific band selection – would have the largest influence in the accuracy of the output data set.

CHAPTER V: SUMMARY AND CONCLUSIONS

SUMMARY

The research described in this dissertation is part of a collaborative effort organized and funded by the National Oceanic and Atmospheric Administration (NOAA), through the Environmental Science Cooperative Science Center (ECSC). A series of hyperspectral imaging flights were executed over Texas Coastal Bend areas, including over Redfish Bay, located between Aransas Pass and Port Aransas, Texas. One of several planned uses of this imagery was to discriminate between species of seagrasses in Redfish Bay.

This hyperspectral imagery was collected with an AISA (Airborne Imaging Spectroradiometer for Applications) Eagle Hyperspectral sensor capable of collecting spectral data in the range of 400 – 1000 nm, in as many as 272 bands (Green and Cole 2005). For these missions, 63 bands were collected, each about 9-10 nm wide. Imagery is collected in a 'pushbroom' fashion, one line containing 1024 pixels at a sweep, followed by the next line, and so forth. The instrument incorporates an integrated inertial system, GPS and gyroscope, so that imagery and positional data are collected simultaneously and stored synchronously (Bertels *et al.* 2005).

Prior to imagery collection, a field survey team visited approximately 250 randomly selected sites, and recorded the location with an RTK-enabled GPS, noting depth, and species presence, absence and makeup. These were transcribed into an Excel spreadsheet, which was then converted into an ESRI (Environmental Systems Research Institute) shapefile for later use.

Georectified imagery was saved on a portable hard drive and was atmospherically corrected before delivery. This project used 9 of the delivered images, each covering approximately 1 km width, and 8 – 14 km in length. The images were mosaicked to form one image, covering approximately 3250 hectares. From this image, 5 bands were selected, based on recommendations found in literature (Fyfe 2003, Cho and Lu 2010).

The selected bands were then corrected for depth, using an algorithm developed by Cho (2010), using an average depth of 65 cm that was applied to the individual bands in ENVI (ENvironment for Visualizing Images) 4.8, using the 'Band Math' function, and the formula

$$(R_w/10 - R_w) / (1- A_w/200)^2 \quad (5.1)$$

where R_w is the percent surface and volumetric reflectance, and A_w is the coefficient for water absorption in the water column in both up and down directions.

After depth correction, the image was opened in ENVI EX 4.8, and a classification workflow initiated. In this workflow, the image is segmented into groups of like pixel values, and then classified into 25 classes of similar segments. These classes were aggregated into no fewer than 9 similar pixels, and exported as an ESRI shapefile.

This shapefile was then opened in ESRI's ArcGIS 10.0, and a classification was selected. Using this selection, all points representing field sites that fell within selected polygons were then selected, as shown in Table 5.1. Each polygon that contained a field site point was then attributed with the type of seagrass found there. This was repeated until all 25 classes were exhausted. Once all the classes were reclassified, the 'Mixed' classes were then exported for use as a mask for the next iteration.

Table 5.1. ArcGIS data table with classification data for Redfish Bay. Note that the first line of the table contains fieldnames.

CLASS_NAME	AREA	MainSpecie	grassType
Class 1	47	1 H100	*Halodule*
Class 1	150,020	1 H75T25	MixedMono
Class 1	4,687	* 1 H100, 1	Mixed
…	…	…	…
Class 2	12	* 1 B100, 3	Mixed
…	…	…	

The image was then reopened in ENVI, and the classification/segmentation process repeated for only those areas within the newly created mask. The ENVI output was then subjected to the same process in ArcGIS. This reiterative processing was repeated through 3 iterations, and then again, using a 'supervised' classification. All output files were then merged into a single shapefile (see Table 5.2) and an accuracy assessment was performed, with the results as shown in Table 5.3.

Table 5.2. The final number of polygons and sums of the areas of each classification from the initial processing.

Classification	Number of Polygons	Total Area in Class
Bare	2,954	3,537,991
Bare/*Halodule* Mix	2,245	587,547
Bare/*Thalassia* Mix	25,343	3,476,164
Halodule	13,968	3,608,193
Mixed	19,108	4,362,722
MixedMono	19,511	3,701,172
Ruppia	12,656	3,585,130
Syringodium	2	38,009
Thalassia	22,038	4,976,130
TOTALS	117,825	27,873,058

Table 5.3. The accuracy assessment from the initial processing.

Producer's Accuracy		User's Accuracy	
Bare	66.67%	Bare	69.57%
Halodule	29.03%	*Halodule*	39.13%
Thalassia	46.15%	*Thalassia*	40.00%
Ruppia	0.00%	*Ruppia*	0.00%
MixedMono	23.33%	MixedMono	22.58%
Overall Accuracy	37.93%		
Cohen's Kappa	0.2988		

To further understand these results, we returned to Redfish Bay with an Ocean Optics Jaz portable spectrometer and collected reflected radiance spectra. These samples were collected over areas with 100% coverage of *Halodule* or *Thalassia* at various depths up to 110 cm. The sensor was placed at three positions: above the surface of the water, just below the air/water interface, and at the canopy level. Each spectral sample was imported into an Excel spreadsheet, where it was converted from spectral irradiance to percent reflectance. Mean spectra of both species at each level were plotted (see Figure 5.1) and analyzed. We found that there are detectable spectral differences between *Halodule* and *Thalassia*, at all three positions.

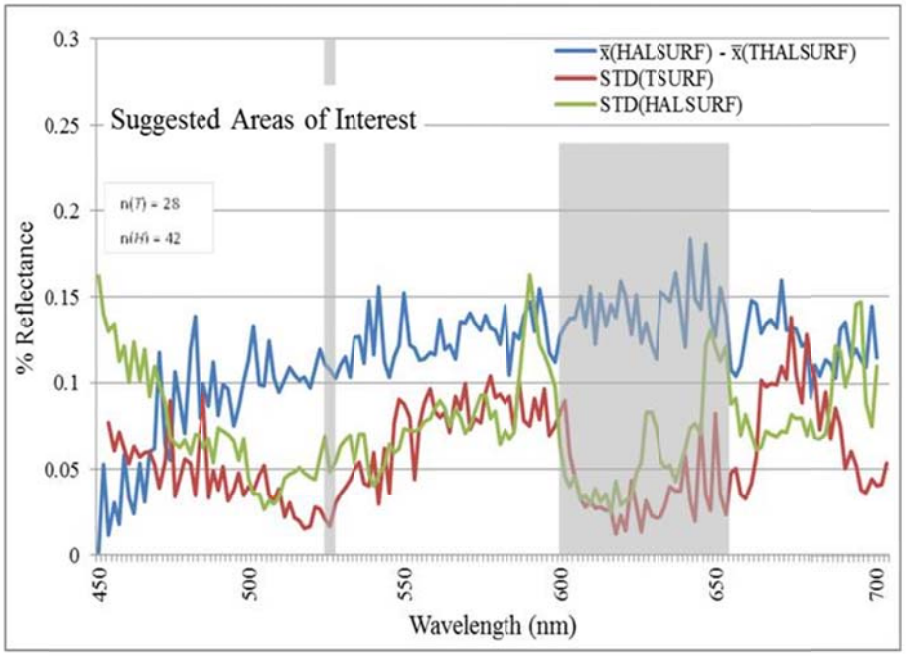

Figure 5.1. Suggested areas for band selection would be between 600 – 660 nm, as well as 535 nm for a reference point where there is little difference between the bands. These areas are selected because there is a detectable amount of difference between the species at these wavelengths and no overlap in the standard of deviations of the spectral curves.

We also noted that, for subsurface and canopy levels, there was considerable overlap of the standard deviations of the spectral curves. However, there was no overlap for spectral curves of above-surface spectral measurements. This indicates that areas with larger differences in the mean spectral curves, but having smaller standard deviations, would be acceptable recommendations for bands discriminating between the species.

Armed with this new information, we returned to the original hyperspectral imagery collected over Redfish Bay. We selected from the original, uncorrected 63 band imagery 5 bands, centered on 535, 600, 619, 638 and 656 nm. These bands were separated and individually corrected for depth, using a depth raster that had been reclassified as coefficients for water absorption and water scattering relative to each

bandwidth. The bands were then re-stacked, and classified in ENVI, then reclassified to species in ArcGIS, following the same iterative procedures detailed earlier. Accuracy assessments were performed for the output classified polygons, and the results of that assessment are shown in Table 5.4.

Table 5.4. Results of the accuracy assessment performed on the output from the second processing of the hyperspectral imagery of Redfish Bay. The results were considerably better with the new band selections and depth corrections applied via a depth raster (bathymetry).

Producer's Accuracy		**User's Accuracy**	
Bare	73%	Bare	70%
Halodule	63%	*Halodule*	67%
Ruppia	0%	*Ruppia*	0%
Thalassia	50%	*Thalassia*	57%
MixedMono	42%	MixedMono	35%
Overall Accuracy	57%		
Kappa Coefficient	.4459		

CONCLUSIONS

Shortcomings

As with most research, there are several shortcomings related to this study. A good bathymetry dataset is critical to the analysis of hyperspectral imagery. This critical component to many research projects is severely lacking not only in Redfish Bay and in Texas, but throughout the estuarine research community. A 1999 survey by the NOAA Coastal Services Center identified near-shore bathymetry, coastal topography and bay bathymetry as "very useful" by at least two-thirds of the respondents, and who listed it in the top ten data needs (Gesch and Wilson 2001). Studies of these dynamic environments

that experience both erosion and accretion require a high-resolution, up-to-date measurements. Besides being a huge asset to planning, navigation and field site placement, bathymetry is a necessary component for depth correction, which is critical for analysis at subsurface levels. Fortunately, the need for highly accurate bathymetry is recognized, and the USGS and NOAA's National Ocean Service and others are working collaboratively to develop tools and techniques for meeting that need. Two leading technologies are emerging: LiDAR and Optical Analytical both offer hope for high resolution datasets with accuracies approaching 15 cm and the ability to cover large areas (Sánchez-Carnero *et al.* 2012).

Another shortcoming recognized within this research is that benthic coverage by drift macroalgae is basically ignored, although it can and does cover as much as 90% of the benthic habitat. Drift macroalgae is ephemeral, drifting over the top and settling on the seagrass beds and in depressions such as scars. As the currents change, the drifting algae shift positions. Drift material is a valuable resource because it tends to have elevated nitrogen levels (Britton-Simmons *et al.* 2012). In this study, macroalgae is treated more as a confounding element rather than a substantial contribution to the benthic community.

Likewise, another important benthic habitat is considered as 'Bare', when it deserves its own classification. Oyster reefs found in numerous locations throughout the study area remain classified as 'Bare', although they are often far from being bare, but rather are recognized as a productive benthic habitat in their own right, serving multiple ecologic functions including improving water clarity and providing shoreline protection (Pollack *et al.* 2011).

Future research

Research in this area will no doubt continue, and should include the use of spectrometer sampling at numerous locations, expanding to include not only seagrass beds, but several other benthic habitat types such as oyster reefs and shell hash bare areas. Collection of signatures from several types of bare areas could allow discrimination of these important habitat types, as well as aid in discrimination of seagrass types.

Future studies of this type will benefit from incorporating bathymetric measuring systems such as LiDAR. There are several studies being conducted that will aid in melding the spectral and bathymetric data sets. As well, future studies should also include mapping both real and potential biomass, as well as predicting areas of species expansion based on contemporary conditions. Finally, future studies should examine the relationship between accretion of sediment and decreases in bathymetry in relationship to sea level rise.

Literature Cited

Ackleson, S. and V. Klemas. 1987. Remote sensing of submerged aquatic vegetation in Lower Chesapeake Bay: a comparison of Landsat MSS to TM imagery. Remote Sensing of Environment 22:235-248.

Agawin, N. S. R. and C. M. Duarte. 2002. Evidence of direct particle trapping by a tropical seagrass meadow. Estuaries and Coasts 25:1205-1209.

Albert, A. and C. Mobley. 2003. An analytical model for subsurface irradiance and remote sensing reflectance in deep and shallow CASE-2 waters. Optics Express 11:2873-2890.

Armstrong, R. A. 1993. Remote-sensing of submerged vegetation canopies for biomass estimation. International Journal of Remote Sensing 14:621-627.

Artigas, F. J. and J. Yang. 2004. Hyperspectral remote sensing of habitat heterogeneity between tide-restricted and tide-open areas in the New Jersey Meadowlands. Urban Habitats 2.

Artigas, F. J. and J. Yang. 2006. Spectral discrimination of marsh vegetation types in the New Jersey Meadowlands, USA. Wetlands 26:271-277.

Artigas, F. J. and J. S. Yang. 2005. Hyperspectral remote sensing of marsh species and plant vigour gradient in the New Jersey Meadowlands. International Journal of Remote Sensing 26:5209-5220.

Baden, S., M. Gullström, B. Lundén, L. Pihl, and R. Rosenberg. 2003. Vanishing seagrass (*Zostera marina, L.*) in Swedish coastal waters. AMBIO: A Journal of the Human Environment 32:374-377.

Ball, G. H. and D. J. Hall. 1965. ISODATA, a novel method of data analysis and pattern classification. Contract Nonr 4918(00), DTIC Document, Menlo Park.

Barbier, E. B., E. W. Koch, B. R. Silliman, S. D. Hacker, E. Wolanski, J. Primavera, E. F. Granek, S. Polasky, S. Aswani, and L. A. Cramer. 2008. Coastal ecosystem-based management with nonlinear ecological functions and values. Science 319:321-323.

Barillé, L., M. Robin, N. Harin, A. Bargain, and P. Launeau. 2010. Increase in seagrass distribution at Bourgneuf Bay (France) detected by spatial remote sensing. Aquatic Botany 92:185-194.

Beck, M. W., K. L. Heck Jr, K. W. Able, D. L. Childers, D. B. Eggleston, B. M. Gillanders, B. Halpern, C. G. Hays, K. Hoshino, and T. J. Minello. 2001. The identification, conservation, and management of estuarine and marine nurseries for fish and invertebrates. BioScience 51:633-641.

Beck, M. W., W. L. Kruczynski, and P. F. Sheridan, editors. 2007. Conclusions: importance of Gulf of Mexico seagrasses. U.S. Geological Survey Scientific Investigations Report 2006-5287.

Bertels, L., B. Deronde, P. Kempeneers, and E. Tortelboom. 2005. Potentials of airborne hyperspectral remote sensing for vegetation mapping of spatially heterogeneous

dynamic dunes, a case study along the Belgian coastline. Pages 153-163 *in* Proceedings 'Dunes and Estuaries' – International Conference on Nature Restoration Practices in European Coastal Habitats. VLIZ Special Publication 19, Koksijde, Belgium.

Beyer, T. G., M. Rasser, and S. Morehead. 2007. Development of a comprehensive habitat map for the Mission Aransas NERR using the NERRS habitat classification scheme: Matagorda Island, Texas. Mission-Aransas National Estuarine Research Reserve.

Bittler, K. 2011. Salinity Gradients in the Mission-Aransas National Estuarine Research Reserve. Research Paper. University of Texas, Austin, Texas.

Boström, C., E. L. Jackson, and C. A. Simenstad. 2006. Seagrass landscapes and their effects on associated fauna: a review. Estuarine, Coastal and Shelf Science 68:383-403.

Bréda, N. J. J. 2003. Ground‐based measurements of leaf area index: a review of methods, instruments and current controversies. Journal of Experimental Botany 54:2403-2417.

Britton-Simmons, K. H., A. L. Rhoades, R. E. Pacunski, A. W. E. Galloway, A. T. Lowe, E. A. Sosik, M. N. DEthier, and D. O. Duggins. 2012. Habitat and bathymetry influence the landscape-scale distribution and abundance of drift macrophytes and associated invertebrates. Limnology and Oceanography 57:176.

Burfeind, D. D. and G. W. Stunz. 2006. The effects of boat propeller scarring intensity on nekton abundance in subtropical seagrass meadows. Marine Biology 148:953-962.

Buskey, E. J. and C. J. Hyatt. 1995. Effects of the Texas (USA) 'brown tide' alga on planktonic grazers. Marine Ecology Progress Series 126:285-292.

Buskey, E. J., B. Wysor, and C. Hyatt. 1998. The role of hypersalinity in the persistence of the Texas ‘brown tide’ in the Laguna Madre. Journal of plankton research 20:1553-1565.

Casazza, G., C. Silvestri, and E. Spada. 2002. The use of bio-indicators for quality assessments of the marine environment: Examples from the Mediterranean Sea. Journal of Coastal Conservation 8:147-156.

Chen, Z., F. E. Muller-Karger, and C. Hu. 2007. Remote sensing of water clarity in Tampa Bay. Remote Sensing of Environment 109:249-259.

Cho, H. J. and D. Lu. 2010. A water-depth correction algorithm for submerged vegetation spectra. Remote Sensing Letters 1:29 - 35.

Cho, H. J., D. Mishra, and J. Wood. 2012. Remote Sensing of Submerged Aquatic Vegetation,.*in* D. B. Escalante, editor. Remote Sensing - Applications. InTech.

Ciraolo, G., E. Cox, G. La Loggia, and A. Maltese. 2006. The classification of submerged vegetation using hyperspectral MIVIS data. Annals of Geophysics 49:287-294.

Cohen, J. 1960. A coefficient of agreement for nominal scales. Educational and psychological measurement 20:37-46.

Cohen, J. E., C. Small, A. Mellinger, J. Gallup, and J. Sachs. 1997. Estimates of coastal populations. Science 278:1209.

Coles, C. 2004. Marine mapping and monitoring. The Futurist 38:11.

Congalton, R. G. 1991. A review of assessing the accuracy of classifications of remotely sensed data. Remote Sensing of Environment 37:35-46.

Costanza, R., R. d'Arge, R. De Groot, S. Farber, M. Grasso, B. Hannon, K. Limburg, S. Naeem, R. V. O'Neill, and J. Paruelo. 1997. The value of the world's ecosystem services and natural capital. Nature 387:253-260.

Cowper, S. W. 1978. The drift algae community of seagrass beds in Redfish Bay, Texas. Contributions in Marine Science 21:125-132.

Cracknell, A. 1999. Remote sensing techniques in estuaries and coastal zones an update. International Journal of Remote Sensing 20:485-496.

Craig, S. E., S. E. Lohrenz, Z. Lee, K. L. Mahoney, G. J. Kirkpatrick, O. M. Schofield, and R. G. Steward. 2006. Use of hyperspectral remote sensing reflectance for detection and assessment of the harmful alga, Karenia brevis. Applied Optics 45:5414-5425.

Dash, J. and P. Curran. 2004. The MERIS terrestrial chlorophyll index. International Journal of Remote Sensing 25:5003-5013.

Dekker, A. G., V. E. Brando, and J. M. Anstee. 2005. Retrospective seagrass change detection in a shallow coastal tidal Australian lake. Remote Sensing of Environment 97:415-433.

Diaz, R. J., M. Solan, and R. M. Valente. 2004. A review of approaches for classifying benthic habitats and evaluating habitat quality. Journal of Environmental Management 73:165-181.

Dobson, E. and P. Dustan. 2000. The use of satellite imagery for detection of shifts in coral reef communities. Proceedings, American Society for Photogrammetry and Remote Sensing, 22-26 May, Washington, DC.

Duarte, C. and H. Kirkman. 2001. Methods for the measurements of seagrass abundance and depth distribution. Pages 141-154 *in* F. Short, and Coles, RG, editor. Global seagrass research methods. Elsevier Press, Amsterdam.

Duarte, C. M. 1999. Seagrass ecology at the turn of the millennium: challenges for the new century. Aquatic Botany 65:7-20.

Duarte, C. M. and J. Cebrian. 1996. The fate of marine autotrophic production. Limnology and Oceanography 41:1758-1766.

Dunton, K., W. Pulich, and T. Mutchler. 2011. A seagrass monitoring program for Texas coastal waters: multiscale integration of landscape features with plant and water quality indicators. Coastal Bend Bays & Estuaries Program.

Dunton, K. H. 1994. Seasonal growth and biomass of the subtropical seagrass *Halodule wrightii* in relation to continuous measurements of underwater irradiance. Marine Biology 120:479-489.

Dunton, K. H. and S. V. Schonberg. 2002. Assessment of propeller scarring in seagrass beds of the south Texas coast. Journal of Coastal Research 37:100-110.

Durand, D., J. Bijaoui, and F. Cauneau. 2000. Optical remote sensing of shallow-water environmental parameters: A feasibility study. Remote Sensing of Environment 73:152-161.

Edgar, G. J. and A. I. Robertson. 1992. The influence of seagrass structure on the distribution and abundance of mobile epifauna: pattern and process in a Western Australian *Amphibolis* bed. Journal of Experimental Marine Biology and Ecology 160:13-31.

Ferwerda, J. G., J. de Leeuw, C. Atzberger, and Z. Vekerdy. 2007. Satellite-based monitoring of tropical seagrass vegetation: current techniques and future developments. Hydrobiologia 591:59-71.

Finkbeiner, M., B. Stevenson, and R. Seaman. 2001. Guidance for benthic habitat mapping: an aerial photographic approach. NOAA Coastal Services Center, National Oceanic and Atmospheric Administration.

Fonseca, M. and J. S. Fisher. 1986. A comparison of canopy friction and sediment movement between four species of seagrass with reference to their ecology and restoration. Marine Ecology Progress Series 29:15-22.

Fonseca, M., P. E. Whitfield, N. M. Kelly, and S. S. Bell. 2002. Modeling seagrass landscape pattern and associated ecological attributes. Ecological Applications 12:218-237.

Fonseca, M. S. and J. A. Cahalan. 1992. A preliminary evaluation of wave attenuation by four species of seagrass. Estuarine, Coastal and Shelf Science 35:565-576.

Foody, G. M. 2002. Status of land cover classification accuracy assessment. Remote Sensing of Environment 80:185-201.

Fourqurean, J., A. Willsie, C. Rose, and L. Rutten. 2001. Spatial and temporal pattern in seagrass community composition and productivity in south Florida. Marine Biology 138:341-354.

Fry, B. and P. L. Parker. 1979. Animal diet in Texas seagrass meadows: δ13C evidence for the importance of benthic plants. Estuarine and Coastal Marine Science 8:499-509.

Fyfe, S. K. 2003. Spatial and temporal variation in spectral reflectance: Are seagrass species spectrally distinct? Limnology and Oceanography 48:464-479.

Fyfe, S. K. 2004. Hyperspectral studies of New South Wales seagrasses with particular emphasis on the detection of light stress in eelgrass *Zostera capricorni*. University of Wollongong Thesis Collection:472.

Fyfe, S. K. and A. G. Dekker. 2001. Seagrass species: are they spectrally distinct? Pages 2740-2742 *in* Geoscience and Remote Sensing Symposium. IGARSS'01, Sydney, Australia.

Ganssle, J. 1990. Self Calibrating Systems. Embedded Systems Programming.

Gao, B.-C., M. J. Montes, C. O. Davis, and A. F. H. Goetz. 2009. Atmospheric correction algorithms for hyperspectral remote sensing data of land and ocean. Remote Sensing of Environment 113, Supplement 1:S17-S24.

Gesch, D. and R. Wilson. 2001. Development of a seamless multisource topographic/bathymetric elevation model of Tampa Bay. Marine Technology Society Journal 35:58-64.

Gitelson, A. A. 2004. Wide dynamic range vegetation index for remote quantification of biophysical characteristics of vegetation. Journal of Plant Physiology 161:165-173.

Green, K. and M. Finkbeiner. 2008. Redfish Bay Texas airborne sensor comparison and propeller scar mapping final report.

Green, S. M. and J. A. Cole. 2005. Hyperspectral remote sensing for vegetation surveys.*in* Third symposium on hemlock wooly adelgid in the eastern United States. U.S. Department of Agriculture, Forest Service, Asheville, North Carolina.

Grumbine, R. E. 1994. What is ecosystem management? Conservation biology 8:27-38.

Guimarães, M. H. M. E., A. H. Cunha, R. L. Nzinga, and J. F. Marques. 2012. The distribution of seagrass (*Zostera noltii*) in the Ria Formosa lagoon system and the implications of clam farming on its conservation. Journal for Nature Conservation 20:30-40.

Halpern, B. S., S. Walbridge, K. A. Selkoe, C. V. Kappel, F. Micheli, C. D'Agrosa, J. F. Bruno, K. S. Casey, C. Ebert, and H. E. Fox. 2008. A global map of human impact on marine ecosystems. Science 319:948-952.

Handley, L., D. Altsman, and R. DeMay, editors. 2007. Seagrass status and trends in the northern Gulf of Mexico: 1940-2002. U.S. Geological Survey Scientific Investigations Report 2006-5287.

Harlin, M. M. 1975. Epiphyte-host relations in seagrass communities. Aquatic Botany 1:125-131.

Hirano, A., M. Madden, and R. Welch. 2003. Hyperspectral image data for mapping wetland vegetation. Wetlands 23:436-448.

Holden, H. and E. LeDrew. 2000. Accuracy assessment of hyperspectral classification of coral reef features. Geocarto International 15:7-14.

Holden, H. and E. LeDrew. 2002. Measuring and modeling water column effects on hyperspectral reflectance in a coral reef environment. Remote Sensing of Environment 81:300-308.

Irlandi, E., W. Ambrose Jr, and B. Orlando. 1995. Landscape ecology and the marine environment: how spatial configuration of seagrass habitat influences growth and survival of the bay scallop. Oikos 72:307-313.

Jagtap, T. G., D. S. Komarpant, and R. S. Rodrigues. 2003. Status of a seagrass ecosystem: an ecologically sensitive wetland habitat from India. Wetlands 23:161-170.

Jenness, J. 2011. Repeating shapes for ArcGIS. Jenness Enterprises.

Kelly, N. M., M. Fonseca, and P. Whitfield. 2001. Predictive mapping for management and conservation of seagrass beds in North Carolina. Aquatic Conservation: Marine and Freshwater Ecosystems 11:437-451.

Kornicker, L. S. 1964. A seasonal study of living *Ostracoda* in a Texas bay (Redfish Bay) adjoining the Gulf of Mexico. Pubblicazioni della Stazione Zoologica di Napoli 33:45-60.

Kutser, T., I. Miller, and D. L. B. Jupp. 2006. Mapping coral reef benthic substrates using hyperspectral space-borne images and spectral libraries. Estuarine, Coastal and Shelf Science 70:449-460.

Lee, M. 2003. Benthic mapping of coastal waters using data fusion of hyperspectral imagery and airborne laser bathymetry. Dissertation. University of Florida, Gainesville.

Lewis, I., F. Graham, and A. W. Stoner. 1983. Distribution of macrofauna within seagrass beds: an explanation for patterns of abundance. Bulletin of Marine Science 33:296-304.

Linton, D. M. and G. F. Warner. 2003. Biological indicators in the Caribbean coastal zone and their role in integrated coastal management. Ocean & Coastal Management 46:261-276.

Louchard, E. M., R. P. Reid, F. C. Stephens, C. O. Davis, R. A. Leathers, and T. V. Downes. 2003. Optical remote sensing of benthic habitats and bathymetry in coastal environments at Lee Stocking Island, Bahamas: A comparative spectral classification approach. Limnology and Oceanography 48:511-521.

Lyzenga, D. R. 1981. Remote sensing of bottom reflectance and water attenuation parameters in shallow water using aircraft and Landsat data. International Journal of Remote Sensing 2:71-82.

Major, K. M. and K. H. Dunton. 2002. Variations in light-harvesting characteristics of the seagrass, *Thalassia testudinum*: evidence for photoacclimation. Journal of Experimental Marine Biology and Ecology 275:173-189.

Malthus, T. J. and P. J. Mumby. 2003. Remote sensing of the coastal zone: an overview and priorities for future research. International Journal of Remote Sensing 24:2805–2815.

Maritorena, S. 1996. Remote sensing of the water attenuation in coral reefs: a case study in French Polynesia. International Journal of Remote Sensing 17:155-166.

Matthew, M. W., S. M. Adler-Golden, A. Berk, G. Felde, G. P. Anderson, D. Gorodetzky, S. Paswaters, and M. Shippert. 2002. Atmospheric correction of spectral imagery: evaluation of the FLAASH algorithm with AVIRIS data. Pages 157-163. IEEE.

McGlathery, K. J., K. Sundback, and I. C. Anderson. 2007. Eutrophication in shallow coastal bays and lagoons: the role of plants in the coastal filter. Marine Ecology Progress Series 348:1-18.

McMillan, C. 1991. The longevity of seagrass seeds. Aquatic Botany 40:195-198.

McMillan, C. and F. N. Moseley. 1967. Salinity tolerances of five marine spermatophytes of Redfish Bay, Texas. Ecology 48:503-506.

Merkord, G. W. 1978. The distribution and abundance of seagrasses in Laguna Madre of Texas. Thesis. Texas A&I University.

Mishra, D. R. 2006. Multi- and hyperspectral remote sensing of tropical marine benthic habitats. Dissertation. The University of Nebraska, Lincoln.

Mishra, D. R., S. Narumalani, D. Rundquist, and M. Lawson. 2005. High-resolution ocean color remote sensing of benthic habitats: A case study at the Roatan Island, Honduras. Ieee Transactions on Geoscience and Remote Sensing 43:1592-1604.

Mishra, D. R., S. Narumalani, D. Rundquist, M. Lawson, and R. Perk. 2007. Enhancing the detection and classification of coral reef and associated benthic habitats: A

hyperspectral remote sensing approach. Journal of Geophysical Research 112:1-18.

Montagna, P. A. and R. D. Kalke. 1992. The effect of freshwater inflow on meiofaunal and macrofaunal populations in the Guadalupe and Nueces estuaries, Texas. Estuaries and Coasts 15:307-326.

Mumby, P., C. Clark, E. Green, and A. Edwards. 1998. Benefits of water column correction and contextual editing for mapping coral reefs. International Journal of Remote Sensing 19:203-210.

Onuf, C. P. 1994. Seagrasses, dredging and light in Laguna Madre, Texas, U.S.A. Estuarine, Coastal and Shelf Science 39:75-91.

Onuf, C. P. 1996. Seagrass responses to long-term light reduction by brown tide in upper Laguna Madre, Texas: distribution and biomass patterns. Marine Ecology Progress Series 138:219-231.

Onuf, C. P. and J. J. Ingold. 2007. A GIS analysis of seagrass resources and condition within Padre Island National Seashore, Texas. Open File Report 2007-1261, U.S. Geological Survey.

Oppenheimer, C. H. 1963. Effects of Hurricane Carla on the Ecology of Redfish Bay, Texas. Bulletin of Marine Science 13:59-72.

Orth, R. J., T. J. B. Carruthers, W. C. Dennison, C. M. Duarte, J. W. Fourqurean, K. L. Heck Jr, A. R. Hughes, G. A. Kendrick, W. J. Kenworthy, and S. Olyarnik. 2006. A global crisis for seagrass ecosystems. BioScience 56:987-996.

Peneva, E., J. A. Griffith, and G. A. Carter. 2008. Seagrass mapping in the northern Gulf of Mexico using airborne hyperspectral imagery: a comparison of classification methods.

Phinn, S., C. Roelfsema, A. Dekker, V. Brando, and J. Anstee. 2008. Mapping seagrass species, cover and biomass in shallow waters: An assessment of satellite multi-spectral and airborne hyper-spectral imaging systems in Moreton Bay (Australia). Remote Sensing of Environment 112:3413-3425.

Pollack, J. B., H. C. Kim, E. K. Morgan, and P. A. Montagna. 2011. Role of flood disturbance in natural oyster (*Crassostrea virginica*) population maintenance in an estuary in South Texas, USA. Estuaries and Coasts 34:187-197.

Pulich, W., S. Barnes, and P. Parker. 1976. Trace metal cycles in seagrass communities. Pages 494-506 *in* M. Wiley, editor. Estuarine Processes. Academic Press, New York.

Pulich, W., C. Blair, and W. A. White. 1997. Current status and historical trends of seagrasses in the Corpus Christi Bay National Estuary Program study area. Publication CCBNEP-20, Texas Natural Resource Conservation Commission.

Pulich, W. and C. Onuf. 2004. Statewide summary for Texas. Seagrass status and trends in the northern Gulf of Mexico 2002:7-15.

Pulich, W. M. 2007. Texas coastal bend. U.S. Geological Survey Scientific Investigations Report 2006-5287.

Quammen, M. L. and C. P. Onuf. 1993. Laguna Madre - seagrass changes continue decades after salinity reduction. Estuaries 16:302-310.

Ressom, H., S. Fyfe, P. Natarajan, and S. Srirangam. 2003. Monitoring seagrass health using neural networks. IEEE 2:1019-1024 .

Rooker, J. R., S. A. Holt, M. A. Soto, and G. Joan Holt. 1998. Postsettlement patterns of habitat use by sciaenid fishes in subtropical seagrass meadows. Estuaries and Coasts 21:318-327.

Rozas, L. P. and T. J. Minello. 1998. Nekton use of salt marsh, seagrass, and nonvegetated habitats in a south Texas (USA) estuary. Bulletin of Marine Science 63:481-501.

Rundquist, D. C. 2001. Field techniques in remote sensing: learning by doing. Geocarto International 16:85-90.

Sánchez-Carnero, N., S. Aceña, D. Rodríguez-Pérez, E. Couñago, and J. Freire. 2012. Fast and low-cost method for VBES bathymetry generation in coastal areas. Estuarine, Coastal and Shelf Science. In press.

Sand-Jensen, K. 1977. Effect of epiphytes on eelgrass photosynthesis. Aquatic Botany 3:55-63.

Schalles, J. F. and C. M. Hladik. 2012. Mapping phytoplankton chlorophyll in turbid, case 2 estuarine and coastal waters. Israel Journal of Plant Science Invited; in press.

Short, F., T. Carruthers, W. Dennison, and M. Waycott. 2007. Global seagrass distribution and diversity: A bioregional model. Journal of Experimental Marine Biology and Ecology 350:3-20.

Short, F. T. and C. A. Short. 1984. Seagrass filter: purification of estuarine and coastal waters. Pages 395-413 *in* V. S. Kennedy, editor. The Estuary as a Filter. Academic Press, New York.

Short, F. T. and S. Wyllie-Echeverria. 1996. Natural and human-induced disturbance of seagrasses. Environmental Conservation 23:17-27.

Shull, S. 2000. Mapping seagrass meadows of Padilla Bay, Washington, using a 1996 compact airborne spectrographic imager (CASI) dataset. Western Washington University.

Smith, V. H., G. D. Tilman, and J. C. Nekola. 1999. Eutrophication: impacts of excess nutrient inputs on freshwater, marine, and terrestrial ecosystems. Environmental pollution 100:179-196.

Strahler, A. H., L. Boschetti, G. M. Foody, M. A. Friedl, M. C. Hansen, M. Herold, P. Mayaux, J. T. Morisette, S. V. Stehman, and C. E. Woodcock. 2006. Global land cover validation: Recommendations for evaluation and accuracy assessment of global land cover maps. European Communities, Luxembourg:51.

Stunz, G. W., T. J. Minello, and P. S. Levin. 2002. Growth of newly settled red drum *Sciaenops ocellatus* in different estuarine habitat types. Marine Ecology Progress Series 238:227-236.

Tamilarasan, V., S. K. Sharma, and S. R. Nagabhushana. 1983. Optimum spectral bands for land cover discrimination. Advances in Space Research 3:287-290.

Tang, D., D. R. Kester, I. H. Ni, Y. Qi, and H. Kawamura. 2003. In situ and satellite observations of a harmful algal bloom and water condition at the Pearl River estuary in late autumn 1998. Harmful Algae 2:89-99.

Tassan, S. 1996. Modified Lyzenga's method for macroalgae detection in water with non-uniform composition. International Journal of Remote Sensing 17:1601-1607.

Thorhaug, A., A. D. Richardson, and G. P. Berlyn. 2007. Spectral reflectance of the seagrasses: *Thalassia testudinum, Halodule wrightii, Syringodium filiforme* and five marine algae. International Journal of Remote Sensing 28:1487-1501.

Tolan, J. M., S. A. Holt, and C. P. Onuf. 1997. Distribution and community structure of ichthyoplankton in Laguna Madre seagrass meadows: potential impact of seagrass species change. Estuaries and Coasts 20:450-464.

Tomasko, D. and B. Lapointe. 1991. Productivity and biomass of *Thalassia testudinum* as related to water column nutrient availability and epiphyte levels: field observations and experimental studies. Marine Ecology Progress Series 75:9-17.

Tunnell, J. W. and F. W. Judd. 2002. The Laguna Madre of Texas and Tamaulipas. TAMU Press.

Uhrin, A. V. and J. G. Holmquist. 2003. Effects of propeller scarring on macrofaunal use of the seagrass *Thalassia testudinum*. Marine Ecology Progress Series 250:61-70.

Valiela, I., K. Foreman, M. LaMontagne, D. Hersh, J. Costa, P. Peckol, B. DeMeo-Andreson, C. D'Avanzo, M. Babione, and C. H. Sham. 1992. Couplings of watersheds and coastal waters: sources and consequences of nutrient enrichment in Waquoit Bay, Massachusetts. Estuaries and Coasts 15:443-457.

Wabnitz, C. C., S. Andréfouët, D. Torres-Pulliza, F. E. Müller-Karger, and P. A. Kramer. 2008. Regional-scale seagrass habitat mapping in the Wider Caribbean region using Landsat sensors: Applications to conservation and ecology. Remote Sensing of Environment 112:3455-3467.

Wang, C. K. and W. D. Philpot. 2007. Using airborne bathymetric lidar to detect bottom type variation in shallow waters. Remote Sensing of Environment 106:123-135.

Ward, T. J. 1987. Temporal variation of metals in the seagrass *Posidonia australis* and its potential as a sentinel accumulator near a lead smelter. Marine Biology 95:315-321.

Watts, J. D., S. L. Powell, R. L. Lawrence, and T. Hilker. 2011. Improved classification of conservation tillage adoption using high temporal and synthetic satellite imagery. Remote Sensing of Environment 115:66-75.

Weng, Q. 2002. Land use change analysis in the Zhujiang Delta of China using satellite remote sensing, GIS and stochastic modelling. Journal of Environmental Management 64:273-284.

Wood, E., W. E. Odum, and J. C. Zieman. 1969. Influence of seagrasses on the productivity of coastal lagoons. Mem. Simp. Intern, Lagunas Consteras, UNAM-UNESCO.

Xie, F., Y. Lin, and W. Ren. 2011. Optimizing model for land use/land cover retrieval from remote sensing imagery based on variable precision rough sets. Ecological Modelling 222:232-240.

Yamamuro, M., K. Nishimura, K. Kishimoto, K. Nozaki, K. Kato, A. Negishi, K. Otani, H. Shimizu, T. Hayashibara, and M. Sano. 2002. Mapping tropical seagrass beds with an underwater remotely operated vehicle (ROV). Page 6 *in* Techno-Ocean 2002 International Symposium, Kobe Port Island, Japan.

Zomer, R. J., A. Trabucco, and S. L. Ustin. 2009. Building spectral libraries for wetlands land cover classification and hyperspectral remote sensing. Journal of Environmental Management 90:2170-2177.